The University of Jordan

Authorization Form

I, Ibtisam el-Beik , authorize the University of Jordan to supply copies of my Thesis/ Dissertation to libraries or establishments or individuals on request, according to the University of Jordan regulations.

Signature: ابتسام البيك

Date: 25.04.2011

الجامعة الأردنيـــــة
كلية الدراسات العليا

التاريـــخ: / /

نموذج رقم (١٨)
اقرار والتزام بالمعايير الأخلاقية والأمانة العلمية
وقوانين الجامعة الأردنية وأنظمتها وتعليماتها
لطلبة الماجستير

أنا الطالب: ابتسام محمد درويش البيك الرقم الجامعي: (8081397)

تخصص: الجيولوجيا الكليـــــة: العلوم

عنوان الرسالة: Spatial Variability of Heavy Minerals and Radioactivity in the Vicinity of Wadi el-Meerab, Southeast Jordan, and Their Exploration Bearing.

اعلن بأنني قد التزمت بقوانين الجامعة الأردنية وأنظمتها وتعليماتها وقراراتها السارية المفعول المتعلقة باعداد رسائل الماجستير عندما قمت شخصيا" باعداد رسالتي وذلك بما ينسجم مع الأمانة العلمية وكافة المعايير الأخلاقية المتعارف عليها في كتابة الرسائل العلمية. كما أنني أعلن بأن رسالتي هذه غير منقولة أو مستلة من رسائل أو كتب أو أبحاث أو أي منشورات علمية تم نشرها أو تخزينها في أي وسيلة اعلامية، وتأسيسا" على ما تقدم فانني أتحمل المسؤولية بأنواعها كافة فيما لو تبين غير ذلك بما فيه حق مجلس العمداء في الجامعة الأردنية بالغاء قرار منحي الدرجة العلمية التي حصلت عليها وسحب شهادة التخرج مني بعد صدورها دون أن يكون لي أي حق في التظلم أو الاعتراض أو الطعن بأي صورة كانت في القرار الصادر عن مجلس العمداء بهذا الصدد.

توقيع الطالب: ابتسام البيك ibey التاريخ: ٢٥ / ٤ / ٢٠١١

تعتمد كلية الدراسات العليا
هذه النسخة من الرسالــــة
التوقيع ... التاريخ ...

SPATIALVARIABILTY OF HEAVY MINERALS AND RADIOACTIVTY IN THE VICINITY OF WADI EL-MEZRAB, SOUTHEAST JORDAN, AND THEIR EXPLORATION BEARING

By
Ibtisam M. Beik

Supervisor
Dr. Ghazi A. Saffarini, Prof.

Co-supervisor
Dr. Harald G. Dill, Prof.

This thesis was submitted in Partial Fulfillment of the Requirements for the Master's Degree of Science in Geology

Faculty of Graduate Studies
The University of Jordan

April, 2011

COMMITTEE DECISION

This Thesis (Spatial Variability of Heavy Minerals and Radioactivity in the Vicinity of Wadi el-Mezrab, Southeast Jordan, and Their Exploration Bearing) was Successfully Defended and Approved on March 31, 2011.

Examination Committee	**Signature**
Dr. Ghazi A. Saffarini, (Supervisor) Prof. of Economic Geology	----------------------------
Dr. Harald G. Dill, (Co-Supervisor) Prof. of Mineralogy and Economic Geology	----------------------------
Dr. Belal S. Amireh, (Member) Prof. of Sedimentology	----------------------------
Dr. Ghaleb H. K. Jarrar, (Member) Prof. of Hard Rocks Petrology & Geochemistry	----------------------------
Dr. Khalil M. Khader, (Member) Assist. Prof. of Applied Mineralogy (The Hashemite University)	----------------------------

Dedication:

To my family and dearest friends,

God bless you…

Acknowledgment

I would like to express my biggest and most sincere gratitude and thankfulness to my supervisor Prof. Dr. Ghazi Saffarini, for supporting me all through this work, for believing in me and for his understanding and endless effort. I would also like to thank Prof. Dr. Harald Dill, for his help, advice and providence with scientific material necessary. Thanks are also due to the members of the examining committee for their rich full discussion and comments that contributed to the improvement of the work.

I am endlessly grateful to Prof. Dr. Belal Amireh for all the help which he provided me during this work and for his generous guidance, detailed instructions and endless patience. I thank Dr. Najel Yaseen also for his guidance all through the course of this work.

I am also most grateful to Dr. Saleem Mahmoud from Natural Resources Authority (NRA), for his generous help during the hard tedious field work and afterwards.

I would like to address many thanks to Mr. Nael al-Abbadi and Mrs. Amina al-Kurdi for grain mounts preparation and to Mrs. Manar Saleh for her laboratory technical assistance. I am sincerely grateful to Mr. Yousef Abu Salha for all his help with the SEM analysis and Mr.Mahmood Hasoneh for his endless encouragement and support.

I also need to express my extreme praise to my great friends and colleagues Mrs. Samiha Adar'awi, Miss. Reem Zaiter and Mr. Anas al-Otaiby, who gave me great deal of assistance in the field work and during the first stages of samples preparations.

And finally, I am endlessly thankful and grateful to my family and closest friends, for they have been supportive, patient and understanding all through the way.

Table of Contents

COMMITTEE DECISION II
Dedication III
Acknowledgment IV
Table of Contents V
List of Tables VI
List of Figures VII
List of Appendices VIII
LIST OF ABBREVIATIONS IX
ABSTRACT X
CHAPTER ONE: Introduction 1
CHAPTER TWO: Geographic and Geologic setting and Stratigrpahy 10
CHAPTER THREE: Methodology and Analytical Techniques 20
CHAPTER FOUR: Gamma Surveying 30
CHAPTER FIVE: Heavy Mineral Assemblages and Gamma Ray Readings 37
CHAPTER SIX: Geostatistical Analysis 60
CHAPTER SEVEN: 90
CHAPTER EIGHT: Conclusions and Recommendations 94
References 97
Appendices 103
Abstarct (in Arabic) 111

List of Tables

Number	Table Caption	Page
2.1	Stratigraphic units and nomenclature of the Khrayim Group	17
3.1	Selected heavy minerals, their general chemical composition and specific gravity	25
4.1	Potassium bearing minerals	33
4.2	Thorium bearing minerals	34
4.3	Uranium bearing minerals	34
5.1	EDS microanalysis of zircons and rutiles	45
5.2	Summary statistics for the variables studied	50
5.3	Pearson's linear correlation coefficient values between different pairs of variables	57
6.1	Parameters characterizing the best fit semi-variogram model chosen using log transformed data	67
6.2	Parameters characterizing best fit models adopted to produce best spatial variability maps.	72
6.3	Results of XRF for the selected samples: DBS7, DBS 23, DBS24 and DBS46	89
7.1	Resistance to chemical weathering of common transparent heavy minerals, inferred using different methods	93

List of Figures

Number	Figure Caption	Page
2.1	Study area location map	12
2.2	Stratigraphic columnar section showing Dubaydib Sandstone Formation Members	18
2.3	Simplified Geologic map of the study area	19
3.1	Sampling location points in the study area	23
3.2	Google Earth satellite image of the study area with sampling location points	24
5.1	Photomicrographs (taken under plane polarized light) of some zircon grained from samples in the study area	40
5.2	Photomicrographs (taken under plane and crossed polarized light) of some zircon grained from samples in the study area	41
5.3	Photomicrographs (taken under plane polarized light) of some zircon grained from samples in the study area	42
5.4	SEM secondary electron images	43
5.5	SEM EDS plots	44
5.6	Photomicrographs (taken under plane polarized light) of some tourmaline grained from random samples in the study area	47
5.7	Photomicrographs (taken under plane and crossed polarized light) of some tourmaline grained from samples in the study area	48
5.8	Photomicrographs (taken under plane and cross polarized light) of some rutile grained from random samples in the study area	51
5.9	Frequency distribution of the variables studied	56
5.10	Pearson’s correlation coefficient plots	58
6.1	Ideal shapes for most common semi-variograms (best fit models)	65

List of Figures (continued)

Number	Figure Caption	Page
6.2	Fitted experimental semi-variograms	68
6.3	Spatial variability map for the gamma radiation (Log CPS), according to the IDW method	71
6.4	Fitted experimental semi-variograms after modifications on the original data and number of neighborhood samples	73
6.5	Spatial variability maps for Log CPS according to the Spherical model	75
6.6	Spatial variability maps for Log THM % according to the IDW method	77
6.7	Spatial variability maps for Log THM% according to the Spherical model	78
6.8	Spatial variability maps for Log THM% (38 samples) according to the Spherical model	80
6.9	Spatial variability maps for Log HM% according to Exponential model	82
6.10	Spatial variability maps for Log (Zrn/THM%) according to Spherical model	84
6.11	Spatial variability map for Log (TurTHM%) according to the IDW method	86
6.12	Spatial variability maps for Log (Rt/THM%) according to Exponential model	87

List of Appendices

Number	Appendix Title	page
A	Sample locations given in both International Geographic and UTM systems	104
B	Gamma radiation readings as CPS and THM % values with corresponding Log transformed values	105
C	HM% values and corresponding Log transformed values	106
D	Zircon % values and corresponding Log transformed values	107
E	Tourmaline% values and corresponding Log transformed values	108
F	Rutile % values and corresponding Log transformed values	109
G	Minor and trace heavy minerals as % from THM found in the wadi alluvium	110

LIST OF ABBREVIATIONS

CPS: Counts per second

DBS: Dubaydib Sandstone

HM%: Volume percentage of ‘transparent heavy minerals” in total heavy minerals.

IDW: Inverse distance weighing.

(Rt/THM%): volume percentage of “rutile mineral” in total heavy minerals.

SD: standard deviation.

THM%: weight percentage of “total heavy minerals” in the bulk alluvium sample.

(Tur/THM%): volume percentage of “tourmaline mineral” in total heavy minerals.

(Zrn/THM%): volume percentage of “zircon mineral” in total heavy minerals.

SPATIALVARIABILTY OF HEAVY MINERALS AND RADIOACTIVTY IN THE VICINITY OF WADI EL-MEZRAB, SOUTHEAST JORDAN, AND THEIR EXPLORATION BEARING

By
Ibtisam M. Beik

Supervisor
Dr. Saffarini A. Ghazi, Prof.

Co-supervisor
Dr. Harald G. Dill, Prof.

ABSTRACT

Accessory heavy minerals (HM) species (i.e. zircon, rutile, apatite and monazite) bear eminent economic importance, contributed by their elemental constituents (e.g., Zr, Ti, Th and REE) which have wide spectrum of industrial and technological modern life applications. Economic deposits of heavy minerals are defined as those containing more than 1% Total Heavy Minerals (THM) by weight and are typically of siliciclastics sedimentary type.

In the present study; recent wadi alluvium was examined, from wadies dissecting the siliciclastic sedimentary rocks of Dubaydib Formation (Southeast Jordan) relatively rich with HM, in order to determine the mineral species present and give inferences about the possible relationship between heavy minerals abundances and prevailing radioactivity in the study area and accordingly the suitability of using gamma ray spectrometry technique in exploration for heavy minerals. For this purpose 40 samples were taken on a 3 km^2 random grid and at each location point Gamma Ray readings were recorded. Traditional heavy minerals separation was performed and grain mounts prepared to examine the heavy fraction types and concentrations. Counting of the transparent HM species revealed the presence of 3 major heavy mineral species; zircon, rutile and tourmaline along with minor amounts of anatase, garnet, dolomite, micas, staurolite, apatite and brookite. Scanning electron microscopy (SEM) was used to examine separate grains, in order to get some inference of the surface chemistry of the different mineral species present. Relative percentages of the heavy mineral species were calculated after counting and the data obtained was used to draw spatial variability maps using kriging techniques. The constructed maps were used to examine the possible spatial association between HM concentrations and prevailing radioactivity.

The amounts of heavy minerals found were not much appreciable economically, however the maps show that concentrations increase in the SE-NW direction in the lower part of the area. Further, only few samples showed radiation anomalies and were analyzed using XRF, which revealed that most of radiation, is due to the presence of Thorium and its decay series and less to Uranium. Correlation data measured and constructed maps indicated that there is a relationship between radiation and zircon content in the THM. The study concluded with recommendations regarding carrying out further studies on vast areas to verify results of this study. With as much relevant chemical analysis possible, for as it seems, radioactive and other economic elements (i.e. Zr, Ti, REE) could be present in high concentrations way above the background but are rather ambiguously distributed. Further studying would also form better perspective of the HM distribution pattern in similar environments and help in guiding towards economic concentrations, using the applied techniques in this study.

CHAPTER ONE:
Introduction

1.1 Preface

This work is presented as a partial requirement for an M.Sc degree in Geology at the University of Jordan. The main focus in this work is on the Heavy Minerals (HM) occurrences, abundances and spatial distribution in wadi deposits in the vicinity of wadi el-Mezrab, Southeast Jordan, mainly for opening the way in the future for further intense investigations of these valuable mineral occurrences in the country.

1.2 General

Heavy minerals (HM) are rock forming or accessory minerals, with densities above 2.8g/cc. (Mange and Wright, 2007). Examples of rock forming minerals are amphiboles, pyroxenes and micas, while zircons, apatite, rutile, tourmaline and ilmenite are some of many examples of accessory minerals occurring in different rock types and typically comprise around 1% of the siliciclastics sediments (Mange and Maurer, 1992).

Heavy minerals have wide range of application in modern geologic scientific researches, as for constraining sediments provenance and source lithology (e.g., Bateman and Catt, 2007; Harald, 1998; Haredy, 2008) as well as palaeotransport (Mange and Wright, 2007).

Also many researchers have based their work on analyzing heavy mineral assemblages, for evaluating weathering conditions (i.e. Van Loon and Mange, 2007), diagenetic evolution (i.e. Miliken, 2007; Morton and Hallsworth, 2007), paleogeographic and paleoclimatic features (Amireh, 1990), tectonic events and even for stratigraphic correlations (Amireh, 1994).

In these researches, geochemistry of the heavy minerals, surface textures, high resolution heavy mineral analysis (HRHMA) and numerical data analysis have been involved to make scientific based inferences regarding the research issue (Mange and Wright, 2007).

In many cases spatial distribution of heavy minerals and their assemblages has been employed in the source studies such as those carried out by Haredy, 2008 and Huisman and Klaver, 2007.

The importance of heavy minerals goes beyond the researching and academic work. It is truly incised in the economic value of these minerals and their elemental constituents.

Titanium minerals (e.g., **rutile, anatase, brookite, ilmenite and leucoxene**) are used worldwide for the manufacturing of TiO_2 pigments, with this application covering 95% of TiO_2 consumption, (Williams and Steenkamp, 2006). Though most of ilmenite is used in the previous application, minor amounts of this heavy mineral is used for foundry sand, filter-bed sand and in oil drilling industry (Mange and Wright, 2007). Rutile has its own applications in welding rods, metallurgy and electronic applications.

On the other hand, **zircon** is mostly used in ceramic industries, refractories, foundry sands, manufacture of zirconia (ZrO_2) chemicals, and other applications in decreasing order of use according to Warland, (2006). Zircon contains 67.22% ZrO_2 by mass (Elsner, 2010). Hafnium is readily incorporated in the zircon crystal as a solid solution between zircon and hafnon ($HfSiO_4$), due to which natural zircons contain HfO_2 between 1 and 3 % by weight (MacRae et al, 2003). Both zirconium and hafnium are the main structural and absorbing materials of thermal nuclear reactors (Shatalov et al, 2008). Also zircon grains contain high

levels of Th and U oftenly, either as inclusions of monazite and uraninite or as solid solution substituting for zirconium (MacRae et al, 2003).

Monazite is the most important mineral in terms of being the source for REE (Ce, La, Sm…etc) and Yttrium. Cerium group of rare earths is employed mostly as catalysts in different industries (Hedrcik, 2005), while Yttrium is used in lasers, high temperature lenses and similar applications (Garnar, 1985).

Epidote mineral group still has no commercial applications and **tourmaline** still doesn't have a separate market (Mange and Wright, 2007).

Economically significant concentrations of heavy minerals are found within siliciclastics sediments or sedimentary rocks. Processes of selective sorting and separation of heavy minerals from the light mineral grains within the sediments may form economic heavy mineral deposits, known as placer deposits (Mange and Wright, 2007). Placers could be formed in different environments and are classified according to the way of their formation to residual, eluvial, stream, glacial, bajada, eolian and beach placers (Jenkins, 1964). Stream (alluvial, fluvial) placers are most important of all types and have been handed most attention in literature.

Not much has been researched or written regarding desert placers, especially in cases where source rocks are the sedimentary cover strata. The reason mostly is that these strata are formed from rocks with a relatively low average density compared to igneous and metamorphic rocks and could provide only trivial amounts of heavy minerals (Mange and Wright, 2007). The placers formed from these sources tend to contain relatively high abundance of the ultra-stable heavy minerals zircon, tourmaline and rutile (ZTR) due to

their ability to survive sediments recycling events. In this study, heavy minerals contained within wadi deposits in Southeastern Jordanian desert have been examined for their abundances, spatial variability and possible exploration radiation based techniques (Gamma-radiation). The studied wadi deposits are derived from sedimentary strata (Dubaydib Sandstone) by means of ephemeral streams and winnowing.

The Dubaydib formation is one of the most promising "heavy minerals" host rocks in Jordan. The formation is middle to late Ordovician in age.

It mainly outcrops in Sahl al-Khrayim (South Jordan), where its base is delineated by the appearance of huge populations of vertical burrows of *Sabellarifex* (Skolithos), whereas the top is considered to be below the first bed of a decimetric-thick sandstone facies that gives a characteristic landscape of mesas and cuestas to the overlaying Mudawwara formation. The Dubaydib formation has been subdivided into three parts (Members) (Amireh et al, 2001):

1. The lower part consists of horizontally bedded silty sandstone penetrated largely by Skolithos.

2. The middle part consists of channel fills intercalated within horizontally bedded sandstone.

3. The Upper part consists of horizontally fine grained sandstone facies enriched with Skolithos.

Several phases Jordanian Natural Resources Authority (NRA) researches in the area as (Madanat et al, 2006) summed up with revealing that the important portion of the heavy minerals is deposited in the middle member of Dubaydib Sandstone Formation (DB2). The thickness of the heavy minerals bearing bed ranges from 1.5-5 m, whereas the overburden, consisting mainly of sandstone, ranges from 0-18.7 m in thickness.

In their studies, zircon was found to be the dominant heavy mineral followed by monazite, Ti-oxides (mostly rutile), ilmenite and epidote. Also zircon concentrations in the sandstone range from 0.67-3.75%, Cerium from 499-2168 ppm and Lanthanum from 224-1065 ppm, while TiO_2 from 1.61-4.91 ppm.

The sandstone of DB2 was found to be highly radioactive due to its content of U and Th, with thorium concentration reaching 400 ppm.

It should also be mentioned that quartz, iron oxides, mica, kaolinite and feldspar are the main constituents found as gangue minerals in the deposit.

During the first phase of the NRA detailed exploration program (1997-1999) rough estimate of the total heavy minerals reserve in DB2 was mounted up to 96.000 metric tons. Second phase of the program was carried in 2004, but the reserves of the heavy minerals from this phase were not determined.

1.3 Previous studies

Bender (1974) was the first to describe and define the boundaries of the "Sabellarifex sandstone unit", which was later amended to the "Dubaydib sandstone formation". The

name taken from Jabal/Wadi Dubaydib, near Sahl As Suwwan, by the National Resources Authority during the 1:50000 mapping program (Abu Lihie, 1988).

Bender (1974) described the geology and geologic setting of Dubaydib Formation.

Makhlouf (1994) studied the occurrences and distribution of the hummocky cross stratified units in the upper Dubaydib Member, and the subaqueous channel patterns of the middle member of the formation. In his study he concluded that both sedimentary features are diagnostic of inner shelf storm deposits, and have been attributed to the action of strong storm-wave surges which prevailed during the Late Ordovician.

Makhlouf (1997) studied the channel sandstone facies of Dubaydib formation and concluded that they were confined to the middle member of the formation and are partially overlain by the hummocky cross-stratified facies. Individual channels are superimposed on each other forming more complex, compound channel forms. According to Makhlouf, (o.ct.,) the channel formation is attributed to storm generated offshore rip currents in the subtidal zone and individual beds within each channel body is thought to record successive storm surge events, during prevailing tempestitie conditions.

Amireh, et al (2001) studied the fluvial-shallow marine-glaciofluvial depositional environments of the Ordovician system in Jordan. The Dubaydib formation of the late Ordovician had been subdivided into three parts: Lower, Middle and Upper according to the litho-facies and architectural elements found. The depositional paleoenviroment for each member has been interpreted.

Natural Resources Authority (**NRA**) carried out several studies on Wadi al-Mezrab area, among which:

- Masri, in 1988 produced a geological map of Wadi Al-Mezrab area scale 1:10.000 which encompassed the area of zircon deposits.
- In 1997, NRA carried out the first phase of an exploration program for zircon and heavy minerals. The study included drilling 39 boreholes and 7 trenches, sampling and reserve determination.
- In 1999, many samples were sent to the international laboratories for analysis. Results were good regarding the presence of zircon and rare earth elements (REE).
- In 2002, bulk samples (500 kg) were prepared and sent to the Egyptian Geological Survey laboratories for mineral processing. The result of this study indicated that zircon could be concentrated with 80% purity.
- In 2004, NRA carried out the second phase of the exploration program for zircon and heavy minerals in new localities and this study is still under evaluation.

1.4 Aims of the study

The aims of this study as previously mentioned, briefly could be outlined as follows:

1. Investigating the occurrences and abundances of heavy minerals in the whole area including wadi el-Mezrab and the surrounding wadies.

2. Examining the different heavy mineral species present.

3. Understanding the spatial distribution and dependence of the heavy minerals species found in the study area, using the Kriging geostatistical technique.

4. Determining whether the applied exploration techniques would lead to the already known HM source, which is Dubaydib Formation.

5. Evaluating the usefulness of gamma-ray surveying in the exploration of heavy minerals in similar wadi deposits.

6. Opening the way for further investigations by mining and exploration companies for heavy minerals in Jordan, particularly in the south, where Dubaydib Formation is easily accessible and promising as shown in several Natural Resources Authority reports and individual researches.

CHAPTER TWO:
Geographic and Geologic setting and Stratigrpahy

2.1 Geographic Setting

2.1.1 Location and Accessibility:

The wadi el-Mezrab area (Fig 2.1) is located about 300 km south of Amman and 90 km east of Aqaba. The study area is rectangular in shape and includes wadi el-Mezrab and few adjacent wadies. It can be delineated by the coordinates (29° 25’ 48”N, 35° 45’ 36”E) and (29° 24’ 05”N, 35° 47’ 26”E) corresponding to the UTM coordinates (767770mE 3258800mN) and (770815mE 3255700mN) in zone 36R.

The area is accessible from the Rum triangular cross road which is reached either from the Amman-Dead Sea highway (road 65) or the the Desert highway (road 15), or it can be accessed from Ma’an via the Ma’an- Mudawwara road (road 5). It is in the direction of Qa’a el Disi, and though the area contains many non-asphaltic tracks that can be crossed by 4-wheel drive vehicles, many parts of it are inaccessible.

2.1.2 Topography:

The topography of the study area is a reflection of tectonics, mainly faulting which led to subsidence and was followed by erosion that gave rise to the principle wadies.

There are three prominent wadies in the area, two of which drain towards southwest into Dubaydib major wadi, and a third one draining into the west.

The study area is part of the Southern Mountainous Desert Province (Masri, 2007).

2.1.3 Climate and Vegetation:

The dry Sahara climate characterizes the study area, such that it has warm and dry climate with short rainy winter (December-March). The annual rainfall is less than 50 mm. The mean daily minimum and maximum temperatures are 2° and 40° C, respectively. Vegetation in the study area is very rare and mainly consists of annual grasses in the wadi courses (Masri, 2007).

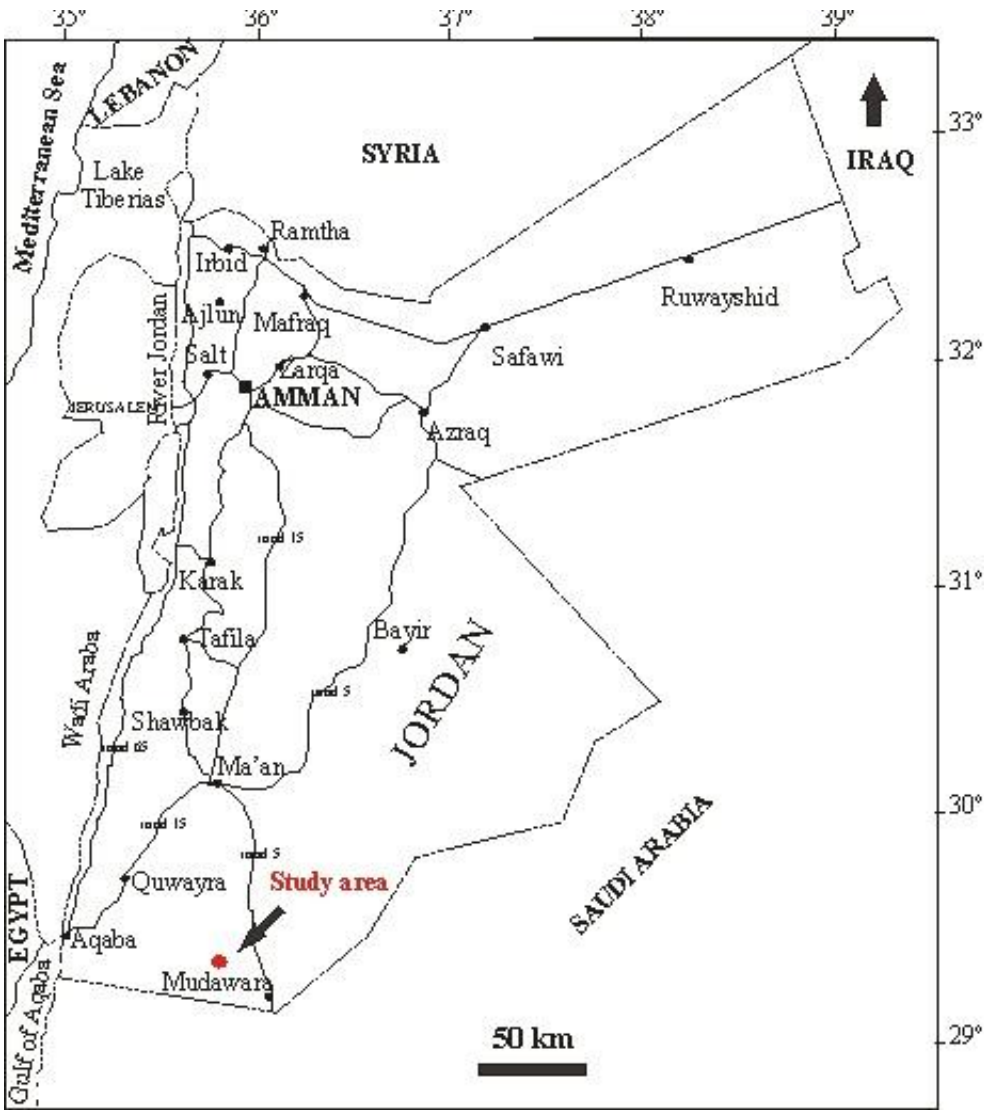


Figure 2.1 Study area location map

2.2 Geological Setting

Southern –southeastern Jordan is covered by different fluvial and marine siliciclastic sedimentary facies ranging from sandstones to mudstones. These are from Ordovician-Silurian (Paleozoic) to Pleistocene and Holocene in age (Masri, 2007).

The origin of the siliciclastics is accounted for by the erosion and further deposition of the calc-alkaline granitoides' sediments in fluvial, fluvio-marine and marine environments. The granitoides are the major constituents of the Arabian-Nubian Shield in Jordan, (McCourt, 1987; McCourt and Ibrahim, 1990).

In the period between 630-540 Ma, Jordan as a part of the Arabian-Nubian Shield was subjected to intensive faulting in what is known as the Najd Fault System. The faults are in SE-NW direction with two movements on them, one is strike slip sinistral (left-lateral) and the other is vertical. The vertical movement along the faults belonging to this system led to the formation of depositional basins, in which the Paleozoic sediments have been deposited at a later stage. Accompanied with the Najd Faults was also magmatic activity, where both plutonic and volcanic magmatic rocks formed the Araba Complex in Jordan. This previous period dominated by extension is the final phase of the so-called Pan African Orogeny (900-543 Ma) (Kennedy, 1964). By the end of which, the surface of the Arabian Shield in Jordan became irregular, with erosional and depositional processes taking control, until the Peneplanation event took place, which though made the area more regular, it also created the perfect environment for sedimentary deposition that took place later in the Paleozoic and after as mentioned previously (Abed, 2000).

Paleozoic sedimentation started with fluvial deposition under humid climate in the Cambrian, then in the late Cambrian and Early Ordovician rivers draining in the Northern direction were propagating the entire country (Powell, 1989). The sedimentary sequence deposited is represented by Ram Group, which ends with the Um Sahm Formation, of Areing age, during which marine influence was more pronounced. Then in middle Ordovician (lower Llanvirn) a major change in deposition took place (Khrayim Group), caused by major marine transgression from the E-NE directions, transforming the depositional environment into shallow marine, with fluctuating water depth until the rest of Ordovician (Powell, 1989). Sheet sandstones, siltstones and mudstones accumulated on a subsiding shelf under the influence of oscillatory waves and tide and storm-driven currents.

2.3 Stratigraphy

The study area is dominated by siliciclastic sedimentary rocks of Middle – Late Ordovician period (Llanvirn and Llandeilo ages respectively) belonging to the Khrayim Group (Table 2.1.). Khrayim group is so named after Jabal and Qaa' Khrayim in South Jordan. It consists of thick sedimentary marine sequence, and is extending from Ordovician (Llanvirnian age) to Lower Silurian. The sequence is outcropping in large thicknesses in SE of Jordan, present in the NE, but was removed from the Western and Middle parts of Jordan by the erosional processes following the Hercynian (Variscan) orogeny in the middle of Carboniferous (Abed, A. 2000).

Two formations dominate the study area; the Hiswah Sandstone Formation and the overlying Dubaydib Sandstone Formation.

2.3.1 Hiswah Sandstone Formation:

The name of the formation is derived from Wadi/Jibal Hiswah as first used by (Abu Lihie, 1988). It's what (Bender, 1974) named the Graptolite Sandstone. The lithology of the Formation could be divided into two major parts:

1. The lower part consists of red fine grained sandstone with oscillation and interference ripples. Bedding surfaces contain drifted *Didymo-graptus bifidus* and some traces. The Graptolites are found in the mudstones interfering with the siltstone-sandstone beds, and could be a potential source for hydrocarbons. These graptolitic species also indicated a llinvarin age of the formation (Bender, 1963). This lower member is deposited in marine low energy shelf environment.

2. The upper part, consisting of sandstone coarsening upward facies. The sandstone beds bear ripple cross lamination, trough cross bedding and *Harlania* traces (Masri, 2007) and were deposited in marine lower to middle shoreface of a coastal sand barrier or a barrier beach complex (Amireh, 1987).

Top of Hiswah formation is identified by the first appearance of *Sabellarifex* burrow bearing sandstones of the overlying Dubaydib Formation.

2.3.2 Dubaydib Sandstone Formation:

The name Dubaydib is derived from Wadi/Jabal Dubaydib SE of Sahl As Suwwan (Abu Lihie, 1988) and its equivalent to what (Bender, 1974) called the "Sabellarifex Sandstone" after defining its upper & lower boundaries.

The lithology of this formation has been studied by many including the NRA (Natural Resources Authority). All studies revealed that the 120-150 m thick sequence of sandy silt, sandstone and silty shale comprising the Dubaydib formation could be divided into three parts (members) as shown in Fig 2.2:

1. The lower member (DB1): It consists mainly of fine grained sandstone deposited in form of sheet like beds (Abed, 2000), where silty sediments interfinger with these beds and comprise the fine component of the coarsening upward sequence in this member (Masri, 2007). This member is full with *Sabellarifex* burrows (Skolithos) in both facies and occasionally *Harlania* burrows could also be found on the bedding surfaces accompanied with symmetrical ripple marks that have mostly straight crests. (Abed, 2000). This member represents sand flat and indicates shallow marine (lower foreshore) depositional environment (Amireh et al, 2001).
2. The middle member (DB2): consists of 3 distinctive fining up sequences, each comprised of sandstone and silty shale (Makhlouf, 1998). Each sequence was deposited as sub-marine channel fill of low sinuosity in northward direction, showing large lateral paleocurrent variation (Amireh et al, 2001). The channels' floor is scoured and filled with intraformational clasts (Makhlouf, 1998). The most prominent structures in the channel fills are large scale trough cross-bedding in the lower part, then low angle cross-stratification moving upwards into Hummocky cross bedding accompanied with *Sabellarifex* burrows, wavy & interference ripple marks, which all together are strong indicators of subtidal depositional environment with tempestite conditions (Makhlouf, 1998) or high energy mid shelf zone (Powell, 1989).

3. The upper member (DB3): This member consists also mainly of fine grained sandstone which is horizontally bedded and contains hummocky cross-stratification & occasional skolithos. It’s interfingered with green silty shale containing Harlania traces and some Cruziana species (Abed, 2000). The depositional environment here again is lower foreshore to upper shoreface (Amireh et al, 2001).

Table 2.1 Stratigraphic units and nomenclature of the Khrayim Group (after Abed, 2000)

<table>
<tr><th rowspan="2">AGE</th><th rowspan="2">Quennel 1951/ Burdon 1959</th><th rowspan="2">Bender 1968/1974</th><th>Llyods Fm 1968</th><th colspan="3">NRA 1984</th></tr>
<tr><td rowspan="6">Mudawwara (K2)</td><th>Group</th><th colspan="2">Formation</th></tr>
<tr><td></td><td rowspan="7">Um Sahm Sandstone including Zarqa Group (Triassic-Jurasic)</td><td>Worm-Burrowed Sandstone</td><td colspan="3"></td></tr>
<tr><td>Llandovrian</td><td>Reddish Brown, Argillaceous Sandstone</td><td rowspan="6">KHRAYIM GROUP</td><td colspan="2">Khushsha</td></tr>
<tr><td rowspan="3">Caradocian</td><td rowspan="2">Nautiloid Sandstone</td><td rowspan="3">Mudawwara</td><td>Ratiya Member</td></tr>
<tr><td>Batra Member</td></tr>
<tr><td>Conularia Sandstone</td><td>Tubeiliyyat Member</td></tr>
<tr><td>Llandelian</td><td>Sabellarifex Sandstone</td><td rowspan="2">Khreim</td><td colspan="2">Dubaydib</td></tr>
<tr><td>Llavirnian</td><td>Graptolite Sandstone</td><td colspan="2">Hiswah</td></tr>
</table>

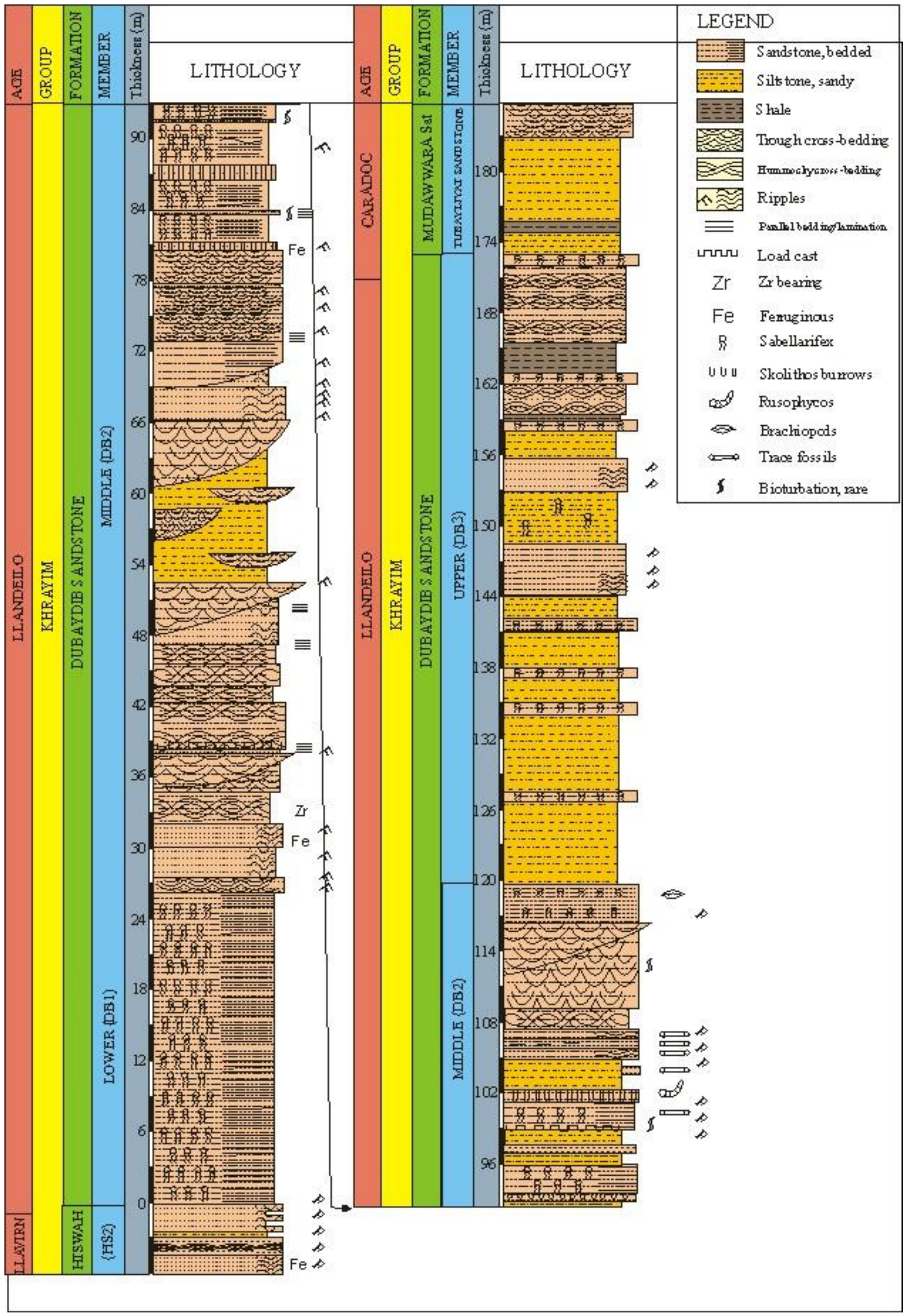


Figure 2.2 Stratigraphic columnar section showing Dubaydib Sandstone formation Members (after Masri, 2007).

The NRA Geological Survey Division examined Dubaydib sandstones for their heavy minerals' content, and subjected wadi el-Mezrab area to detailed exploration program in two phases (1997-1999 & 2004). The results indicated that the middle member (DB2) contains large reserves of heavy minerals in 1.5-4.2 m thick bed, overlain by 0-20 m thick sandstone overburden (Madanat et al., 2006). It is worth mentioning that part of the study area is cross passed by two large NW-SE normal faults, having downthrows in opposite directions, forming the known AlMuzayribat Graben (Fig 2.3) according to (Madanat et al, 2006 and Masri, 2007).

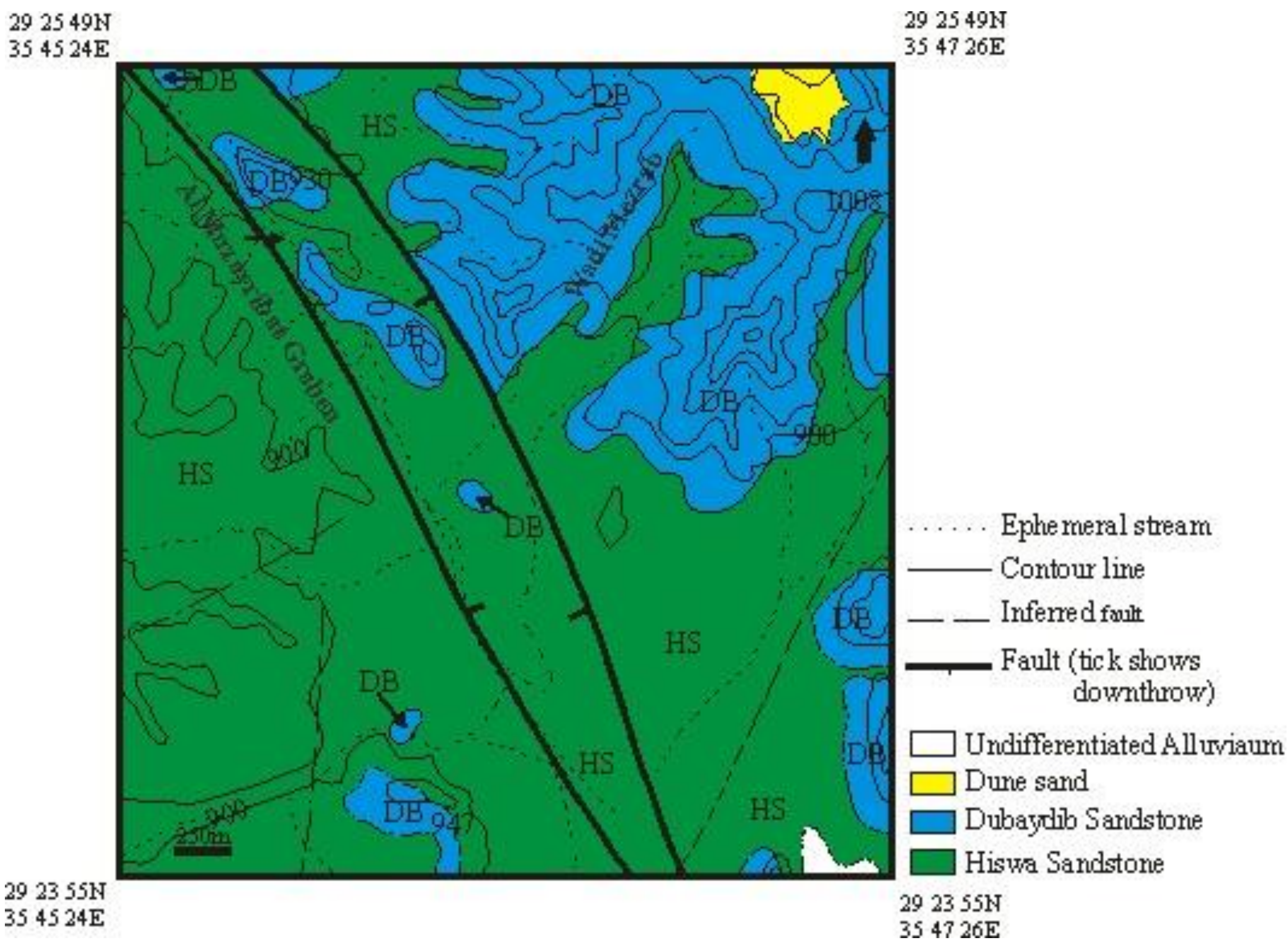


Figure 2.3 Simplified Geologic map of the study area (after Madant et al, 2006).

CHAPTER THREE:
Methodology and Analytical Techniques

3.1 Introduction

To fulfill the aims of this study a staged program was set forth. The following is a detailed account of its items.

3.1.1 Desk studies (duration: one month):

These included:

1. Preliminary desk studies. Considering the study area and its geological setting, stratigraphy, topography....etc., and getting the appropriate geologic maps.

2. Literature review relevant to the thesis topic including local and international previous studies, NRA reports, geologic maps, satellite images....etc.

3. Delineation of the study area.

3.1.2 Field Work:

One day field trip (orientation survey) was conducted first to get the proper orientation for further work, then it was followed by another 4 days field trip (routine survey)(April 2010) for sampling purposes. Sampling was made along a group of lines lying in the NE-SW direction whenever possible for the later application of Kriging techniques i.e., to facilitate the study of the spatial distribution of heavy minerals in the study area.

3.1.3 Laboratory Work:

Laboratory work was performed in two months period and included:

1. Gentle mechanical disaggregation and sieving of samples to obtain the desired size fraction from each sample.
2. Heavy liquid separation and calculation of the THM % by weight.
3. Petrographic analysis of the non-opaque HM portion using polarized light microscope.
4. Calculating individual and total transparent heavy mineral species volume percentage from THM from grain mounts by grain counting.
5. Preparing and studying representative samples using SEM (scanning electron microscopy) and XRF (X-ray Fluorescence) for elemental analysis.

3.1.4 Data Interpretation:

This included:

1. Processing and interpreting the collected data from the field and laboratory work through relevant software program (e.g. GS+ for Kriging).
2. Evaluating the results and drawing final conclusions regarding the presence and abundance of the heavy minerals in the study area on one hand and the exploration techniques used in this study on the other.

3.2 Field work (sampling)

Samples were collected along lines lying in the NE-SW direction forming a randomly stratified grid aligned in the NW-SE direction (Fig 3.1), with the sampling interval ranging from 300 to 400 m in the NE-SW direction, and few samples taken at 150 and 200 m interval, for acquiring better semi-variogram later on i.e., to account for the small scale

spatial variability. Gamma radiation using BGS-3 scintillation counter was recorded at each sampling location point. Figure 3.2 represents the corresponding Google Earth satellite image of the study area with sampling location points.

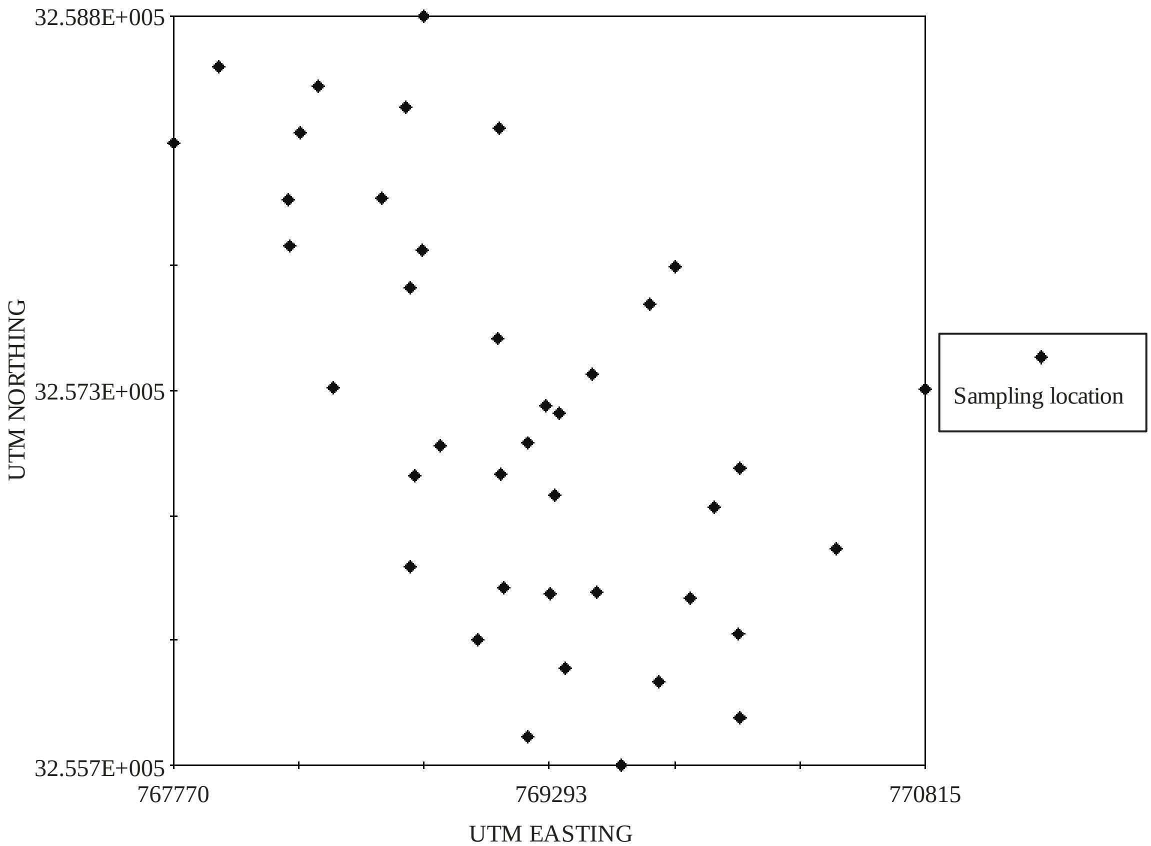


Figure 3.1 Sampling location points in the study area (UTM zone 36).

3.3 Laboratory Work

3.3.1 Heavy Minerals Separation and Grain Mounting:

Heavy minerals are high density minerals found in the siliciclastics sediments, that could originally either be rock forming minerals (e.g. amphiboles, pyroxenes, micas) , or are

accessory constituents (e.g. zircon ,apatite ,tourmaline, etc .) in different types of rocks (Mange and Maurer 1992). Those minerals are deposited and sorted according to differences in the size, shape and density of the grains (Paldmal et al, 1998; Komar, 2007). Densities and composition of the heavy minerals of interest to this study are listed in Table 3.1.

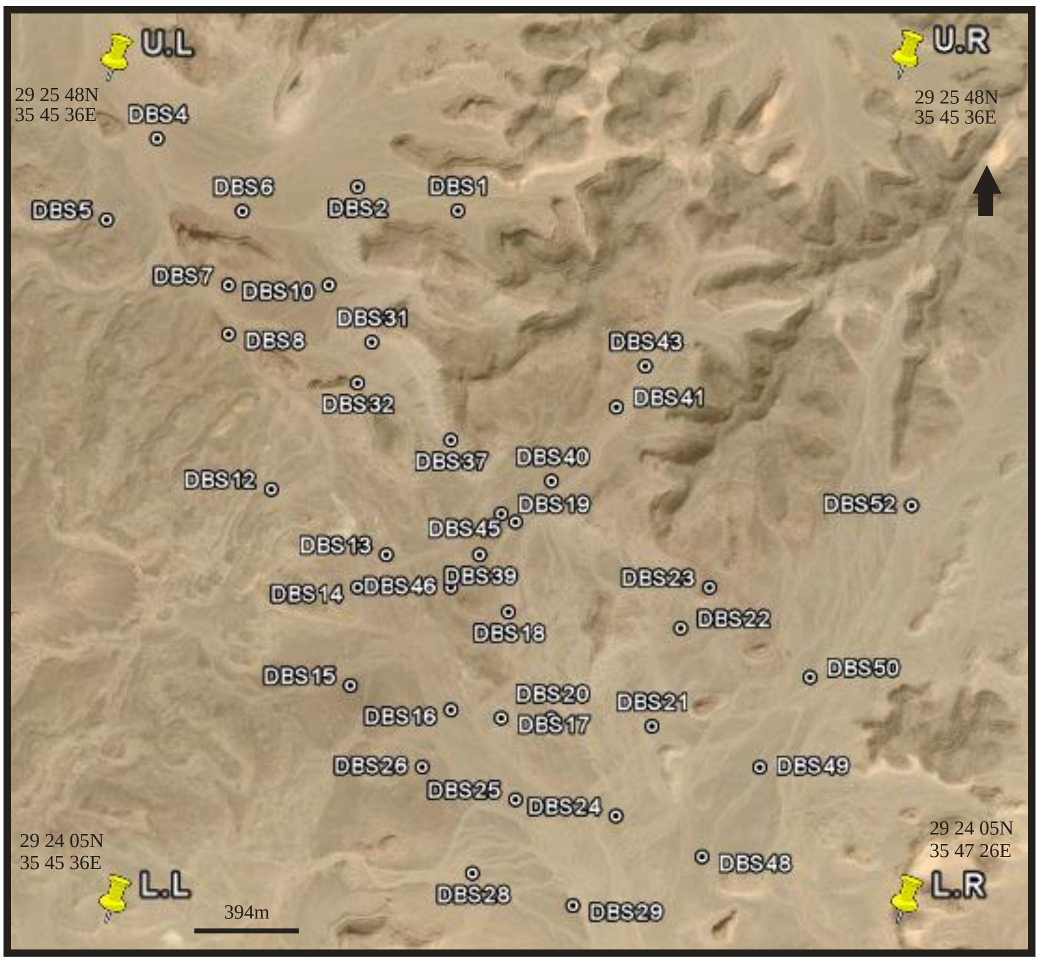


Figure 3.2 Google Earth satellite image of the study area with sampling location points.

Table 3.1 Selected heavy minerals, their general chemical composition and specific gravity (after Klein and Dutrow, 2008).

Mineral name	Mineral composition	Specific gravity
Anatase	TiO_2	3.9
Rutile	TiO_2	4.18-4.25
Apatite	$Ca_5(PO_4)_3$ (F,Cl,OH)	3.15-3.2
Brookite	TiO_2	3.9-4.1
Epidote	$Ca_2(Al,Fe)Al_2O(SiO_4)$	3.35-3.45
Garnet group	$(Mg,Fe^{2+},Mn^{2+})_3Al_2Si_3O_{12}$-$Ca_3(Fe^{3+},Al,Cr^{3+})_2Si_3O_{12}$	3.13-4.32
Illmenite	$FeTiO_3$	4.7
Monazite	$(Ce,La,Y,Th)PO_4$	4.6-5.4
Tourmaline	$(Na,Ca)(Fe^{2+},Li,Mg,Al,Mn)_3(Al,Fe^{3+})_6(BO_3)_3$ $(Si_6O_{18})(OH)_3(OH,F,O)$	3.0-3.25
Staurolite	$Fe_{3-4}Al_{18}Si_8O_{48}H_{2-4}$	3.65-3.75
Zircon	$ZrSiO_4$	4.68

Since the heavy minerals have relatively high densities, the most used technique to separate them from the remaining mineral components of the rocks or sediments containing them, is through a high density liquids, such that the immersion of the sample in a heavy liquid of intermediate density will produce two mineral fractions ; heavy (sinking part) and light (floating part).

The heavy liquid (high density liquid) used in this study was bromoform $BrCH_3$ (tribromoethane) with density 2.86-2.89 g/cc, following the procedure described below .

The separation procedure:

After mixing (homogenizing) each of the original samples brought from the field, 500 g were weighed from each sample, gently disaggregated mechanically and dry sieved through two fraction sizes (0.038-.25mm). For calculation purposes the fraction in between was weighed again, then washed with water and dried. The amount lost on washing (dust

and clays) was calculated as well, and eventually 40 g from the sample were taken for the heavy liquid separation (HLS).

Using a separation set and $BrCH_3$ heavy liquid, each 40 g were immersed in the HL, and left to separate for 3 hours, with periodic stirring. After 3 hours, the heavy fraction was removed, washed with acetone, then with water using a shaker to separate any adhered grains, then were dried and weighed.

The possible errors in the separation should be taken into consideration when presenting the data, therefore 7 subsamples (of 10 g) from one original sample (DBS21) were separated under same previous circumstances then THM weight per each was measured. The results are displayed below:

0.0473g/ 0.0459g/0.0428g/0.0364g/0.0617g/0.0527g/0.0436g

The mean, the standard deviation and following the error in the separation was estimated using the following equation (Journel and Huijbregts, 1978): p = V*T/ n^0.5, where:

P: error in the work

V: Variation Coefficient; V = STD/mean

T: factor (taken T=1)

N: number of samples

The results were:

Mean = 0.0472

STD = 0.008074 and P = 0.065

This indicated that the error is 6.5 %, and it should be considered when making conclusions regarding the THM quantities measured.

After the heavy minerals fraction was gained and weighed from each sample, grain mounts were prepared using Epoxy resin and hardener in proportions 15:2 by volume (manufactured by Struers). Multiple quartering was performed on the each heavy fraction sample before spread on the glass slide, to assure that the grain mounts indeed are representative in terms of the different mineral constituents and their proportions. For the purpose of this study and due to facilities available, 200-400 grains of heavy minerals were examined and counted, but only the non-opaque portions were identified using the cross-polarized light microscope. The number of the grains counted provides reliability to the estimations of the mineral proportions and the detection of rare species (Mange and Maurer, 1992).

Counting was performed in Ribbons, and involved both opaque and non opaque grains as mentioned. The proportions of different non-opaque (transparent) heavy minerals species were calculated as volume percentages as:

1. Transparent heavy minerals/Total heavy minerals%.

2. Individual transparent heavy mineral specie/Total heavy minerals%.

3.3.2 Chemical Analysis:

For the purpose of chemical analysis, two techniques were used; the Scanning Electron microscope and X-ray Fluorescence.

The techniques are further explained in the following section.

3.3.2.1 Scanning Electron Microscopy (SEM):

Selected mineral grains from the heavy fractions were handpicked under the binocular microscope, such that grains which apparently belonged to same species were grouped together. The grains were put on the aluminum stubs, coated by platinum and analyzed using the "Inspect SEM" (manufactured by FEI) available at the University of Jordan (JU).

Topographic images of the mineral grains were produced using both secondary electron and back scattered electron detection techniques, while the chemical analysis depended on the EDS technique (Energy Dispersive x-ray Spectroscopy).

3.3.2.2 X-ray Fluorescence (XRF):

Four selected samples were analyzed using the X-ray Fluorescence which was performed at the Natural Resources Authority (NRA). The selected portions for the XRF analysis represent the size fraction 0.038-.250 mm from the bulk sediments samples DBS7, DBS23, DBS24 and DBS46. The logic behind selecting these particular samples will be explained in later chapters.

The preparation of the samples for this analysis was performed according to the following steps:

Samples were sieved again through 0.1 mm sieve and all passed through it.

From each of the four samples, two subsamples of 1 gm each were weighed and heated at 1000 ˚ C for 1.5 hours in, then re-weighed ,and the difference in the weight before and after heating was calculated as percentage of 1 g weight in order to find the LOI (Loss on Ignition). For all the four samples the LOI was less than 10%.

Fused pellets were prepared in crucibles by mixing 1.25 g of sample with 10 g of Lithium Tetra Borate and Lithium Bromide mixture acting as a fluxing material. Crucibles were heated at 1100-1200˚C for 25 minutes, and the content was poured in the pellets' molds and cooled.

Pressed pellets were prepared as well. However in this case 4 g of sample with 1 g of Cellulose powder was mixed, and pressed on also a Cellulose base by pressuring it with 31.5 tone of weight.

The pellets were taken for the XRF analysis performed by the S4 Pioneer WDXRF (Wave Length Dispersive X-Ray fluorescence) spectrometer (manufactured by Bruker AXS). Standard-less evaluation was done for the major elements, while for the 4 elements of most importance for this study (i.e. Zr, Hf, U & Th) a calibration preceded the analysis, such that the lowest standard at the NRA available is around 50 ppm for the Th and 125 ppm for U detection.

Results of both SEM and XRF are presented in the following chapters.

CHAPTER FOUR:
Gamma Surveying

4.1 Introduction

Atoms of an element having same atomic numbers, but different number of neutrons (i.e. different mass numbers) are known as isotopes (Faure, 1998).

Some isotopes (radioactive isotopes), contain extensive energy and are unstable, tending to disintegrate into more stable nuclei of a different isotope, emitting different radiogenic particles and energy (nuclear radiation) in the process of the nuclear decay (IAEA, 2003).

4.2 Types of decay processes

The radioactive decay is of several types. Alpha decay is where the nucleus emitting an alpha particle (He_2^4) loses two protons and two neutrons. Beta-decay happens when a beta particle (identical to negatively charged electron) is being emitted. Beta + decay involve the emission of a positron. Electron capture and Spontaneous fission are other examples of decay process. The common to most decay processes is that the nucleus undergoing the disintegration is left in an excited state. Therefore it undergoes a second decay to a lower energy state that could be the ground state, which is accompanied by high energy photons (Gamma rays), this is what's known as Gamma Decay (Jewett, 2004).

In this scope Gamma Rays can be defined as: electromagnetic waves (high energy photons) emitted by radioactive nuclei during certain nuclear reactions (Zumdahl and Zumdahl, 2003). They are the highest energy form of the electromagnetic radiation, with the shortest wave length, which gives these rays a high penetration range from 700m in air and up to 50 cm in rocks (IAEA, 2003).

The importance of gamma radiometric data in exploration geology (particularly in geochemical exploration) is that it can ease the exploration procedure and save time and money, whenever a tight correlation is found to exist between these data and the exploration target (e.g. mineral target). In this case the mineral target is said to have a radiometric signature, which consequently is excellent guide for further exploration and for the surface mineral provenance.

Three most important sources for gamma rays are potassium ^{40}K isotope, and uranium and thorium isotopes' decay series. Though other radioactive isotopes experience the gamma ray emission, the detection of the rays is poor due to insufficient energy and intensity that cannot be easily detected by different instruments (Geiger-Muller counter, scintillation counter….etc.) used for this purpose (IAEA, 2003).

4.2.1 Potassium:

Potassium under natural conditions is a monovalent lithophile element. Its abundance in the Earth's upper crust is 2.33 as weight % of K. Table 4.1 lists the most common potassium containing minerals expressed as %K (Mittlefehldt, 1999).

4.2.2 Thorium:

Thorium is one of the Actinide elements with valance 4^{+}in solution, and lower valance in solid state (Krishnaswami, 1999). Its abundance in Earth's crust ranges from 8-12 ppm in average, but could be as low the ranges of ppb (Dickson and Scott, 1997).

As shown in Table 4.2, Th is present in zircon, monazite apatite and other accessory minerals. The highest energetic gamma rays (2.62 MeV) are emitted by the daughter thallium (^{208} Tl), (Krishnaswami, 1999).

Table 4.1 Potassium bearing minerals, (after IAEA, 2003).

Potassium bearing mineral	**Chemical formula**	**%K**
Rock forming silicate minerals :		
Feldspar	$(K,Na)AlSi_3O_8$; $(Na_x,Na_{1-x})\ Al_{2-x}\ Si_{2+x}O_{8(x=0-1)}$	
Alkali-Feldspar	$(K,Na)\ Al\ Si_3O_8$	13
Microcline	$KAlSi_3O_8$	13
Orthoclase	$KAlSi_3O_8$	13
Sanidine	$KAlSi_3O_8$	13
Leucite	$KAlSi_2O_6$	17
Nepheline	$(Na,K)AlSiO_4$	23
Biotite	$K(Mg,Fe)_3(AlSi_3O_{10})(OH)_2$	8
Phologpite	$KMg_3(AlSi_3O_{10})(OH)_2$	8
Muscovite	$KAl_2(AlSi_3O_{10})(OH)_2$	8
Hornblende	$(K,Na)_{0-1}(Na,Ca)_2(Fe,Mn,Mg,Ti,Al)_5(Ai,Al)_8O_{22}(H,F)_2$	1
Other K-minerals:		
Alunite	$KAl_3(SO_4)_2(OH)_6$	
Glauconite	$(K,Ca,Na)_{<1}(Al,Fe^{3+},Fe^{2+},Mg)_2[(OH)_2/Al_{0.35}Si_{3.65}\ O_{10}]$	
Sylvite	KCl	

4.2.3 Uranium:

Average abundance of uranium in the Earth's crust is 3 ppm, it's a reactive metal with 4+ valance in igneous rocks and crystallochemical properties close to Th^{4+} and the LREE (Bea, 1999). Under supergene mobile conditions Uranium valance is 6^+ leading to the formation of many U^{6+} minerals. Table 4.3 contains most common Uranium containing mineral species.

Table 4.2 Thorium bearing minerals, (after IAEA, 2003).

Thorium bearing minerals	**Chemical formula**	**% ThO2**
Minerals with Th as major constituent:		
Huttonite	$ThSiO_4$	80
Thorite, Uranothorite	$ThSiO_4$, $(Th,U)SiO_4$	50,<50
Cheralite	$(Th,Ce,Ca)(SiO_4PO_4)$	30
Thorianite, Uranothorianite	ThO_2, $(Th,U)O_2$	80,<80
Common accessory minerals:		
Monazite	$(REE,Th)PO_4$	10
Xenotime	YPO_4	0.4-1
Zircon	$ZrSiO_4$	0.01-1
Allanite	(Ca,Al,Fe,Mg)silicate	0.1-1
Apatite	$Ca5(PO4)_3(F,Cl,,OH)$	0.001-0.1
Titanite	$CaTiSiO_5$	0.001-0.1
Epidote	$CaFe^{3+}Al_2O.OH(Si_2O_7)(Si_2O_4)$	0.005-0.05

Table 4.3 Uranium bearing minerals, (after IAEA, 2003).

Uranium bearing minerals:	**Chemical formula**	**% UO2/ppm U**
Minerals with U as major constituent:		
Uraninite (Pitchblende)	UO_2	
Betafite	$(U,Ca)(Nb,Ta,Ti)_3O_9.nH_2O$	
Huttonite	$ThSiO_4$	100-20000ppm
Uranospherite	$(BiO)(UO_2)(OH)_3$	
Thorite, Uranothorite	$ThSiO_4$, $(Th,U)SiO_4$	1-35%
Thorianite, Uranothorianite	ThO_2, $(Th,U)O_2$	5%
Common accessory rock forming minerals:		
Zircon	$ZrSiO_4$	5%
Xenotime	YPO_4	5%
Monazite	$(REE,Th)PO_4$	100-20000ppm
Allanite	(Ca,Al,Fe,Mg)silicate	10-2000ppm
Apatite	$Ca_5(PO_4)_3(F,Cl,OH)$	5-200ppm
Sphene	$CaTiSiO_5$	10-500ppm

4.2 Gamma Ray detection (instrument used)

The purpose of this study was to determine the degree of usefulness of gamma ray surveying in the exploration of heavy minerals contained within wadi deposits in the study area. The sources of gamma radiation if present were expected to be the result U or Th decay series occurring within those heavy minerals containing them.

The gamma ray detection instrument used in this study was BGS-3 scintillation counter (manufactured by SCINTREX) provided by the Natural Resources Authority (NRA). In this instrument, gamma rays are detected by a thallium activated sodium iodide crystal (1.6*1.6*1.6 inches in proportions). When the gamma rays strike the crystal, they get absorbed and converted to scintillations whose intensities are proportional to the energy absorbed. Subsequently these scintillations (light photons) are being detected by a photomultiplier tube (PMT) which is coupled with the crystal, and converts the photons to electrical pulses emitted from its cathode. The pulses are being amplified and shaped, then fed to a ratemeter which gives an analogue voltage proportional to the number of gamma rays that strike the crystal in each second. The output is displayed in counts per second (CPS) on a mounted meter. BGS-3 records all the gamma rays in excess of 0.05MeV (BGS-3 operation manual, by SINTREX).

In a flat terrain the readings represent the gamma ray activity from a circular area more or less 10-20 m in diameter, assuming detector is being hold at waist height, whereas lowering the instrument to ground level, the diameter decreases to only 2-3 m. It’s worth mentioning that many factors may influence the counts. These are: removal of the minerals containing radioactive elements by leaching, differences in the cover thicknesses from one location to

another, encounter of water-logged areas (water effectively absorbs the Gamma rays), as well as topographic variations. Positive relief features increase the count rates, while negative decrease them. Therefore all these factors should be taken into consideration during the gamma ray surveying and results interpretation for mineral exploration.

CHAPTER FIVE:
Heavy Mineral Assemblages and Gamma Ray Readings

5.1 Heavy Mineral Assemblages

Grain mounts were prepared as described previously and studied under the polarized light microscope. Prior to grain mounting individual grains were picked under the binocular light reflective microscope and subjected to spot microanalysis using scanning electron microscopy.

The main aim of this was to identify the mineral assemblages present and get some insight about the chemistry of some of the grains of interest.

5.1.1 Mineralogy:

Most abundant mineral species found in the grain mount are zircon, tourmaline and rutile, with minor amounts of anatase. Some traces of apatite, dolomite, mica, garnet, staurolite and brookite were detected. This chapter focuses on the major species which are of importance to this study.

5.1.1.1 Zircon:

Zircon is one of the most stable minerals, (Mange and Maurer, 1992). It belongs to the isolated tetrahedral silicates group, with general chemical formula $ZrSiO_4$ (Perkins, 2002). Substitutions occur frequently within the crystal structure of zircon, those including REE, H_2O, U, Th and most commonly Hf which is incorporated as solid solution between zircon $ZrSiO_4$ and hafnon $HfSiO_4$ (MacRae et al, 2003). The presence of U and Th and their radioactive daughters induces structural damage of the zircons through α-decay and fission tracks from the nuclear fission of ^{238}U (Garver and Kamp, 2002). The production of α

particles and gamma radiation while the decay and the difference in atomic size and charge between mother and daughter isotopes causes this damage in the crystal structure and the product zircons are termed metamict or malacon zircons (Klein and Dutrow, 2008; Mange and Maurer, 1992). Metamictziation is a transitional process from the crystalline to the amorphous (aperiodic) state of a mineral leading to changes in some optical properties of the mineral as well (Ewing, 1994). Inclusions of other minerals bearing U and Th within their structure are possible to be found within the zircon grains and that's counted as additional source of gamma radiation encountered from zircons.

Figures 5.1., 2 and 3 show various zircon grains taken from grain mounts of different samples. All of the zircons across the study area are colorless, euhedral, sub-rounded, oblong, and short or elongated prismatic (Fig.5.3.b and g) with rounded terminations (Fig. 5.1.d, e and f). According to Patyk-kara et al, (2008), the wide variation in the morphology of zircon grains indicates that they underwent different cycles of deposition. Grains also exhibit cracking in many situations, which could be interpreted as fission tracks left from ^{238}U gamma rays emission as mentioned. The cracking is more prominent in grains in (Fig. 5.3) derived from sample DBS 46 which recorded 10100 CPS of gamma rays in the field. Many zircon grains contain inclusions of opaque and other minerals within (Fig.5.1.b, c and e and Fig.5.2.a.

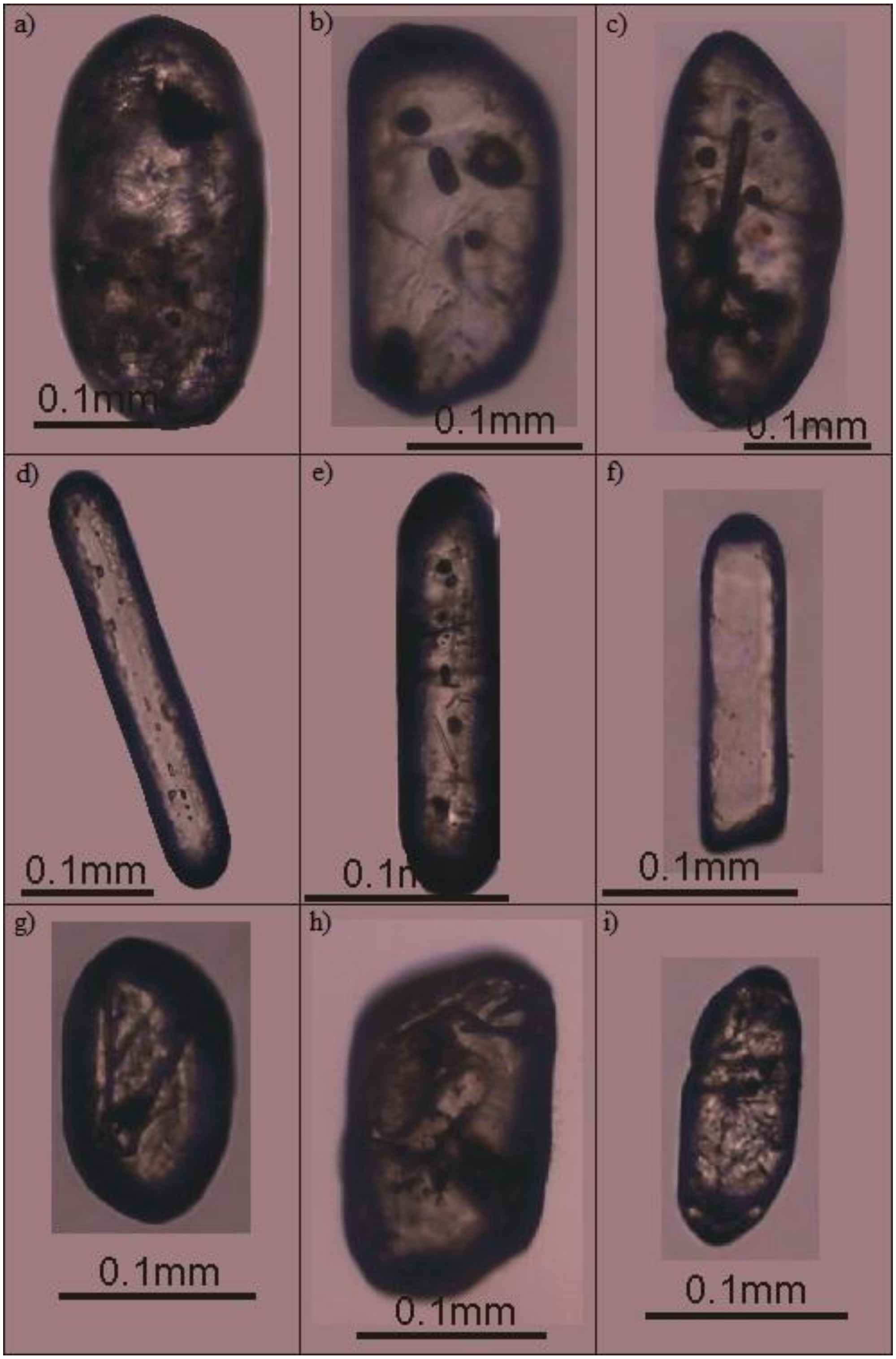


Figure 5.1 Photomicrographs (taken under plane polarized light) of some zircon grained from samples in the study area. a) sub-rounded zircon grain. b) and c) inclusion within zircon. d), e) and f) elongated zircon grains with rounded terminations. g), h) and i) sub-rounded grains with dull appearance.

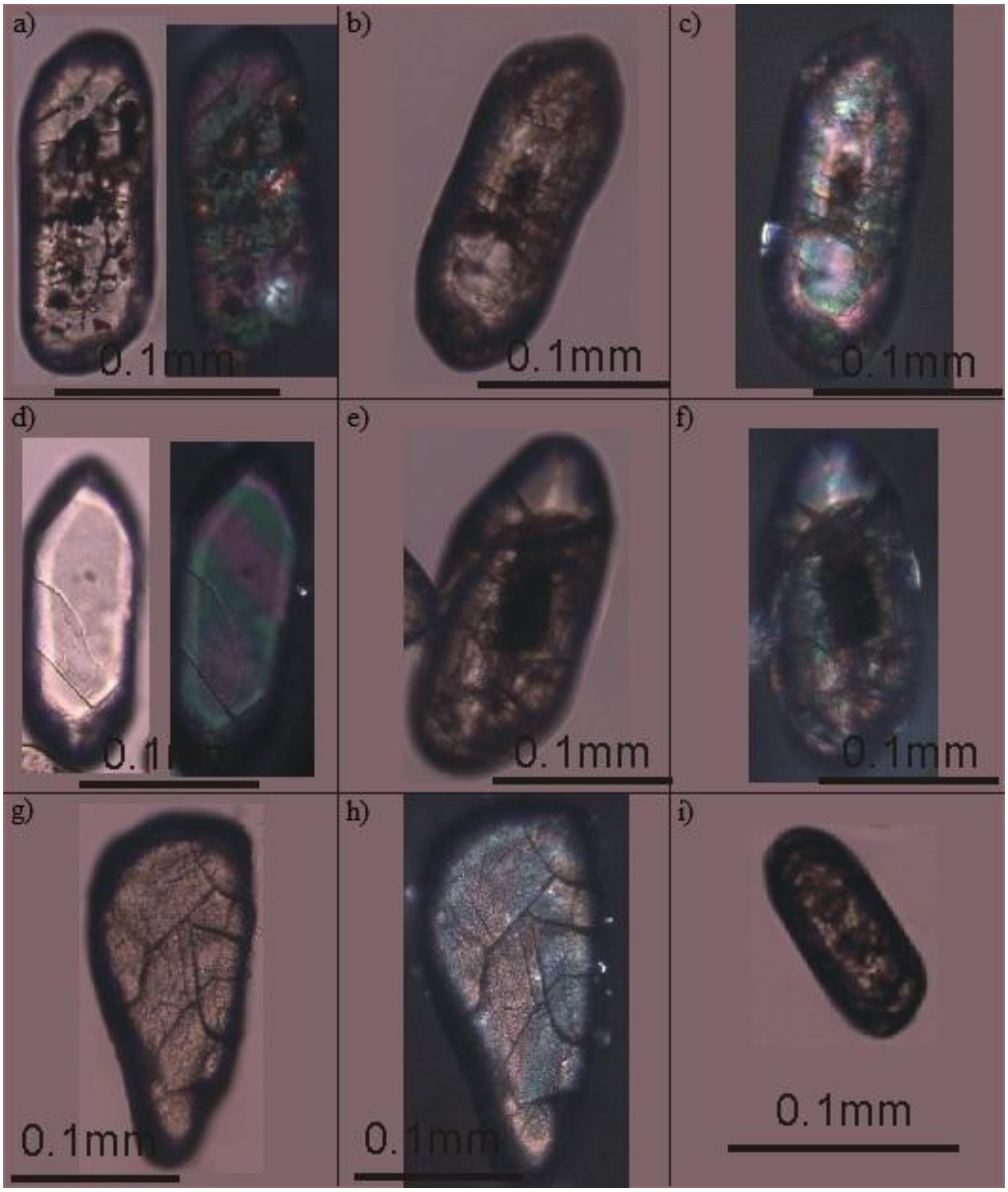


Figure 5.2 Photomicrographs (taken under plane and crossed polarized light) of some zircon grained from samples in the study area.

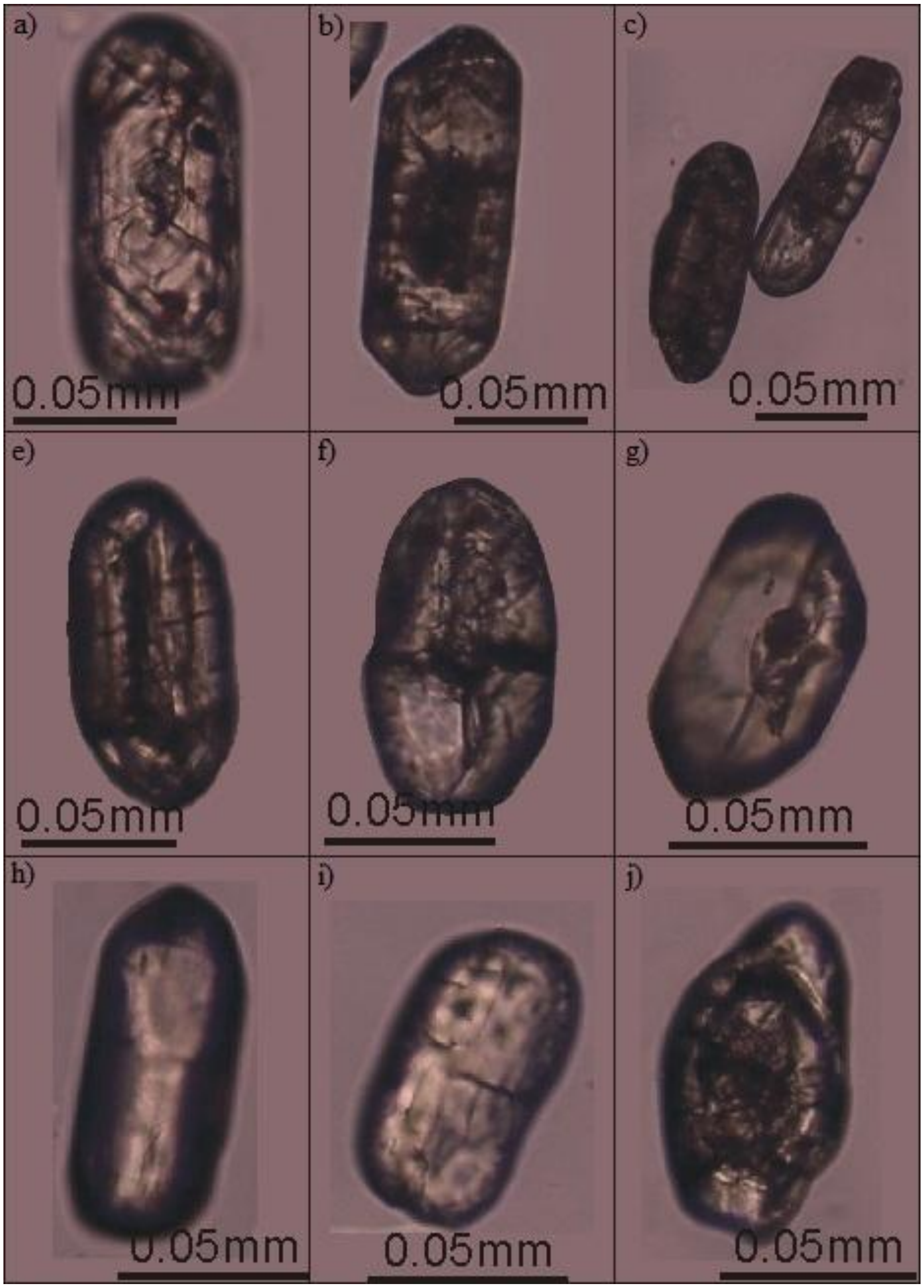


Figure 5.3 Photomicrographs (taken under plane polarized light) of some zircon grained from samples in the study area. Zircon grains derived from sample DBS 46 with prominent cracking and dullness in appearance.

The scanning electron microscopic (SEM) images of selected representative zircon grains, taken using the secondary electron detector (ETD) are shown in Fig.5.4.a and b.

Energy dispersive spectrometric (EDS) analysis of these zircon grains is shown in Table 5.1. As obvious those particular grains contain within range amount of Hf, other than that they represent typical zircons. Figure 5.5.a and b shows the EDS plots for grains zircon 2 and 3, respectively, where clear peak of Hf is evident in Fig.5.5.a.

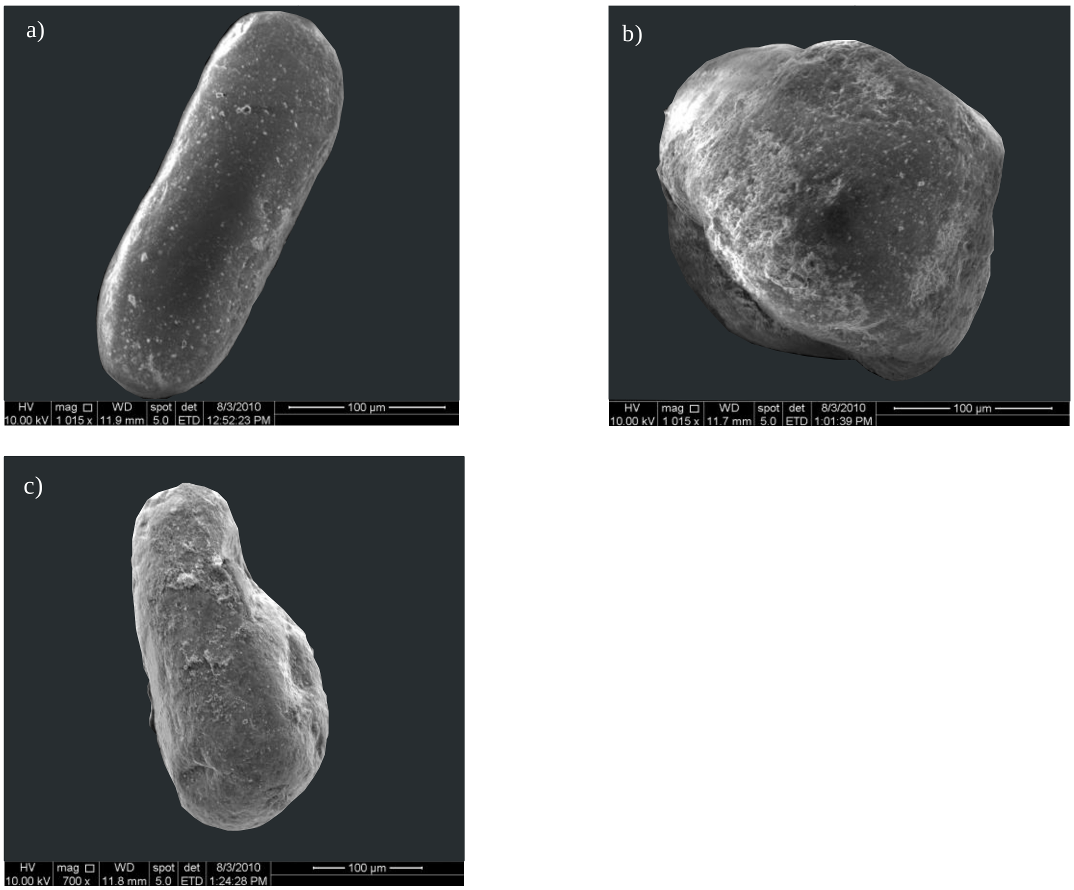
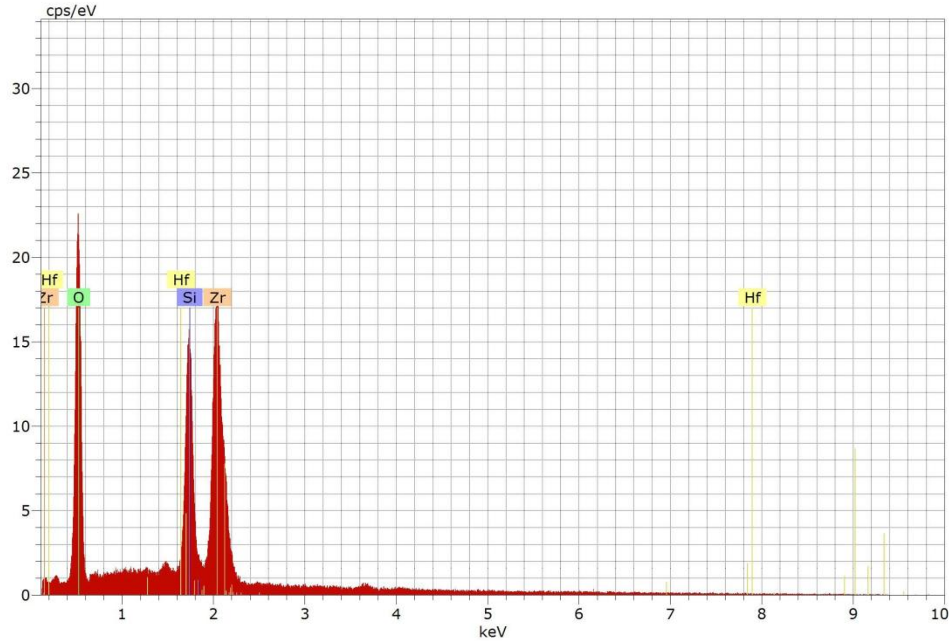


Figure 5.4 SEM secondary electron images of: a, b) zircon and c) rutile from the heavy mineral fraction.

a)



b)

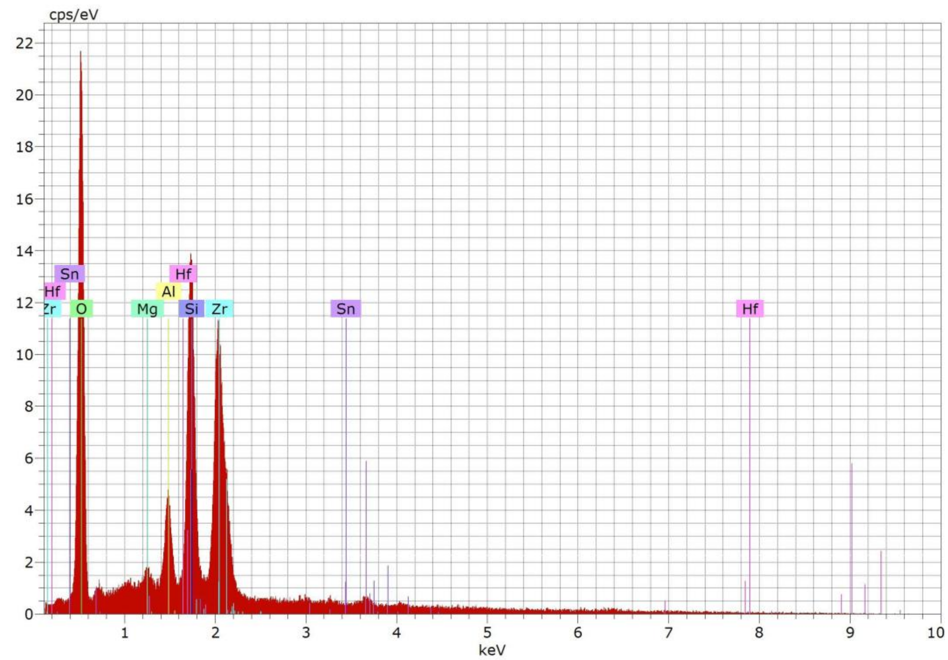


Figure 5.5 SEM EDS plots showing: a) Typical zircon chemistry with Hf = 3.45%, b) Zircon with Hf = 1.23%.

c)

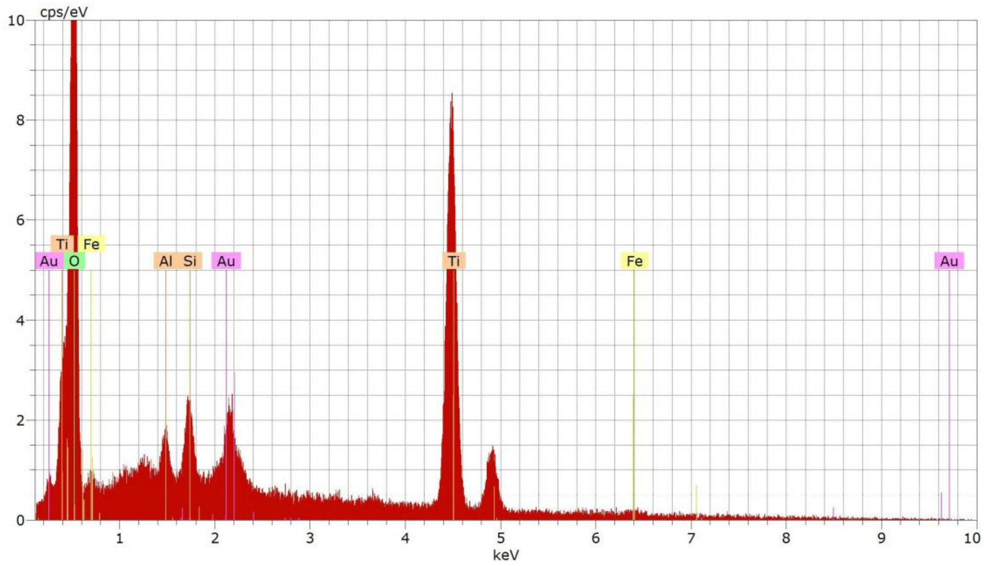


Figure 5.5(continued)….. SEM EDS plots showing: c) a rutile grain form the heavy mineral fraction.

Table 5.1 EDS microanalysis of zircons and rutiles.

Mineral:	**Zircon1**	**Zircon2**	**Zircon3**	**Rutile1**	**Rutile2**	**Rutile3**
Wt%						
O	19.08	30.27	37.67	40.89	33.75	31.12
Mg			0.41		0.96	
Al	0.32		3.28	0.92	1.73	0.46
Si	19.69	16.04	17.24	1.73	4.36	1.62
Zr	57.59	50.23	36.86			
Hf	3.32	3.45	1.23			
Fe					4.85	4.77
Ti				56.47	54.35	55.72
Sn			3.3			
Au						6.31
Total	100	99.99	99.99	100.01	100	100

It should be noted from Table 5.1 that the EDS results are not absolutely accurate quantitatively, which is obvious from the elemental normalized weight (mass) percentages for elements within the same grain. Considering one mole of $ZrSiO_4$ (molar weight =

183.31 g) the mass percentage of Zr, Si and O within the zircon respectively should be 49.76%, 15.32% and 34.91% (Perkins, 2002), which is not completely compatible with the values shown in the previous Table 5.1. The same is found for the rutile grains, and therefore the given results could be treated as qualitative and give inference about the chemical constituents rather than their accurate concentrations.

5.1.1.2 Tourmaline:

Tourmaline is a member of the cyclosilicates, with general chemical formula $(Na,Ca)(Mg,Fe,Mn,Li,Al)_3Al_6[Si_6O_{18}](BO_3)_3(OH,F)_4$ and has three compositional varieties ; dravite, schorl and elbaite which are magnesium rich, iron rich and lithium rich respectively (Mange and Maurer, 1992).

Figures 5.6 and 5.7 shows the varieties of tourmaline grains found in different samples from the study area. Most grains are brown in color indicating richness with respect to magnesium (Perkins, 2002). Shapes vary from irregular to sub-rounded (Fig. 5.6.f), short and elongated (Fig 5.6.d) with sub-rounded terminations. Many tourmaline grains contain other mineral inclusions (Fig.5.6.a, b and e).

5.1.1.3 Rutile and Anatase:

Rutile (TiO_2) is an octahedral oxide, where the TiO_6 octahedra share edges to form chains, which in turn are connected from corners of these octahedra (Perkins, 2002). Ti^4 might be substituted by variety of cations, some of which are U^{6+}, Zr^{4+}, Sn^{4+}, Hf^{4+}, U^{4+}, Fe^{3+}, Fe^{2+} and lesser Mg^{2+}, Zn^{2+} and Mn^{2+} (Meinhold, 2010). Anatase is a polymorph of rutile forming at low temperatures if in igneous or metamorphic rocks (Mange and Maurer,

1992). Therefore it could be detrital in origin in the sedimentary rocks. However authigenic anatase may form in the sediments from unstable Ti-bearing minerals.

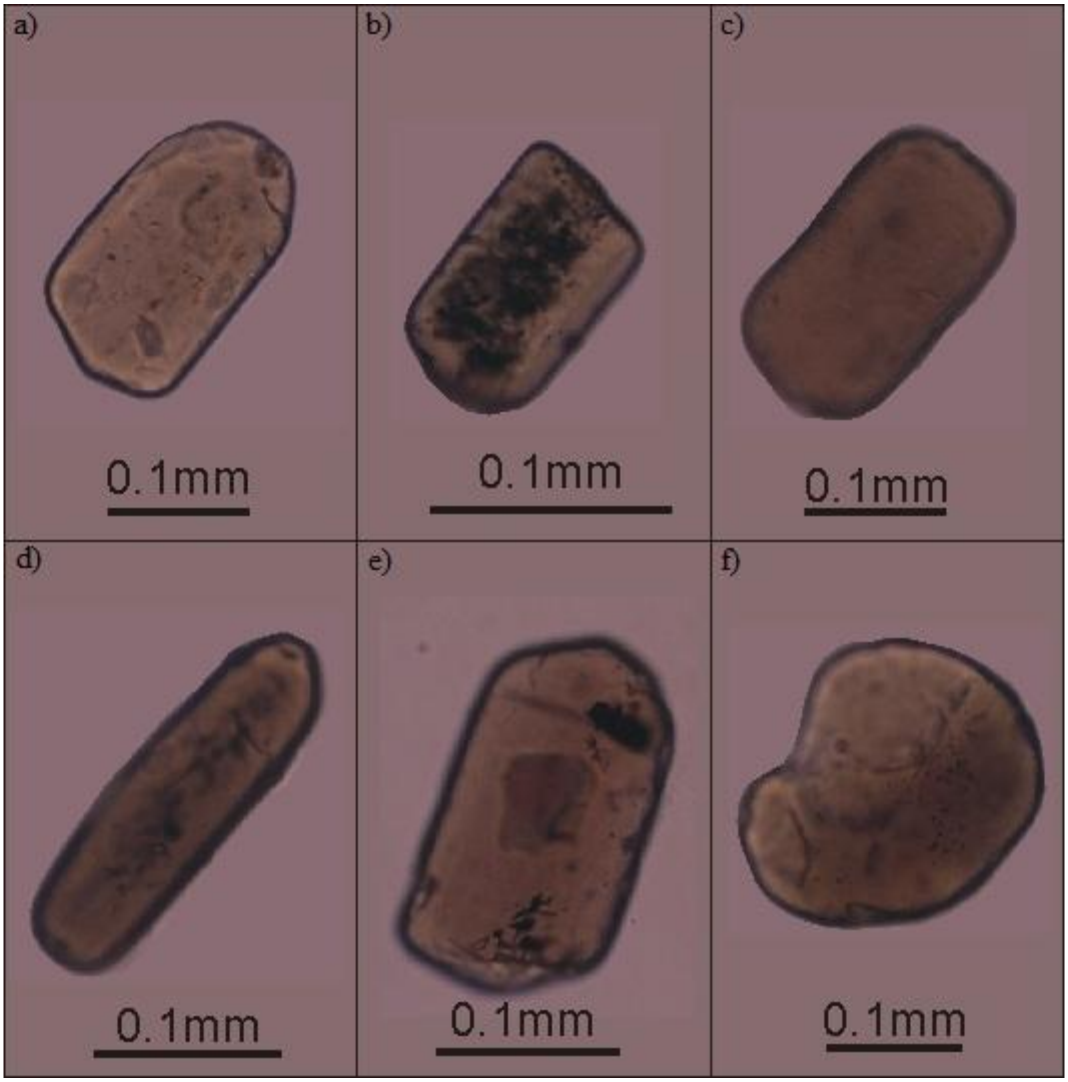


Figure 5.6 Photomicrographs (taken under plane polarized light) of some tourmaline grained from random samples in the study area. a), b), c) tourmaline equant grains with round terminations. d) elongated tourmaline grain with rounded terminations. e) tourmaline with sub-rounded termination and inclusions. f) subrounded tourmaline grain.

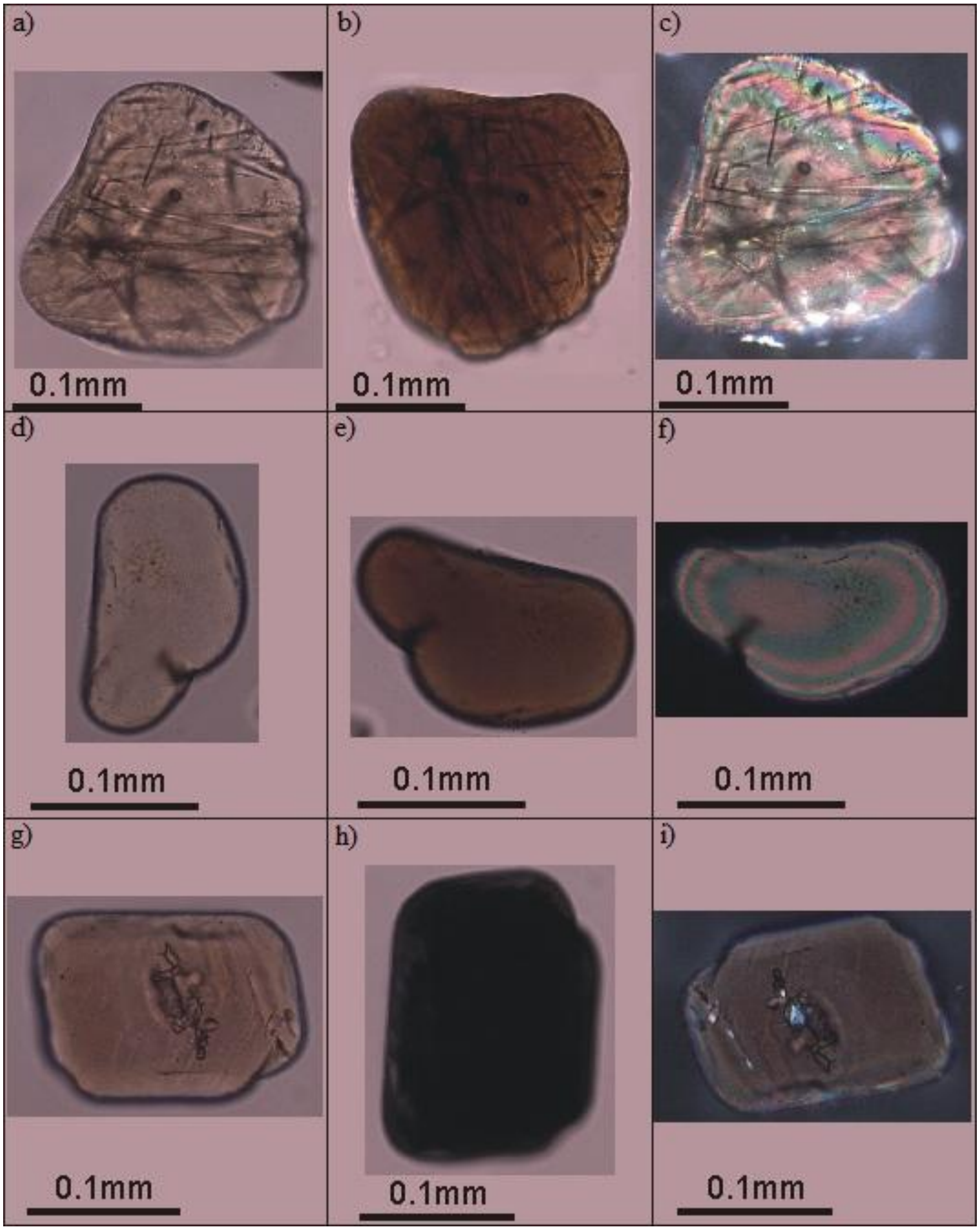


Figure 5.7 Photomicrographs (taken under plane and crossed polarized light) of some tourmaline grained from samples in the study area. a) tourmaline grain exhibiting surface striations (ppl). b) maximum absorption displayed in the previous tourmaline grain (ppl). c) interference colors in tourmaline under crossed polarized light for same grain in a and b. d) and e) sub-rounded tourmaline grain displaying minimum and maximum absorption (ppl) respectively and f) crossed polarized view for the same previous grain. g), h) sub-rounded tourmaline grain displaying minimum and maximum absorption, respectively, containing inclusions (ppl) and i) crossed polarized view for the previous grain.

In the samples present, both rutile and anatase were encountered. Rutile grains varied in color from deep red to yellow, while shapes were rounded, sub-rounded and elongated with rounded terminations, as shown in Fig. 5.8. Anatase grains found are mostly authigenic, with either tabular shape or as small aggregates, indicating Ti-rich pore solutions.

Spot analysis of randomly picked rutile grains submitted to EDS analysis, are shown also in Table 5.1 and (Fig.5.4.c and Fig.5.5.c).

Variability of the heavy minerals in this study was assessed both using traditional statistical methods (descriptive statistics) and followed by more important geostatisticsal analysis used to examine the spatial variability of those minerals in the study area.

5.2 Descriptive statistics

This section shows the quantitative results of the study. The included variables are gamma-ray readings as counts per second (CPS), total heavy minerals weight percentage from bulk sediments sample (THM), transparent heavy minerals volume percentage from total heavy minerals calculated after grain counting (HM), volume percentages of the individual heavy mineral species from the total heavy minerals (i.e. zircon, tourmaline, rutile, anatase……etc) also derived from relative abundances in the grain mounts after counting.

For each variable, the type of frequency distribution was analyzed using skewness and kurtosis as main tools for evaluation. Where transformation of original data to logarithms was performed, the geometric mean and geometric standard deviation were calculated instead of the arithmetic (Limpert et al, 2001), and accordingly the threshold value for each

variable was estimated using the following selected equation for 95% confidence (Bhattacharyya and Johnson, 1977):

T ($_{95}$%) =antilog (geometric mean + (2* geometric STD))

Anomalous samples for each variable were identified, depending on this threshold value. Each variable's minimum and maximum value was recorded as well. Summary of these descriptive statistics is provided in Table 5.2.

Table 5.2 Summary statistics for the variables studied.

Variable:	**CPS**	**THM%**	**Zrn/THM %**	**Tur/THM%**	**Rt/ THM%**	**HM/ THM%**
Type of distribution:	Log-Normal	Log-Normal	Log-Normal	Log-Normal	Log-Normal	Log-Normal
N:	40	40	40	39	39	40
Skewness:	2.72	0.62	-0.17	-0.3	-0.41	-0.31
Kurtosis:	7.45	4.3	-0.59	0.03	-1.05	-0.84
Geometric mean:	286.0882	0.2388	12.0504	4.1908	4.1486	23.3346
Geometric STD:	2.333	3.0967	2.3496	2.0212	2.3583	1.9907
Actual min. value:	150	0.0087	2.218	0	0	5.854
Actual max. value:	10100	15.628	79.051	15.92	16.915	87.154
Threshold value:	1557.0408	2.2898	66.5273	17.1199	23.0728	92.4698
Anomalous samples:	24/46	46	46	None	None	None

Pearson's product correlation coefficient (r) was used as a measure indicating the degree of linear relationship between different variables (Bhattacharyya and Johnson, 1977). Only the significant relationships will be mentioned in the text.

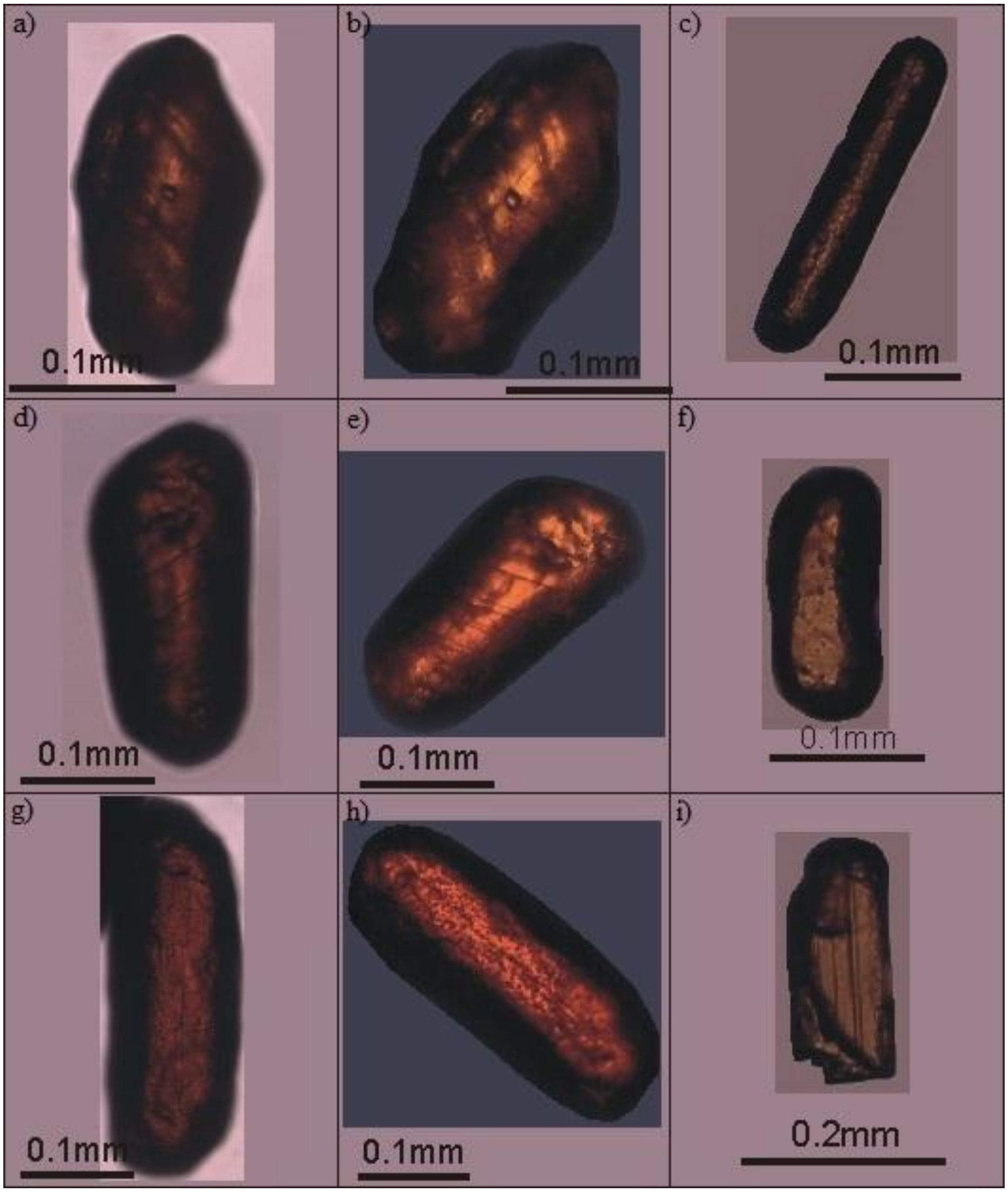


Figure 5.8 Photomicrographs (taken under plane and cross polarized light) of some rutile grained from random samples in the study area.

5.2.1 Gamma-ray readings:

As mentioned previously gamma radiation was detected in the field, using Scintillation counter (BGS-3), such that a gamma radiation reading was taken at each sampling location. The output of results was as counts per second (CPS) and recorded as shown in appendix B.

Original CPS values showed high positive skewness and kurtosis of 5.29 and 27.95 respectively, therefore the data were transformed to log CPS (Fig 5.9.a), however with further skewness and kurtosis of 2.72 and 7.45 respectively. At this point the mean for the 40 samples was calculated and found to equal 286.0882 while the standard deviation was 2.333. The minimum and maximum CPS values were 150 and 10100, respectively. The threshold value was estimated at 95% confidence to equal 1557.0408 CPS , therefore the anomalous samples with respect to CPS were DBS24 (CPS=3100) and DBS46 (CPS =10100). The summary statistics for the gamma-ray readings are show in Table 5.2. Visual inspection of the original CPS frequency distribution in Fig 5.9.a indicated that two other samples are contributing to the high skewness seen and these were DBS7 (CPS=1450) and DBS39 (CPS=1267). Omitting all the 4 original anomalous samples and transformation to log CPS, this time reduced the skewness down to 0.52 and kurtosis to -0.32. However all the original samples were used in the geostatistical analysis as shown later.

5.2.2Total heavy minerals (THM):

The total heavy mineral content was weighed and measured relatively to the bulk weight of the whole sediment sample. The THM% values for each of the 40 samples are given in appendix B.

THM% values as well, show log-normal distribution (Fig 5.9.b), such that the skewness and kurtosis for the transformed values are reduced to 0.62 and 4.3 respectively after the transformation to Log THM%. The minimum THM% values equaled 0.0087 and maximum was 15.628 THM%. The mean of the THM% values was 0.2388 with standard deviation of 3.0967. From those two values and at confidence of 95% the threshold value for the THM% was estimated to be 2.2898 THM % by weight, which excluded sample DBS46 from the THM% data considering it anomalous. The summary statistics for THM % are also shown in Table 5.2. Inspection of the frequency distribution of the THM% values showed that another value DBS37 can be considered anomalously low.

5.2.3 Transparent heavy minerals (HM):

Transparent heavy mineral species were counted separately and their abundance was calculated in respect to THM as volume percentage. Results are listed in appendix C.

The (HM/THM%) values are log-normally distributed (Fig 5.9.c), such that after transformation skewness and kurtosis values equal -0.31 and -0.84, respectively. (HM/THM%) varies from 5.854 to 87.154. The values are centered on the mean of 23.3346 and have standard deviation of 1.9907. Calculated threshold value, again at 95% confidence is 92.4698, and it can be clearly seen that there are no anomalous values for (HM/THM%). Summarized statistical description for HM is given in Table 5.2.

5.2.4 Zircon:

Zircon content in the wadi deposits was calculated from the grain mounts as volume percentage from the total heavy mineral fraction (Zrn/THM%, abbreviated according to

Kretz, 1983). The values of (Zrn/THM%) are given in appendix D. As the previous variables, (Zrn/THM %) also experiences log-normal distribution (Fig 5.9.d).

The distribution after transformation is negatively skewed with value of -0.17, while kurtosis equals -0.59. Minimum and maximum values for Zrn% in THM are 2.218 (DBS29) and 79.051(DBS46). The mean equals 12.0504 while the standard deviation is 2.3496. One sample only, that is DBS46, its content exceeds the threshold value of 66.5273 Zrn/THM%. All these values are summarized in Table 5.2 as well.

5.2.5 Tourmaline:

Tourmaline abundance is also recorded as volume percentage from the total heavy mineral content (Tur/THM%, abbreviated according to Kretz, 1983). For each sampling location the (Tur/THM%) value is given in appendix E.

Tourmaline shows, no differently, a log-normal distribution (Fig. 5.9.e), with skewness and kurtosis of its distribution being -0.3 and 0.03, respectively. Of 40 samples, one gave zero Tur% and wasn't included in any of the calculations and semi-variogram drawing. From the rest 39 samples, minimum (Tur/THM%) value is 0.783 and maximum 15.92. Samples' mean equals 4.1908 and standard deviation is 2.0212. Threshold value equals 17.1199 and clearly there are no anomalous samples encountered.

5.2.6 Rutile:

Rutile abundance is calculated as volume percentage relatively to the total heavy mineral content, and values of (Rt/THM%, abbreviated according to Kretz, 1983) are given in appendix F.

Rutile distribution is log-normal as shown in Fig 5.9.f, with skewness and kurtosis of the log transformed values being -0.41 and -1.05 respectively. One sample shows (Rt/THM%) value near zero and was not included in any calculations or inferences. Rest of 39 samples range in (Rt/THM%) values from 0.659 to 16.915. Mean value of the (Rt/THM%) is 4.1486 with values standard deviation of 2.3583. From the mean and standard deviation, the threshold value was estimated to be 23.0728 and therefore no anomalous samples exist in respect to Rutile content in THM.

5.2.7 Others:

Other non opaque (transparent) heavy mineral species were encountered in the grain mounts during counting, but only in relatively small amounts. Anatase accounts for higher percentage for these species, followed by apatite, dolomite, micas, garnet and staurolite with almost negligible amounts of brookite as shown in appendix G.

At this point, it’s perhaps worthwhile to mention that many samples contained saussurite grains. Saussurite is an assamblege of the minerals epidote, clinozoisite and zoisite and which is formed by the alteration of plagioclase (Mangue and Maurer, 1992). However, since it doesn’t have economic value, it wasn’t given much attention in this section.

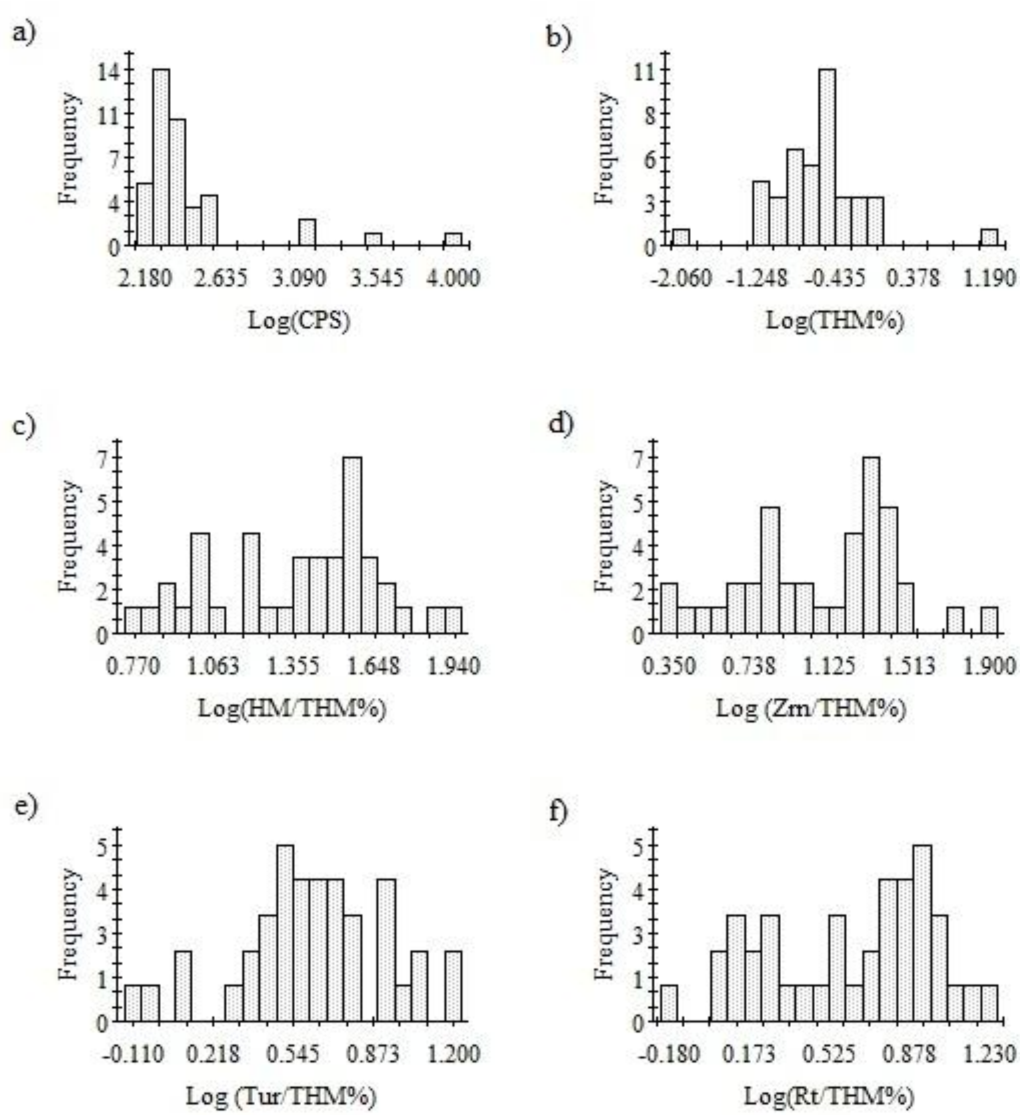


Figure 5.9 Frequency distribution of the variables studied. a) Gamma radiation. b) Total heavy mineral content. c) Transparent heavy mineral content in THM. d) Zircon% content in THM. e) Tourmaline% content in THM. f) Rutile% content in THM.

5.2.8 Inter-variables Relationships:

As mentioned previously variables were examined for their mutual linear relations. Table 5.3 shows the values of linear correlation coefficients calculated between selected variables

of interest. Main purpose of this test is to verify the relationship between the content of the heavy minerals THM% and the gamma radiation detected at different locations in the study area, which proved to be significant at 2f and 95% confidence, with a value of r = 0.962341. Generally the closer the value of r is to -1 or 1, the stronger is the linear relationship between the variables x and y (THM and CPS in this case) according to (Bhattacharyya and Johnson, 1977).

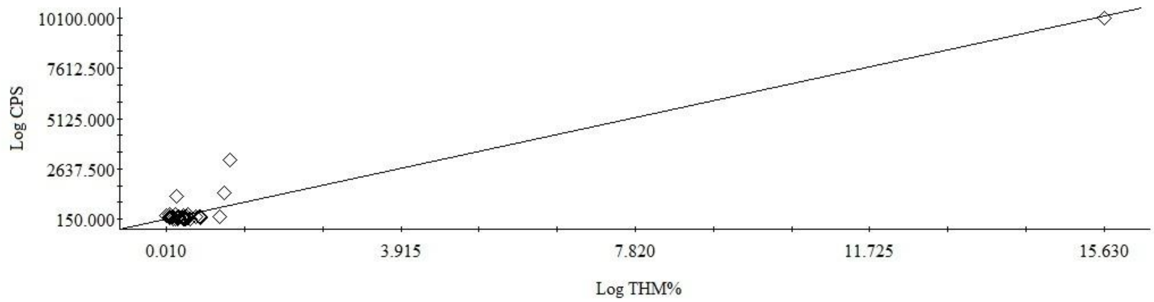
Another significant relationship was determined between the zircon content in the total heavy minerals and the gamma radiation, with r value equaling 0.674995. Though not definite, this relationship could be justified if the source of the gamma-rays is the radioactive elements Th, U or Hf present in the crystal lattices of the zircon grains or in other minerals included within zircon (MacRae et al 2003; Suror et al 2003). The r value of 0.604253 between the zircon and rutile content in the THM indicates that those two minerals are highly related, such relationship exists between tourmaline and rutile as well, while zircon and tourmaline are not showing significant correlation value. This finding is important in economic terms, such that high abundances of zircon would be expected to be accompanied by high rutile contents as well.

Table 5.3 Pearson's linear correlation coefficient values between different pairs of variables. (i.v. = irrelevant value).

Variable	**CPS**	**THM%**	**HM%**	**Zrn%**	**Tur%**	**Rt%**
CPS	1	0.962341	0.52862	0.674995	i.v.	i.v.
THM%		1	i.v.	i.v.	i.v.	i.v.
HM%			1	i.v.	i.v.	i.v.
Zrn%				1	-0.10344	0.604253
Tur%					1	0.369035
Rt%						1

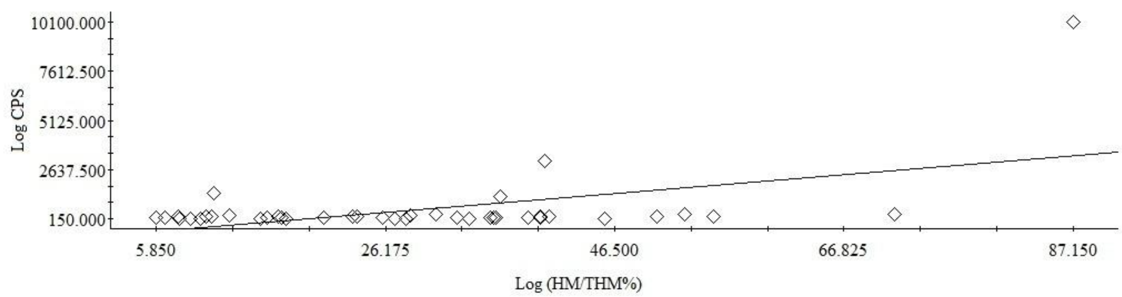
All the previous significant relationships are graphically represented in Fig. 5.10.

a)



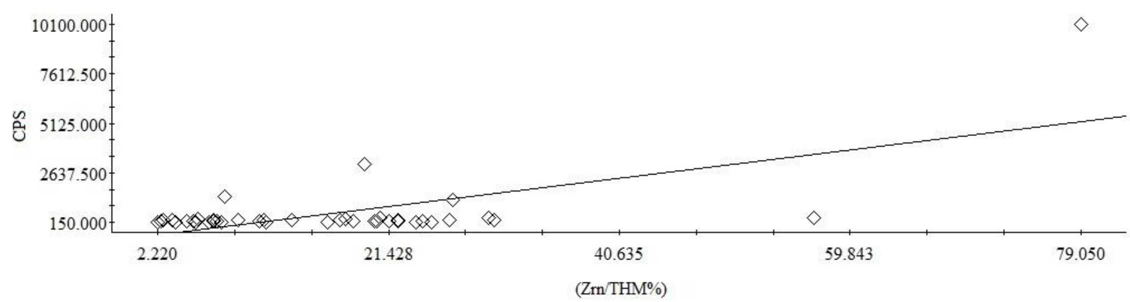
Regression coefficient = 641.2 (SE = 29.4, r2 =0.926, y intercept = 168.0110 , n=40)

b)



Regression coefficient = 47.1 (SE = 12.3, r2 =0.279, y intercept = -750.9266 , n =40)

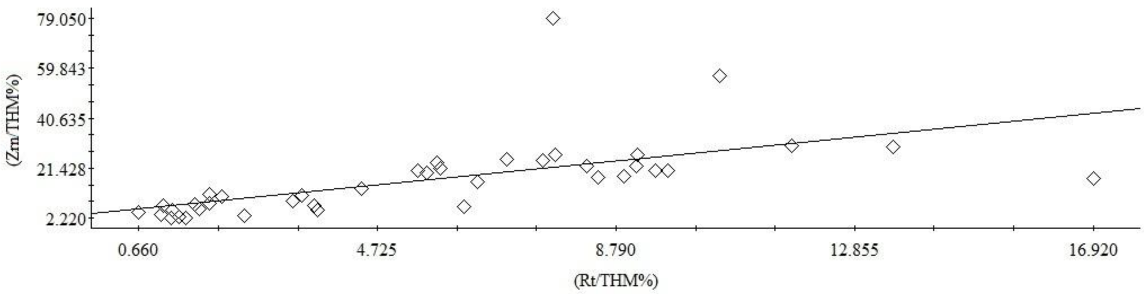
c)



Regression coefficient = 73.9 (SE = 13.1, r2 =0.456, y intercept = -634.7136 , n =40)

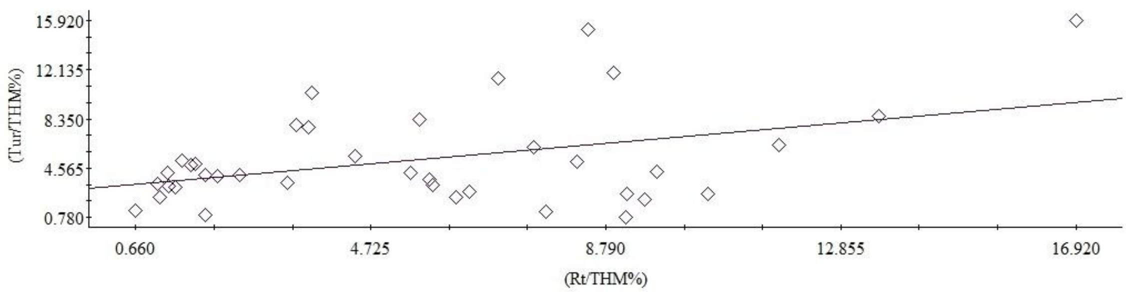
Figure 5.10 Pearson's correlation coefficient plots for: a) Gamma radiation (CPS) Vs Total heavy mineral content (THM%). b) Gamma radiation (CPS) Vs transparent heavy mineral content in THM (HM/THM%). c) Gamma radiation (CPS) Vs zircon content in THM (Zrn/THM%).

d)



Regression coefficient = 2.27 (SE = 0.50, r2 =0.359, y intercept = 4.3087 , n =39)

e)



Regression coefficient = 0.39 (SE = 0.14, r2 =0.173, y intercept = 3.0915, n =38)

Figure 5.10 (continued)…..Pearson's correlation coefficient plots for: d) zircon (Zrn/THM%) Vs rutile content in THM (Rt/THM%). e) tourmaline (Tur/THM%) Vs rutile content in THM (Rt/THM%).

CHAPTER SIX:
Geostatistical Analysis

6.1 Introduction

This chapter is concerned with the main aim of this work that is studying the spatial variability of the heavy minerals and the individual species found in the study area as well as prevailing radioactivity using Kriging technique and accordingly whether the applied techniques would lead to the already known heavy mineral mineralization in the study area.

Kriging is a geostatistical technique used for best local estimation of unknown values of a certain localized variable at an unobserved locations within a given ore deposit or any field, based on the Theory of Regionalized Variables (Clark, 1979) which simply infers to variable's distribution in space in a purely descriptive meaning (Journel and Huijbregts, 1978). The application of this technique in exploration for mineral deposits in arid regions, as occurs in the study area, was checked for by Saffarini and Lahawani (1991) and proved to be useful. Though most of its application is related to ores as mentioned, widespread attempts have been made to test its usefulness in estimating all different kinds of variables from different fields of environmental sciences, hydrology, geochemistry, climatology geography and many others, and the results were positive and highly encouraging. On the other hand, many fields still haven't been approached by this technique and its benefits have not yet been unveiled to different scientific spectra. One of those spectra is the here discussed heavy minerals distribution in arid desert areas, which not only is important for economic studies but also has applications in paleoclimate, paleogeography and provenance studies.

6.1.1 Structural Analysis:

In essence, the kriging technique is an optimal regression technique depending in its successful application on the structure of the spatial distribution of the variable under consideration.

The spatial variation of a variable is best expressed through a model semi-variogram, that is a graph (and/or a mathematical formula) describing the expected difference in value between pairs of samples within a certain direction (Clark, 1979). Assuming that the given data set is stationary (i.e. belongs to same probability distribution), the structure of spatial variability is dependent only on the distance between two values in a certain direction (Jalali, 2007). The experimental semi-variogram is derived from the following equation:

$\boldsymbol{\gamma(h) = 1/2N(h) * (\sum[Z(i)-Z(i+h)]^2)}$ where;

$\gamma(h)$: semivariance for interval distance class h,

Z(i): measured sample value at point i,

Z(i+h): measured sample value at point (i+h) and

N(h): total number of sample couples for the lag interval (h).

The value $2\gamma(h)$ is the variance of the differences between samples (Z) that are (h) distance apart and (n) is the number of sample pairs at that distance. In application after the semi-variogram is drawn for a given variable, a mathematical model is chosen to best fit the semi-variogram and the model's parameters (a: the range of influence) and (C: the sill of

the semi-variogram) are further employed for derivation of kriging weights used in the estimation process later on.

6.1.2 Mathematical models used for semi-variogram fitting:

Of the most common models used for the purpose of fitting experimental semi-variograms are:

1. Spherical (Matheronian) model:

This is a model characterized by the two parameters (a) which is known as the range of influence and is the distance at which samples become independent and the semi-variogram becomes more or less constant and the parameter (C) which is also known as the sill of the semi-variogram and is the $\gamma(h)$ value at which the graph levels off and interestingly it equals the samples variance (Clark, 1979). The spherical model (Fig 6.1.a) is expressed by the following equation:

$$\gamma(h) = C * [(3/2* h/a) - (1/2 * h^3/a^3)] \quad \text{where } h<a$$

$$\gamma(h) = C \quad \text{where } h>= a$$

One case of spherical model should be further noted, that is when the range of influence is approaching zero, and the observed semi-variogram is completely flat. In such case the samples are said to exhibit a “pure nugget effect”, and the following equation is used to describe the semi-variogram (Journel and Huijbregts, 1978):

$\gamma(0) = 0$ and

$\gamma(h) = C_0$, where C_0 is the nugget effect.

2. Exponential model:

Is also a model (Fig 6.1.b) characterized by the parameters (a) and (C), such that:

$\gamma(h) = C\ [1\text{-}\exp(-h/a)]$

3. Gaussian model:

A model shown in Figure 6.1.c and is characterized by (a) and (C) according to the following equation:

$\gamma(h) = C\ 1\text{-}\exp[\ (-h^2/a^2)]$

4. Linear model:

This model speaks for itself; it's a linear model with no sill or range of influence (Fig 6.1.d) and is defined as:

$\gamma(h) = ph$ where; p is the slope of the line and h is the lag distance.

6.1.3 Kriging:

After the best fit model has been selected for the experimental semi-variogram, the kriging process continues with weighing the input data based on the chosen model, such that the sum of weights is adjusted to equal one and the estimation error is as lower possible. This way the operator obtains the Best Linear Unbiased Estimator (BLUE) of the mean along with the kriging variance. For detailed procedure of kriging one may refer to (Clark, 1979) where the author explicatively showed the steps of acquiring the BLUE and the estimation variance through set of linear equations. The final output from applying the kriging steps is spatial variability map for the variable of concern accompanied by a spatial variability map

for the estimation error (kriging standard deviation) committed when using a certain model and its parameters for estimation purposes.

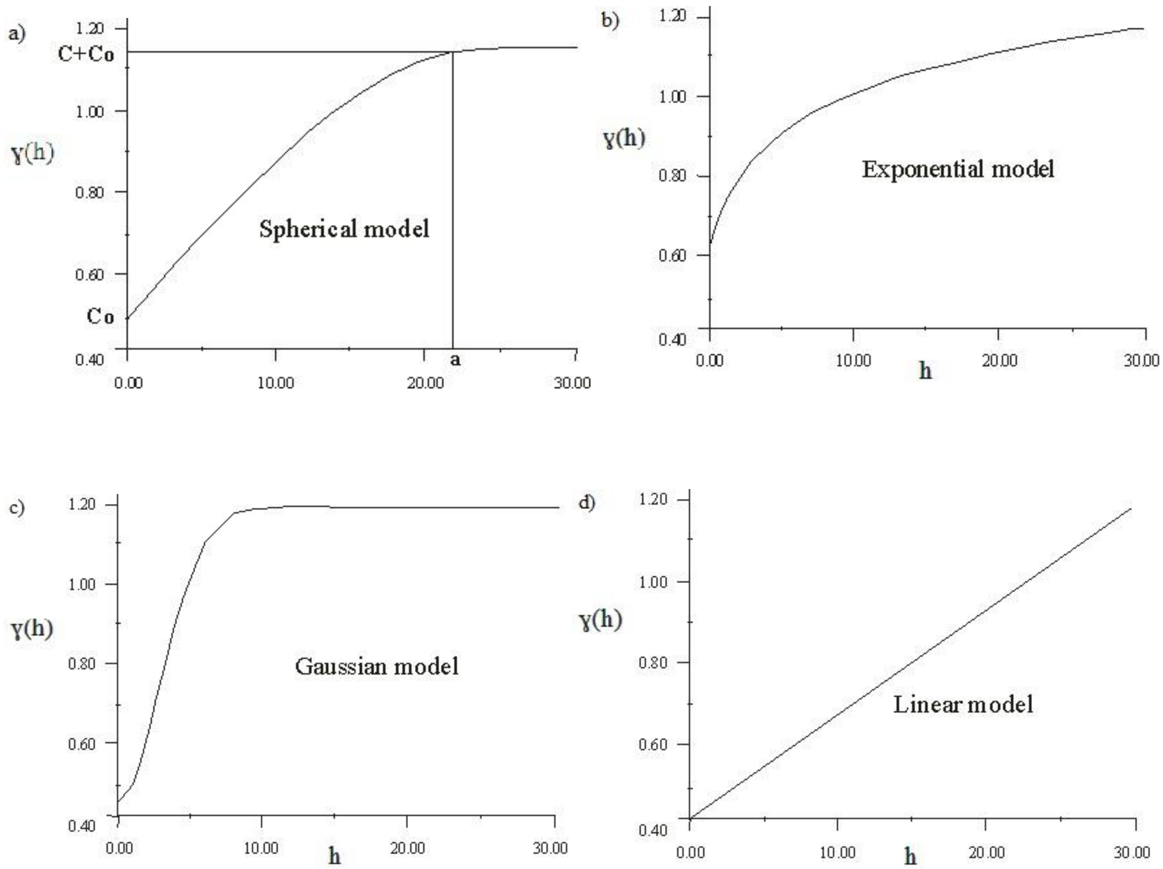


Figure 6.1 Ideal shapes for most common semi-variograms (best fit models). a) Spherical model, showing the range of influence (a), nugget effect (C_o) and the Sill component (C). b) Exponential model. c) Gaussian model. d) Linear model (after Chen and Jiao, 2001).

Semi-variance analysis and kriging was performed using GS+ software (a product of Gamma Design Software 2001) in this study all the way through.

Spatial variability analysis was carried on the same variables from the previous section; CPS, THM, HM%, Zrn%, Tur% and Rt % after transforming the values to their logarithmic form. The semi-variograms were drawn with 22.50^{o} offset tolerance, and then best fit isotropic models were chosen based on a combination of parameters (i.e. residual sum of

squares (RSS), r^2, regression coefficient (RC) and reliability maps). The Residual sum of squares provides an exact measure of how well the selected model fits the semi-variogram, such that the lower the reduced sum of squares, the better is the model fit. The r^2 provides an indication of how fit that same model is, but is not as accurate as the RSS. The final choice however was made upon the regression coefficient (RC), which is a measure of goodness of fit for the least squares models describing the linear regression equation (i.e. the equation showing the linear relationship between the actual measured values and estimated values using the kriged weights depending on the selected best fit model's parameters same observations). As the RC values approaches 1.00 the better the fit is and the model is assumed as the best fit model. Also, careful examination of the reliability map helped in deducing the best model, since areas in the map where the standard error (kriging standard error) is larger than the original samples standard deviation are considered unreliable in respect of their estimated values.

Another important parameter is $C/(C_0+C)$, which according to many authors is an indicator of spatial dependence of the variable (Cambardella et al, 1994; Musoli et al, 2008). This proportion may range from zero when pure nugget effect at selected range (distance), to one in case of high spatial dependence (Musoli et al, 2008).

Geostatistical information is presented in Table 6.1, followed by a detailed discussion for each variable.

6.2 Gamma-ray readings (CPS)

The logarithms of gamma-ray readings recorded as counts/second (CPS), showed a rather random erratic spatial variability described by the nugget effect (Fig 6.2.a) whose

parameter C_o= C = 0.13131. With the proportion C/ (C_o+C) having the value of zero. Therefore for the purpose of constructing a reliable spatial variability map, Inverse distance weighting (IDW) method was applied to the given 40 readings. In IDW the values at unknown locations are estimated given the following equation:

$Zestj = \sum [Zi/(hi+s)^p]/\sum 1/(hi+s)^p]$ Where;

Zestj: estimated value Z at location j,

Zi: measured sample value at location I,

hi: distance between Zestj and Zi,

s: smoothing factor and

p: weighting power (usually ranges between 1-5) .

Table 6.1 Parameters characterizing the best fit semi-variogram model chosen using log transformed data.

Variable	**log CPS**	**log THM%**	**log HM%**	**log Zrn%**	**log Tur%**	**log Rt%**
Best fit model	Nugget Effect	Nugget Effect	Exponential	Spherical	Nugget Effect	Exponential
RSS			1.725E-03	2.271E-03		3.86E-03
r^2			0.652	0.028		0.759
C_o			0.05	0.065		0.0474
Sill	0.13131	0.23599	0.105	0.14	0.09380	0.1978
Range parameter (A_o)			750	350		1166
Effective range (A)			2250	350		3498
C/(C_o+C)	0	0	0.524	0.536	0	0.760
RC	-0.807	-0.858	0.732	0.734	-1.729	0.773
r^2	0.017	0.028	0.119	0.044	0.077	0.185
SE	0.365	0.484	0.281	0.363	0.294	0.336

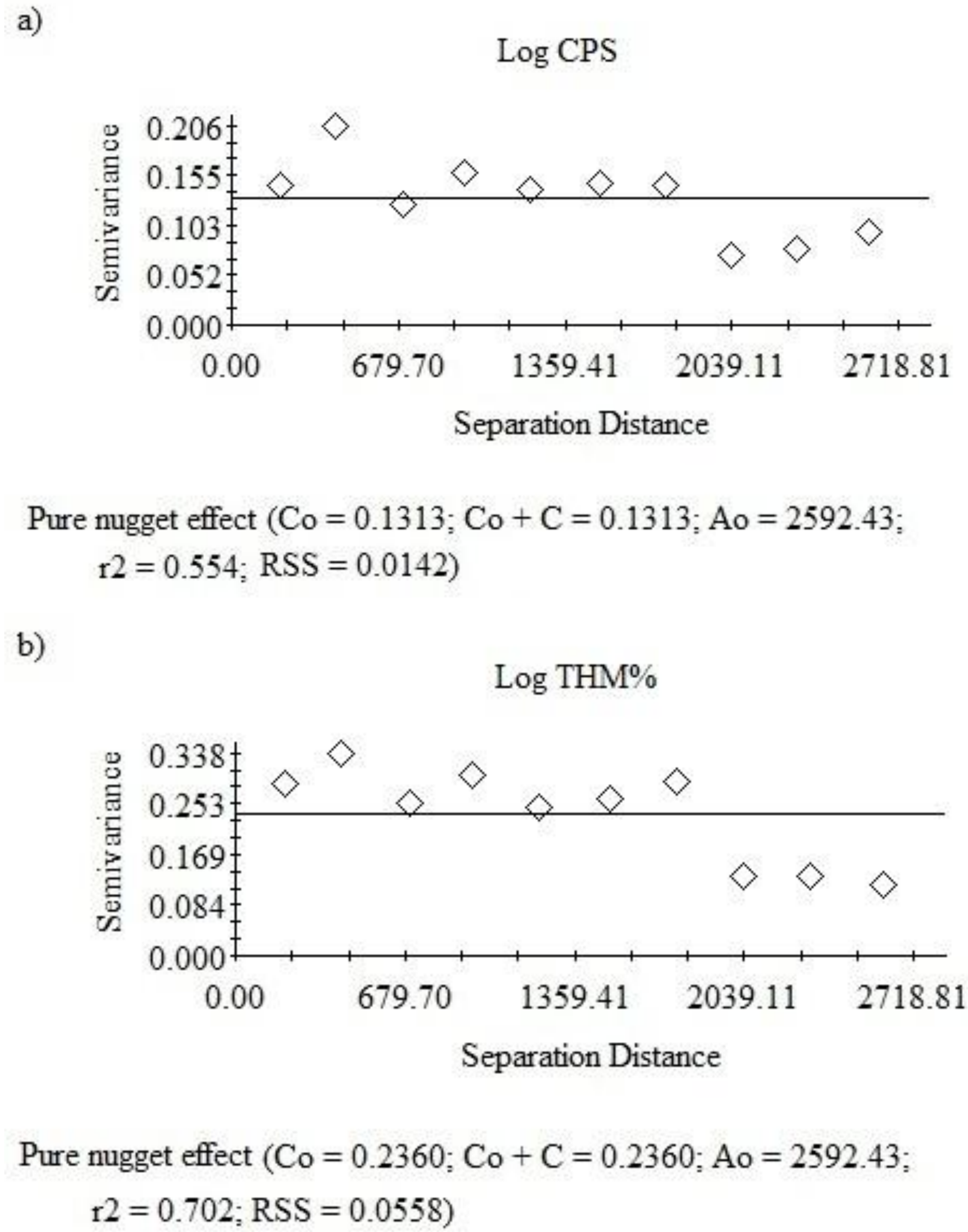
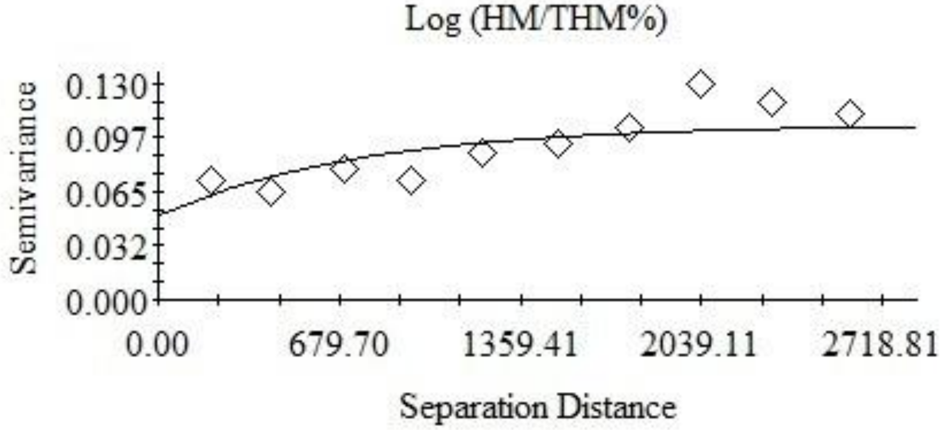


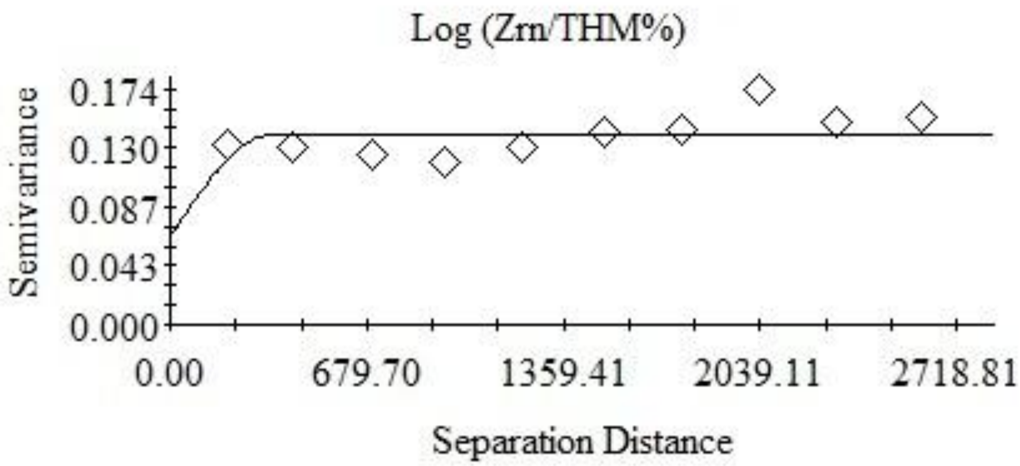
Figure 6.2 Fitted experimental semi-variograms for: a) Gamma radiation as Log CPS (pure nugget effect). b) Total heavy minerals as Log THM% (pure nugget effect).

c)



Exponential model (Co = 0.0500; Co + C = 0.1050; Ao = 750.00; r2 = 0.652; RSS = 1.725E-03)

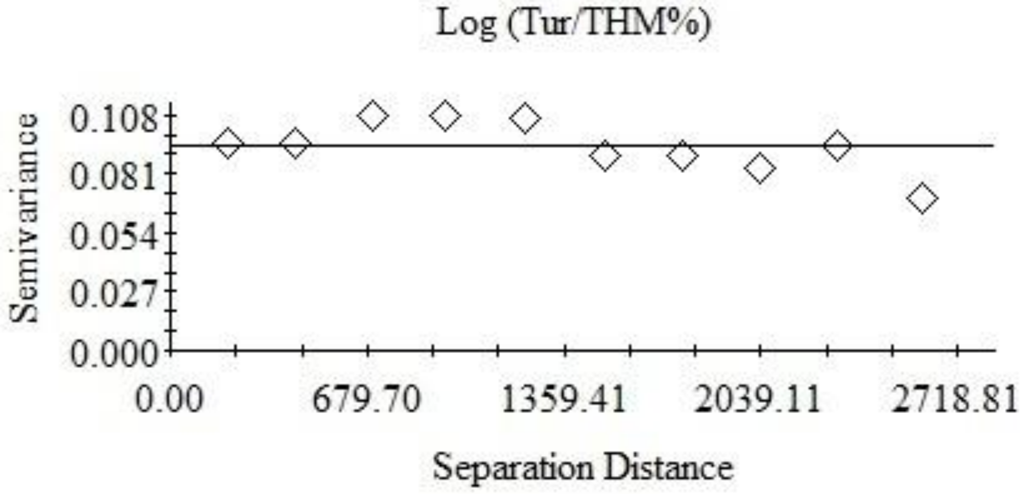
d)



Spherical model (Co = 0.0650; Co + C = 0.1400; Ao = 350.00; r2 = 0.028; RSS = 2.271E-03)

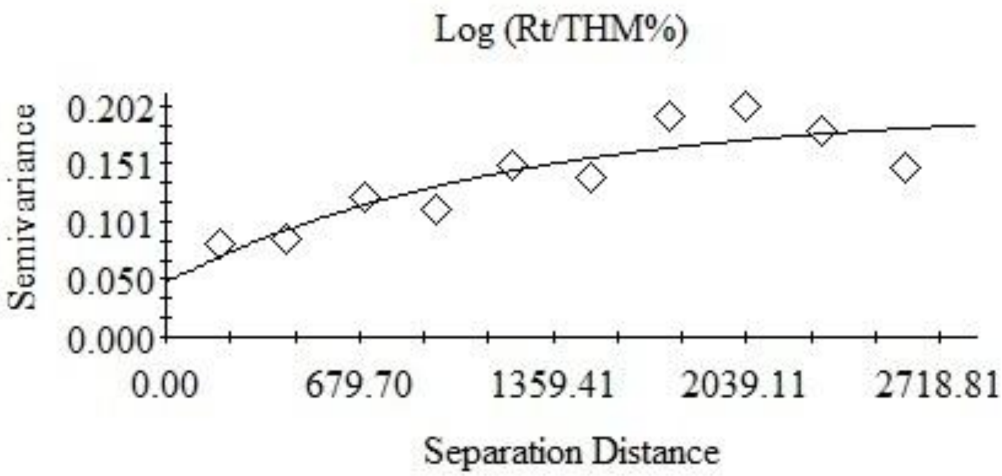
Figure.6.2 (continued)..... Fitted experimental semi-variograms for: c) Transparent heavy minerals as Log (HM/THM%), (exponential model). d) Spherical for Log (Zrn/THM%), (spherical model).

e)



Pure nugget effect (Co = 0.0938; Co + C = 0.0938; Ao = 2592.43;
r2 = 0.468; RSS = 1.288E-03)

f)



Exponential model (Co = 0.0474; Co + C = 0.1978; Ao = 1166.00;
r2 = 0.759 ; RSS = 3.860E-03)

Figure.6.2 (continued)….. Fitted experimental semi-variograms for: e) Log (Tur/THM%), (pure nugget effect). f) Rutile as Log (Rt/THM%), (exponential model).

The map deduced from the IDW for Log CPS, is shown in Fig 6.3. The map shows that most of the study area contains only background radiation values with slight increase from NE to SW direction. It can be also seen that the four anomalous samples are aligned in the NW-SE direction.

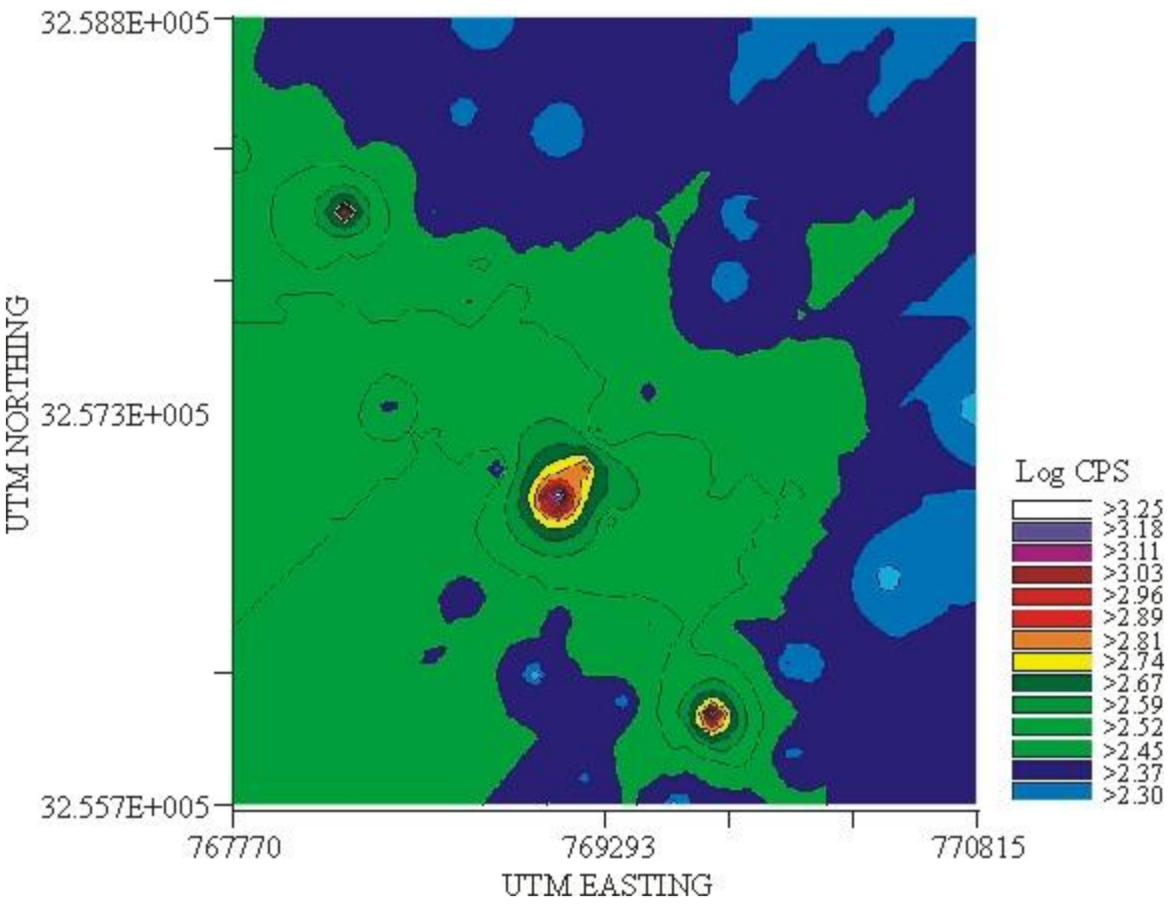


Figure 6.3 Spatial variability map for the gamma radiation (Log CPS), according to the IDW method.

Several trials were made to find a best fit model other than the linear for the experimental semi-variogram for the Log CPS values, but with no success. Only in one case when number of neighborhood was increased to 40 a spherical model with parameters in

Table 6.2 was accepted on the bases of high RC, r^2 and Z SD (kriging standard deviation) map. The increase of neighborhood samples is an approach taken by geostatisticians in cases where variables exhibit pure nugget effect as explained by Heriawan (2006).

Table 6.2 Parameters characterizing best fit models adopted to produce best spatial variability maps.

Variable	**Best fit model**	**RSS**	**r^2**	**C_o**	**Sill**	**A_o**	**A**	**$C/(C_o+C)$**	**RC**	**r^2**	**SE**
log CPS	Spherical	0.0167	0.013	0.0439	0.14	450	450	0.686	1.12	0.103	0.348
log THM%	Spherical	0.0857	0.142	0.0911	0.265	700	700	0.656	0.103	0.001	0.491
log THM% (38 samples)	Exponential	1.162 E-03	0.508	0.09	0.135	1500	4500	0.333	0.871	0.103	0.313

Looking at the RSS and r^2 values for the Spherical model (Fig. 6.4.a), 0.0167 and 0.013, suggests that the selected model isn't a good fit for the semi-variogram, on the other hand the high RC value of 1.12, and the r^2 value of 0.103 (which implies significant correlation at 2f and 95% confidence), indicates that the produced map could have areas of high reliability.

Spatial variability maps for both the estimated values (Z) and kriging standard deviation (SD) are shown in (Fig 6.5.a and b). Again the same spots of high radiation are clearly peaking in the Z values map as in map produced by IDW with rest of the area exhibiting only background CPS values.

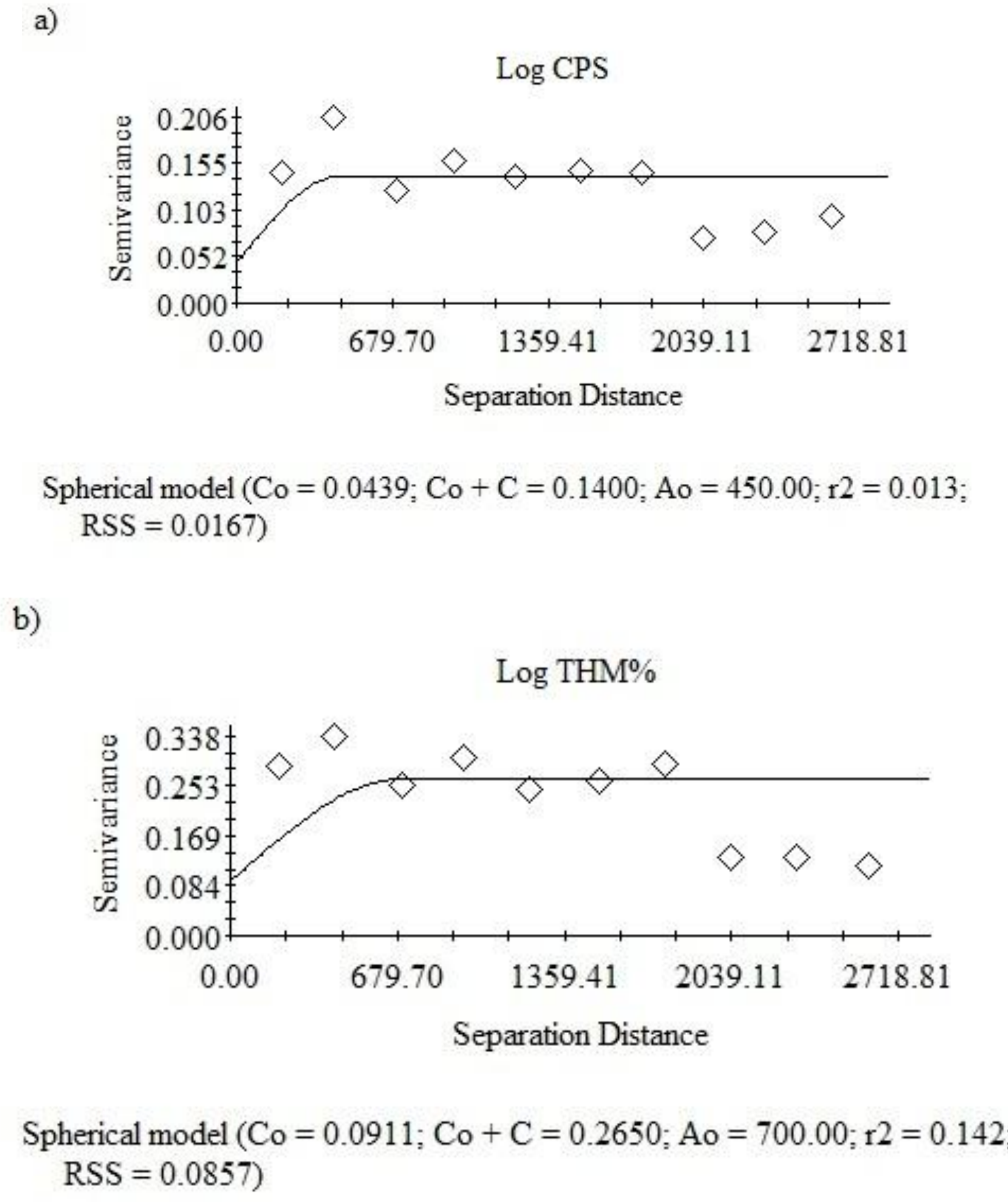
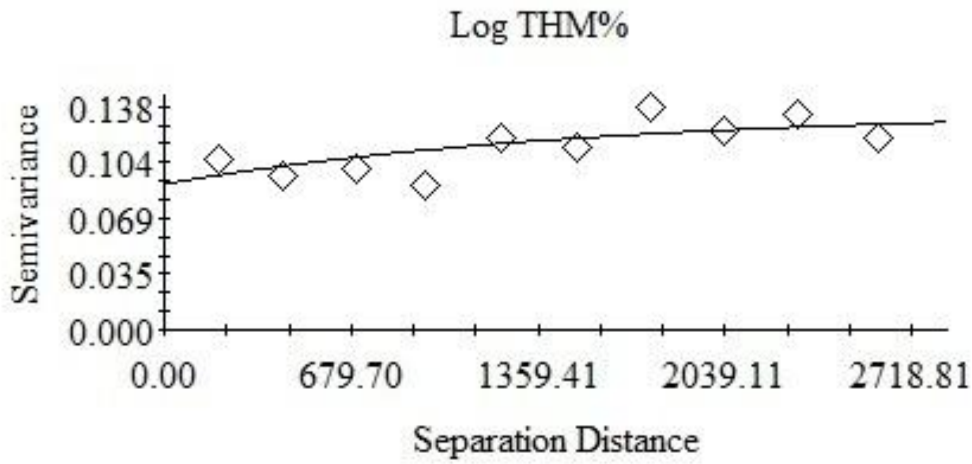


Figure 6.4 Fitted experimental semi-variograms after modifications on the original data and number of neighborhood samples. a) Spherical model for gamma radiation (Log CPS). b) Spherical model for total heavy minerals (Log THM%).

c)



Exponential model (Co = 0.0900; Co + C = 0.1350; Ao = 1500.00; r2 = 0.508; RSS = 1.162E-03)

Figure 6.4 (continued)…..Fitted experimental semi-variograms after modifications on the original data and number of neighborhood samples. c) Exponential model for total heavy minerals (LogTHM%) after omission of anomalous values.

6.3 Total heavy minerals (THM)

Log THM% values also exhibit an erratic distribution at first sight, described by the linear model (Fig 6.2.b) where the C_o= C= 0.23599 and C/ (C_o+C) = zero. Therefore the IDW approach was used here again for the estimation purposes. The RC and r^2 values are -0.858 and 0.028 respectively, and are quite low, however the spatial variability map was produced (Fig 6.6). Based on this map it’s obvious that the Log THM% is lowest in the middle of the study area, increasing in the SE and NW directions similar to the CPS.

Same attempt as in the case of Log CPS was done here, to find a good fitting model for the Log THM% experimental semi-variogram other than the linear.

The model selected was Spherical (Fig 6.4.b) with parameters shown in Table 6.2. Unlike with Log CPS previously suggested model with high RC value, in the case of Log THM% the best fit achieved in terms of RC was 0.103, which is very low, even though in this case the number of neighborhood samples was increased to 40 here as well. The Z and Z SD map are shown in Fig 6.7.a and b, as it can be seen the locations of anomalous samples are same as in the IDW map, other than that the map is not much detailed.

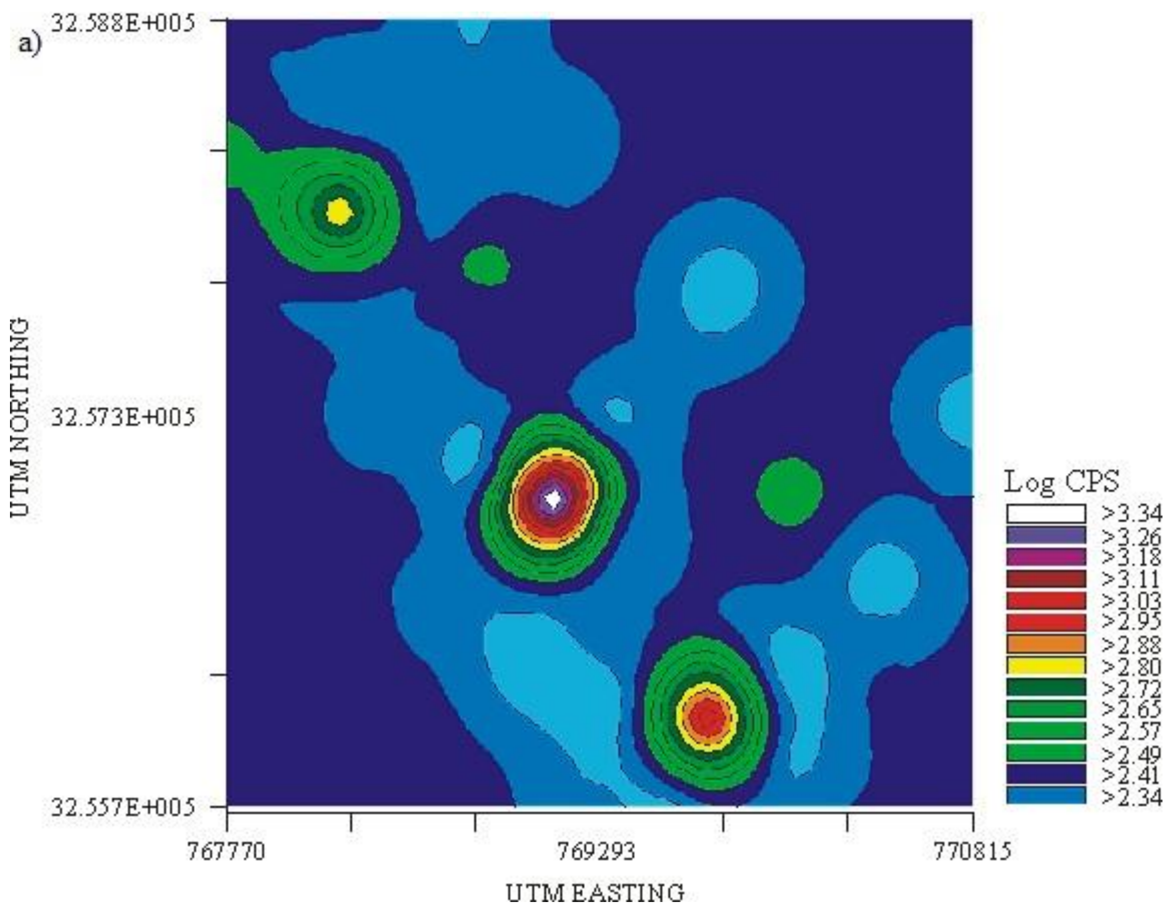


Figure 6.5 Spatial variability maps for Log CPS according to the Spherical model. a) Log CPS values map.

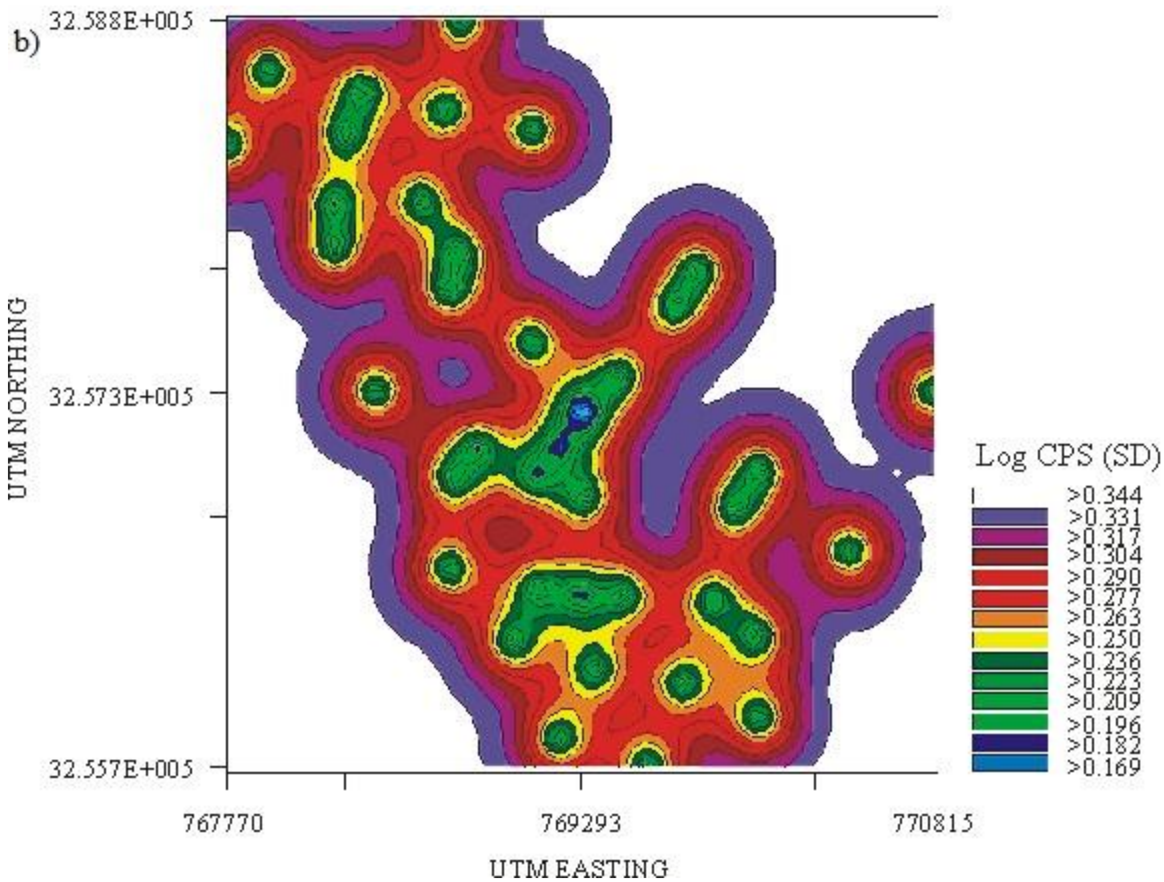


Figure 6.5 (continued)…. Spatial variability maps for Log CPS according to Spherical model. b) Kriging standard deviation map.

Here another issue should be brought up and much attention should be brought upon. According to Jalali (2007) in order to enhance the kriging variance and result in more accurate prediction it is possible to omit the most anomalous values from the data set given. This approach was experimented here and the two samples DBS37 and DBS46 were omitted from the THM% data set. The distribution remained log-normal and the new SD equals 0.3306 (this is important for the reliability map). The experimental semi-variogram for the Log-transformed data was calculated and drawn again using the 38 samples, and

satisfyingly an Exponential model fit the semi-variogram (Fig 6.4.c) with RSS = 1.162 E-03 and $r^2 = 0.508$. The RC value increased up to 0.87 with significant r value (Table 6.2).

Significant reduction of the Sill from 0.265 to 0.135 can be noticed after the omission of the two anomalies. This is important change since the sill was found to equal the original samples variance (Clark, 1979).

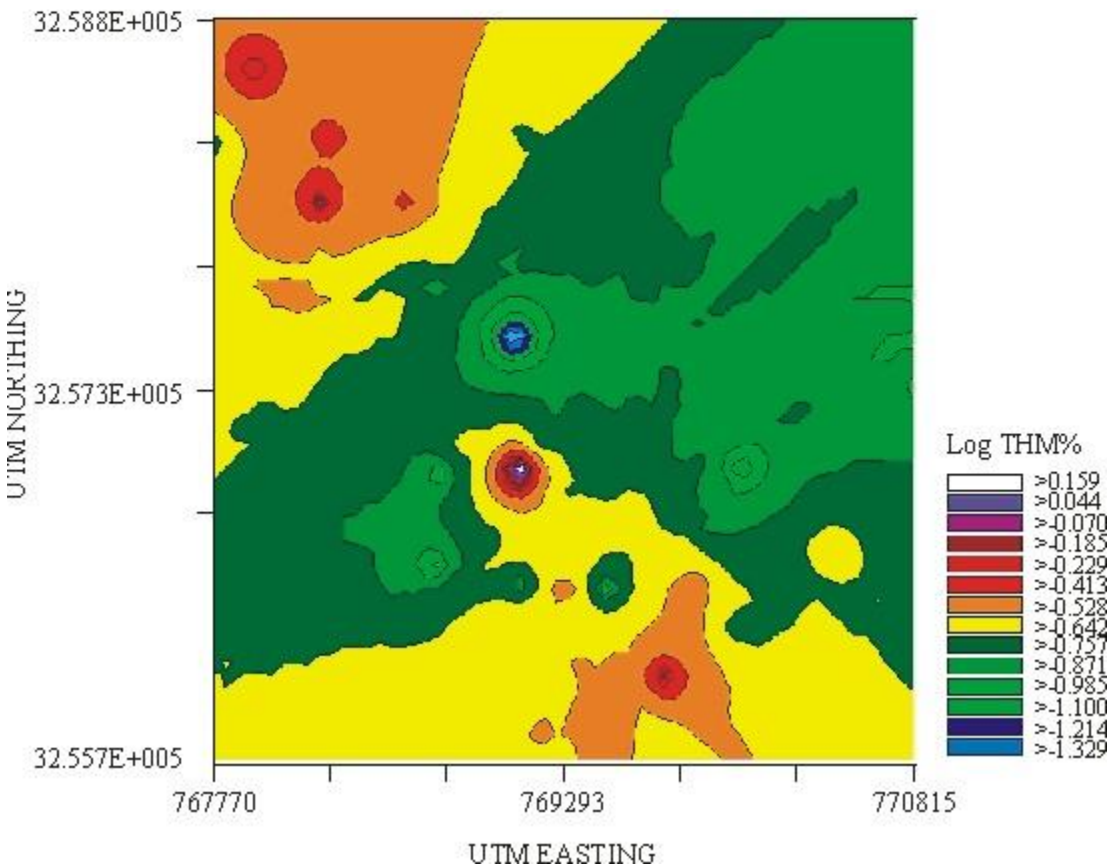


Figure 6.6 Spatial variability maps for Log THM % according to the IDW method.

The spatial variability maps for Z and Z SD are shown in Fig 6.8.a and b. The general trend of the Z variability is better interpolated even visually according to this map, with notice that omission lead to better estimation in the whole area and the spatial variation is more clearly observed. This map is to a certain extent close to the one produced using the IDW

method with same remarks regarding the spatial distribution of the total heavy minerals content in the study area. What should be noticed here is the striking similarity between the spatial variability of radioactivity in the area from both Figure 6.3 and 6.5.a and the spatial variability of Log THM% values in Figure 6.6 and 6.7.a. Another striking feature in these maps is that the Log CPS distribution and total heavy minerals dispersion train points to the opposite direction of the mineralized zone and along the NW-SE diagonal of the study area. This could be attributed to accumulation effect in a low elevated area (al-Muzayribat graben) with the passage of time or due to the accumulation as a result of dispersion from different directions.

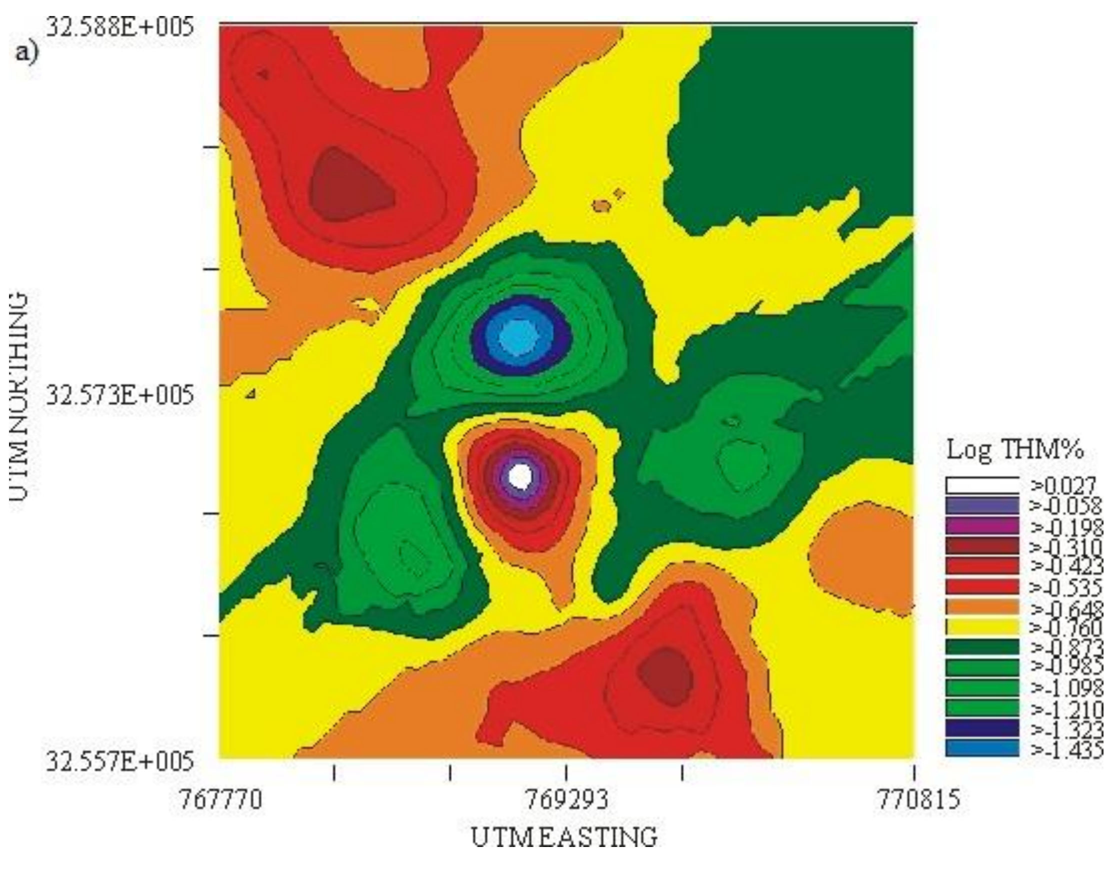


Figure 6.7 Spatial variability maps for Log THM% according to the Spherical model. a) Log THM% values map.

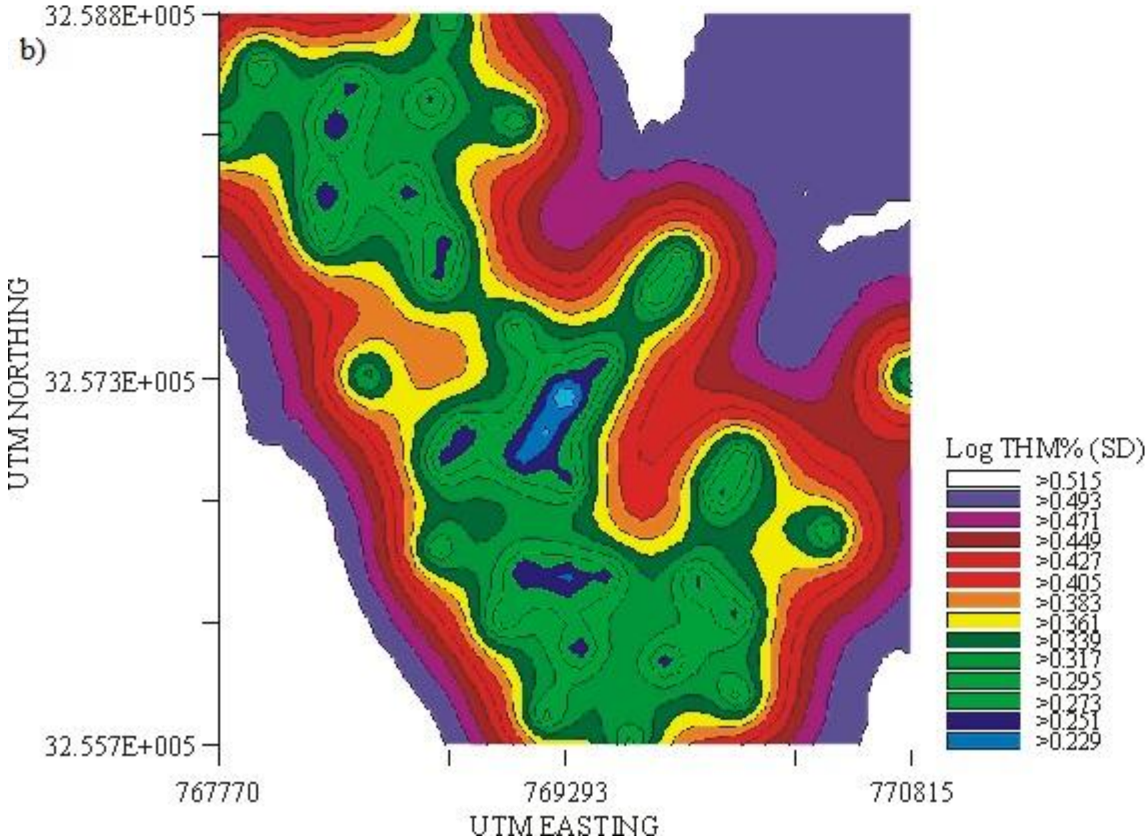


Figure 6.7 (continued)….Spatial variability maps for Log THM% according to the Spherical model. b) Kriging standard deviation map.

6.4 Transparent heavy minerals (HM)

Unlike the preceding two variables, Log (HM/THM%) showed significant spatial dependence with the C/ (C_o+C) ratio reaching 0.524. The exponential model was best fit for the semi-variogram (Fig 6.2.c) with RSS value of 1.725 E-03 and r^2 of 0.652. The nugget effect is minimal with value of 0.05, and sill equals 0.105 according to the adopted model. This indicates a close structured spatial relation between the values of the variable studied and that the randomness in the relationship is minimal.

The adopted best fit exponential model with parameters as listed in Table 6.1 with RC value of 0.732 and r^2 value of 0.119 (significant at 2f and 95% confidence). The Log (HM/THM%) spatial variability map was drawn (Fig 6.9.a) accompanied with the kriging standard deviation map (Fig 6.9.b). The transparent heavy minerals are clearly more concentrated in the lower SW part of the study area, while lowest values are in the northern part as they are a fraction of the total heavy minerals and are expected to maintain similar dispersion trend. The most reliable parts in the constructed map for transparent heavy minerals are those that lie on both sides of the NW-SE diagonal of the study area.

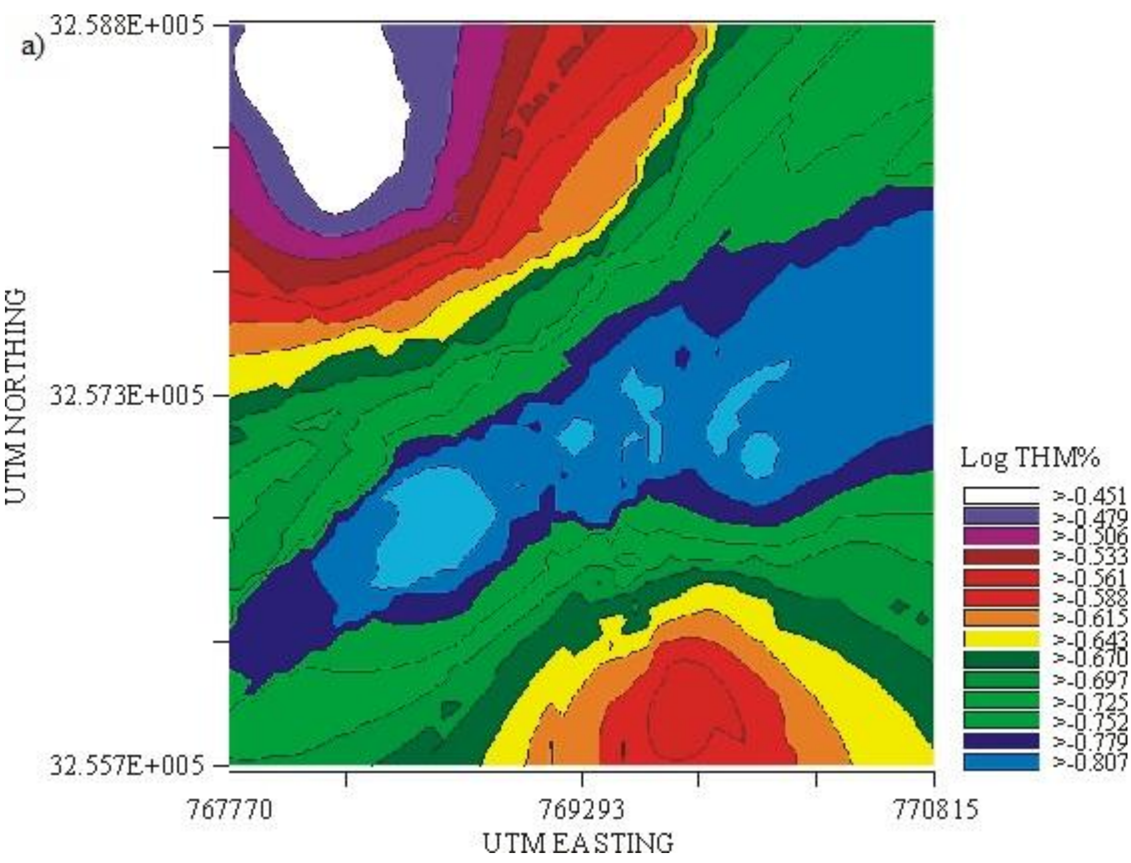


Figure 6.8 Spatial variability maps for Log THM% (38 samples) according to the Spherical model. a) Log THM% values map (The mineralized horizon lies at the NE border of the study area).

6.4.1 Zircon:

Log-transformed zircon content as percentage from total heavy minerals Log (Zrn/THM%), also exhibits a structured spatial variability. The adopted best fit model is Spherical (Fig 6.2.d), with nugget effect (C_o) and sill (C) equal to 0.065 and 0.14 respectively, which are relatively low and indicate low spatial variation and strong spatial dependence as evidenced by the high $C/(C_o+C)$ value which mounts up to 0.536 (Table 6.1). This structured spatial variation lead to the construction of a good and reliable spatial variability map for Log (Zrn/THM%) values within the study area (Fig.6.10.a and b) with the accompanied standard deviation map.

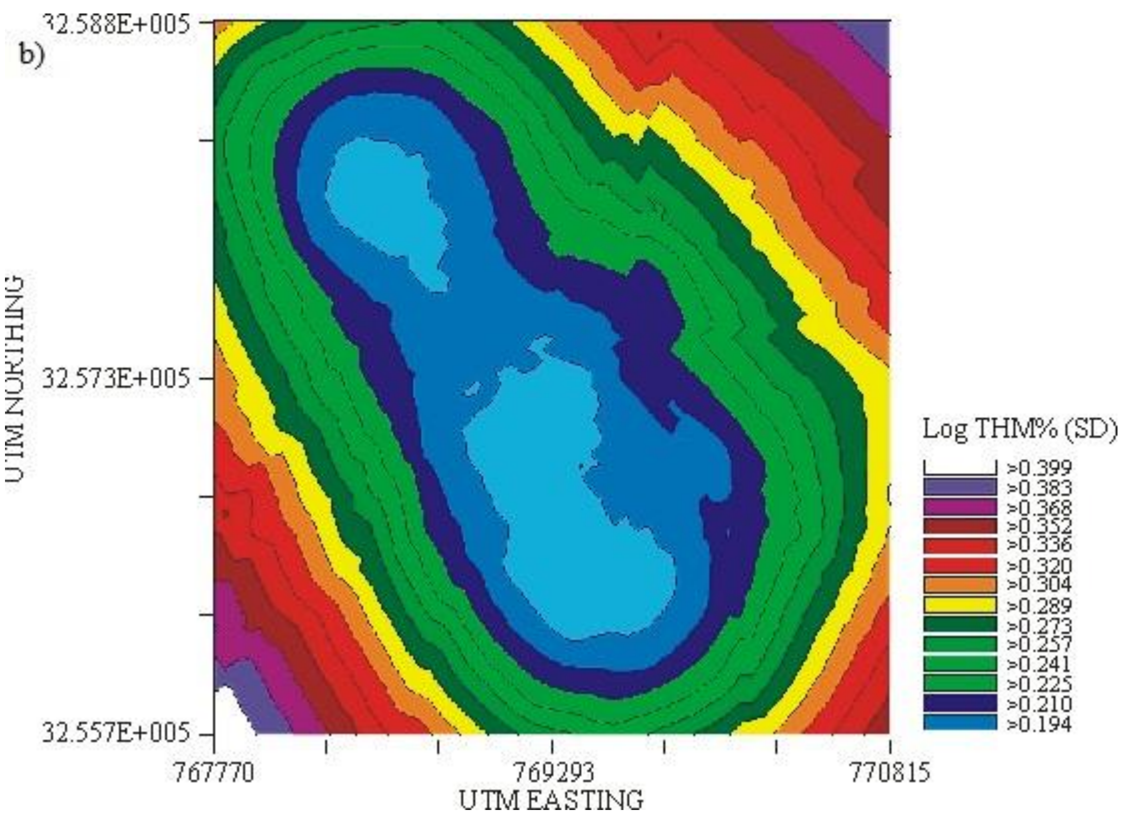


Figure 6.8 (continued)….. Spatial variability maps for Log THM% (38 samples) according to the Spherical model. b) Kriging standard deviation map.

Highest zircon content is in the lower SW part, while it decreases towards the N and NE. It might worth noticing here that the trend of zircon concentration to certain extent coincides with the gamma radiation distribution and the transparent heavy minerals distribution map. Once again this is an ample evidence of the usefulness of applying gamma rat spectrometry in exploration for zircon and Hf bearing minerals.

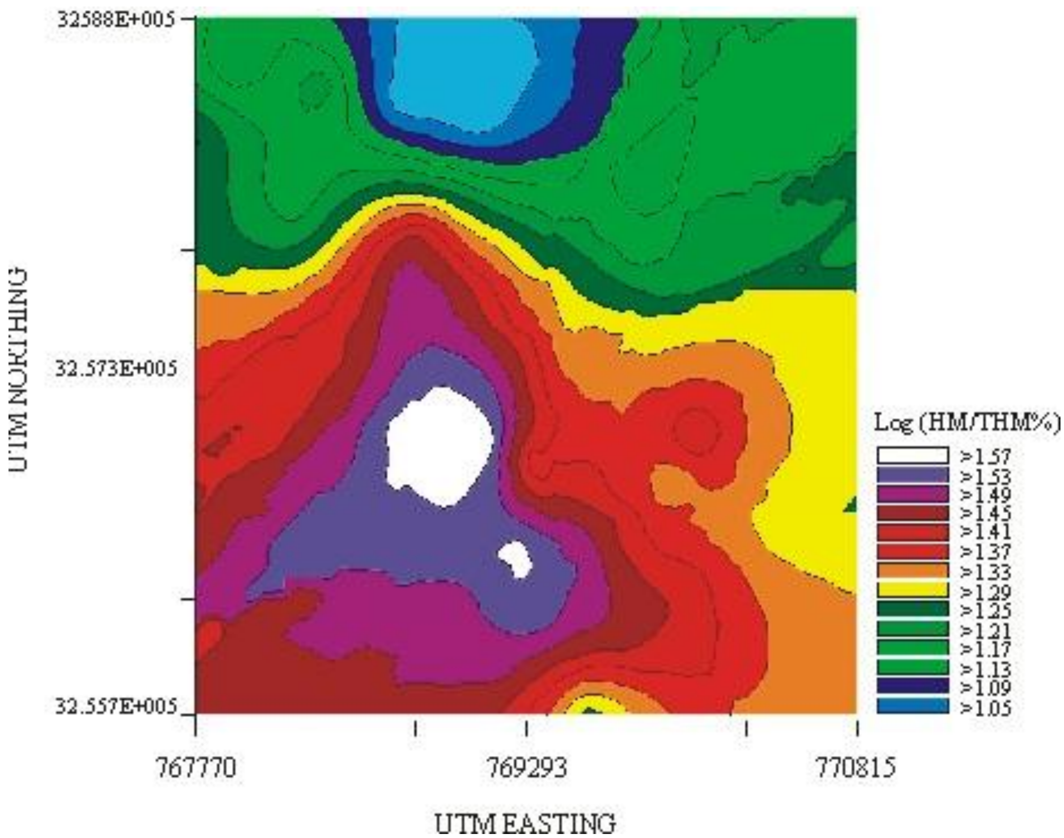


Figure 6.9 Spatial variability maps for Log (HM/THM%) according to Exponential model. a) Log (HM/THM %) values map.

6.4.2 Tourmaline:

Log-transformed tourmaline values (Log Tur/THM%) are randomly distributed and exhibit a pure nugget effect (Fig 6.2.e) with C/ (C_o+C) equal to zero such that C_o =C = 0.09380.

As this is the case, the IDW method was used for interpolation. RCC and r^2 values are listed in Table 6.1 and are relatively low, despite that the spatial variability map was drawn for Tur% values (Fig 6.11).

From the map it is evident that the variations in the Log (Tur/THM%) values across the study area are low as indicated by the low sill, with certain local variations and highest concentration in the middle part of the area. The constructed map exhibits also similar spatial variability trends as those exhibited by zircon (as Log (Zrn/THM%).

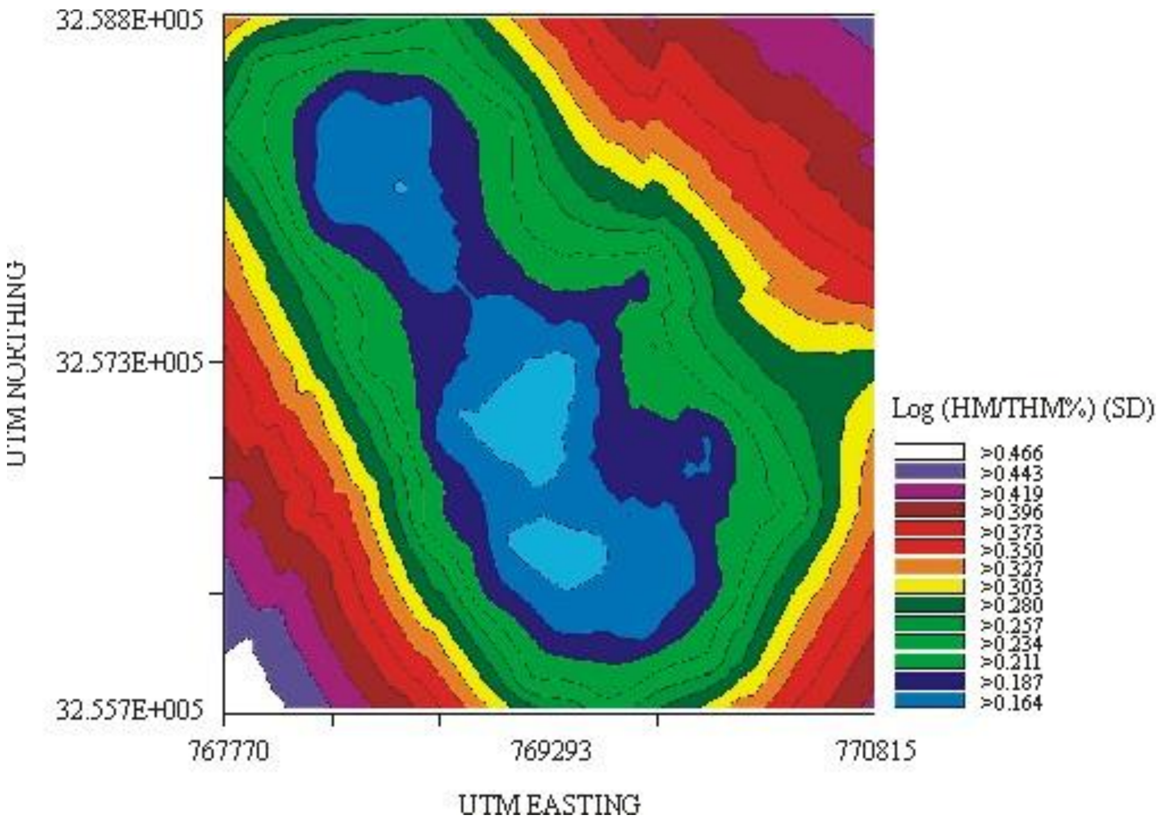


Figure 6.9 (continued)…..Spatial variability maps for Log (HM/THM%) according to Exponential model b) Kriging standard deviation map.

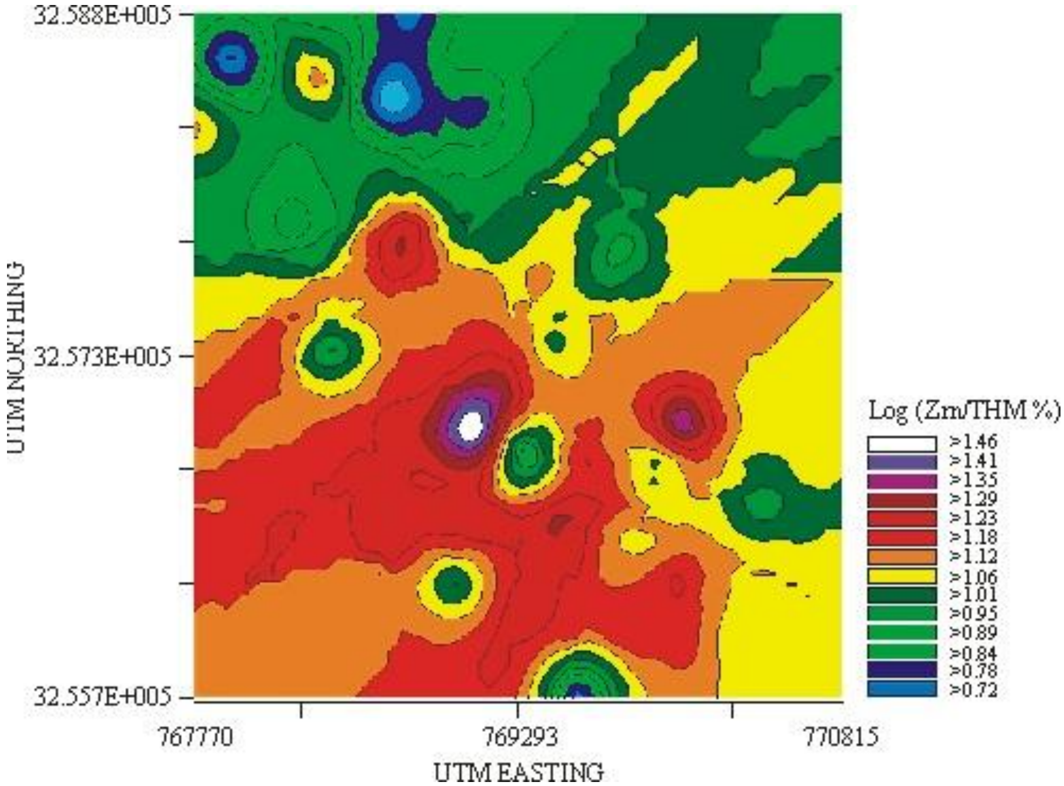


Figure 6.10 Spatial variability maps for Log (Zrn/THM%) according to Spherical model. a) Log (Zrn/THM%) values map.

6.4.3 Rutile:

Log-transformed rutile content, Log (Rt/THM%) from the total heavy minerals, is another variable with evident structured spatial distribution. Exponential model was best fit to the experimental semi-variogram (Fig 6.2.f), with parameters C_o=0.0474, C=0.1978 and A_o=1166. The RSS of this chosen model equaled 3.860E-03 and r^2=0.759. The highest C/ (C_o+C) was recorded and it equals 0.760, indicating strong spatial dependence of Log (Rt/THM%) values. RSS and r^2 values for the proposed model are also high (0.773 and 0.185, respectively, Table 6.1). It's clear from the combination of the previous information regarding the model that the spatial variability map (Fig 6.12.a) will be quite reliable as proved by the kriged rutile standard deviation values map (Fig 6.12.b). As obvious as it is,

the rutile concentration is highest in the SW portion of the study area and decreases in the east and north directions.

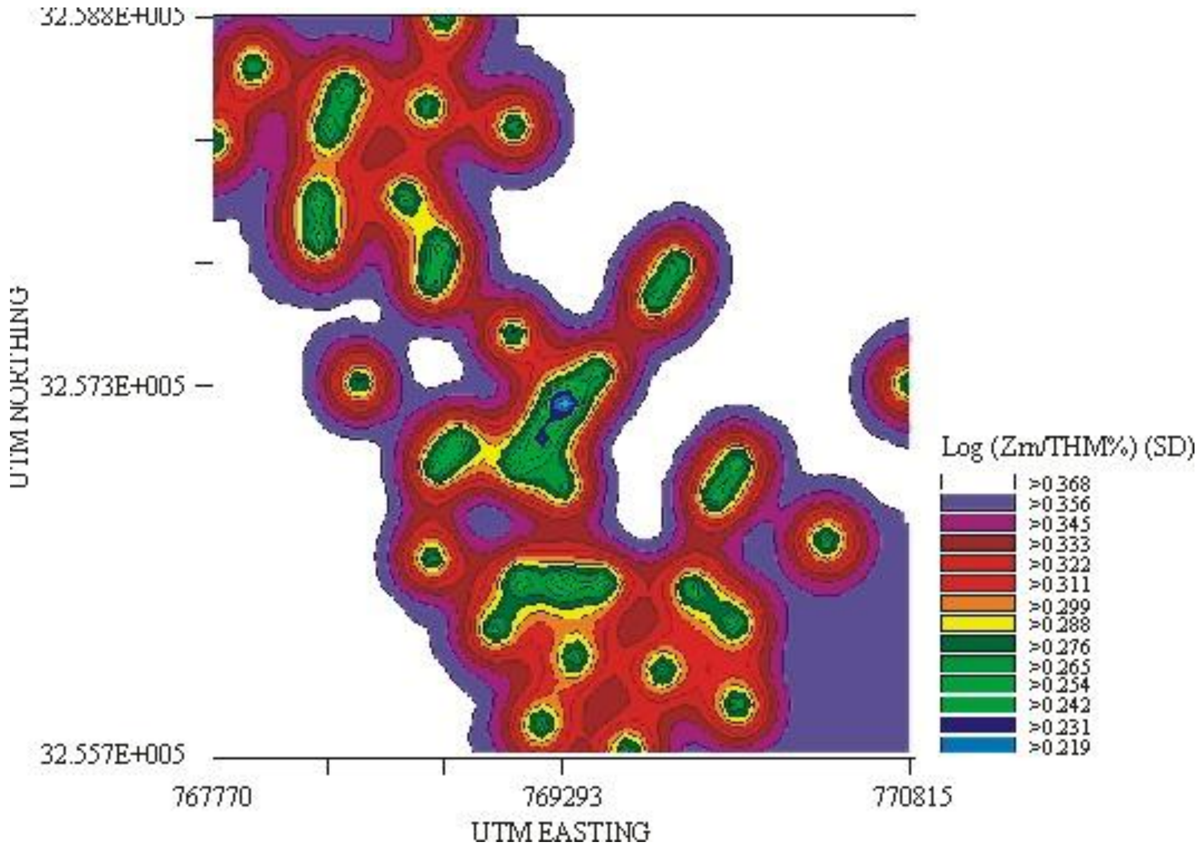


Figure 6.10 (continued)…..Spatial variability maps for Log (Zrn/THM%) according to Spherical model.b) Kriging standard deviation map.

To summarize: spatial studies on wadi sediments in the study area indicate that the encountered transparent heavy mineral abundances as total and zircon and rutile abundances can be quantified using the spherical and exponential models after transformation to logarithmic form. However Log-transformed total heavy mineral abundances and tourmaline contents exhibit pure nugget effect.

The constructed spatial variability maps have their most reliable estimates along the NW-SE direction and the least reliable estimates are those made on the NE-SW corners.

The minimum spatial dependence is exhibited by Log CPS, Log THM% and Log (TurTHM%), whereas the maximum spatial dependence is that of Log (HM/THM%) , Log (Zrn/THM%) and Log (Rt/THM%).

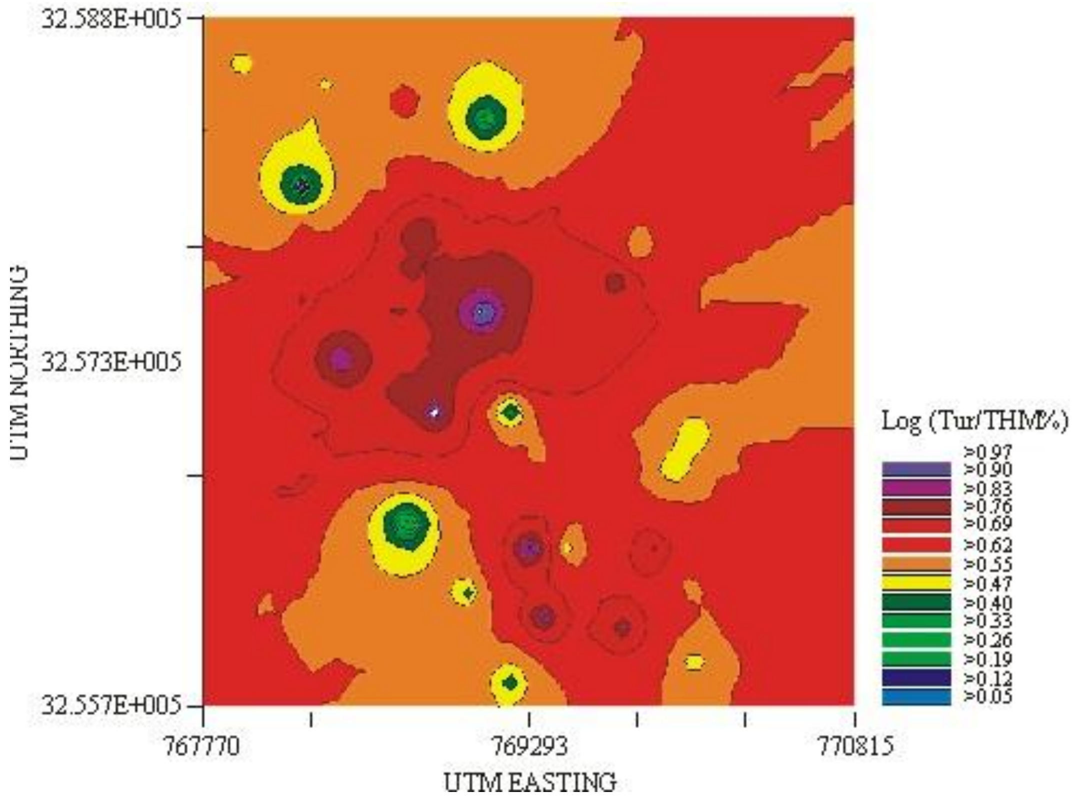


Figure.6.11 Spatial variability map for Log (Tur/THM%) according to the IDW method.

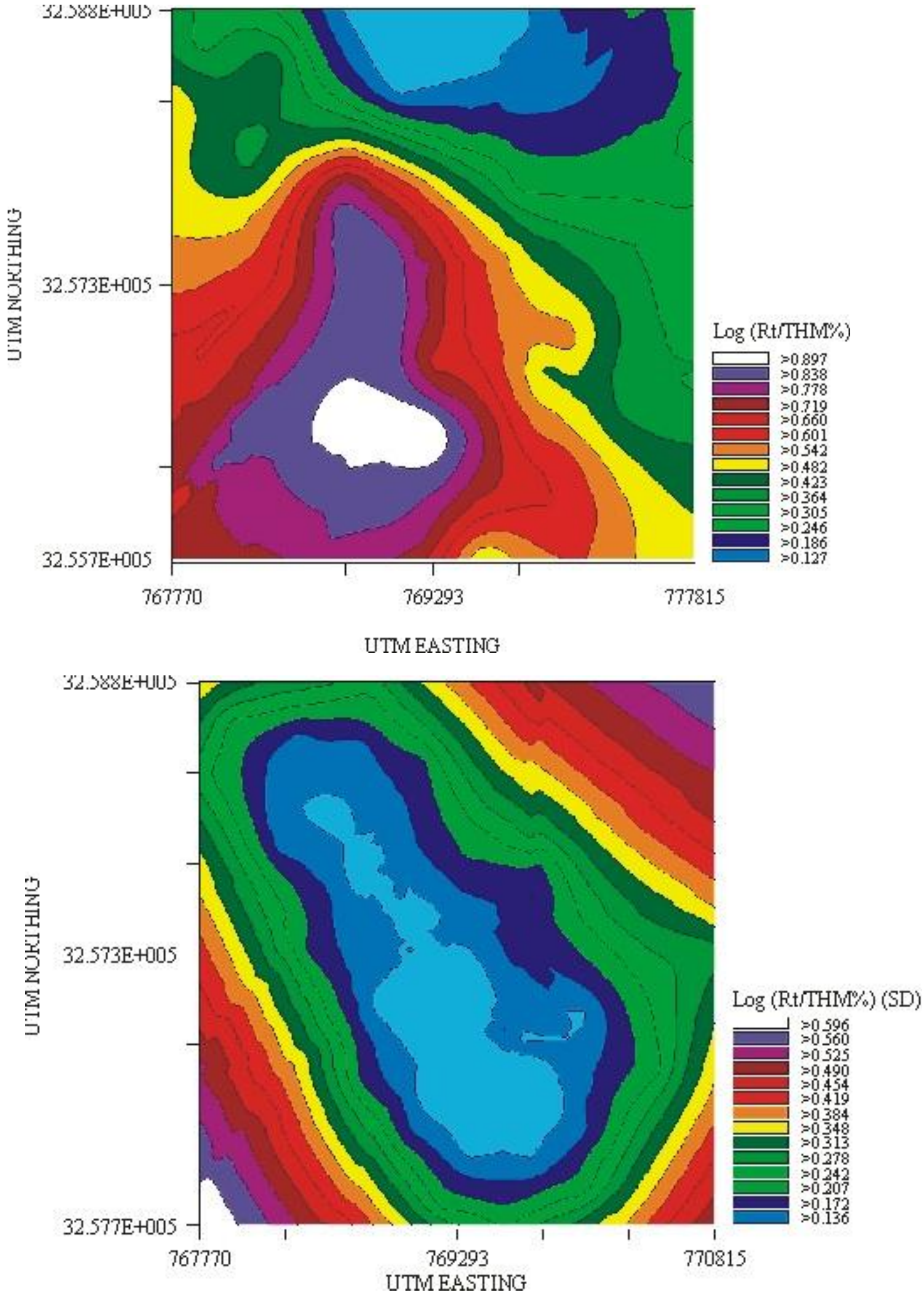


Figure 6.12 Spatial variability maps for Log (Rt/THM%) according to Exponential model. a) Log (Rt/THM% values map b) Kriging standard deviation map.

6.5 X-ray fluorescence analysis

Statistical results verified the presence of anomalous samples as suspected from gamma-ray readings in the field and grain counts results. These observations led to the selection of 4 samples for XRF analysis, in order to identify the elemental source of radiation rather than the minerals bearing this element/s. The analytical results, though not absolutely quantitative due to lack of specific standards, give good impressions about the bulk chemical content of the selected samples.

Samples taken for the analysis are bulk sediments ranging in size from (0.038 to 0.25mm), which is the size most abundant with heavy minerals. Table 6.3 shows the results of the analysis in terms of major Oxides %, Loss on Ignition%, uranium (ppm), thorium (ppm), ZrO_2 and HfO_2 %.

Sample DBS46 was regarded as anomalous ever since gamma-radiation at its sampling location was recorded to equal 10100 CPS, this highly elevated value above the background and is accompanied by the highest content of THM which mounted up to 15.628%. Grain mounts revealed extremely high zircon content ((Zrn/THM%)= 79.051) and almost no opaque grains.

Therefore DBS46 was subjected to XRF analysis and as shown in Table 6.3, the major source of radiation is Th with its content reaching 1880 ppm. Taking into consideration that the Th average content in Earth's crust is 12 ppm as mentioned previously then the analyzed sample DBS46 represents a positive valuable extreme in terms of Th content. It's also an important source for U and Hf.

The other 3 samples don't show high extremities, however in general the values of Th and U, indicate that the source of radiation is mostly Th not U.

Table 6.3 Results of XRF for the selected samples: DBS7, DBS 23, DBS24 and DBS46.

	DBS7	DBS23	DBS24	DBS46
Fe_2O_3 %	7.1	11.2	9.84	4.97
MnO %	0.022	0.042	0.255	0.033
TiO_2 %	1.32	0.89	0.89	5.48
CaO%	6.67	0.76	7.32	1.24
K_2O%	2.06	3.63	1.81	2.13
P_2O_5 %	0.26	0.08	0.62	0.61
SiO_2 %	52	56.4	54.2	68.2
Al_2O_3 %	7.21	16	7.02	6.12
MgO %	1.13	2.31	1.35	0.87
Na_2O %	0.09	0.49	0.06	0.05
SO_3 %	13	0.15	8.34	0.14
Cl%	0.035	1.04	0.060	0.05
L.O.I. %	7.9	6.7	7.3	3.4
U ppm	nd	nd	nd	170
Th ppm	180	nd	41	1880
ZrO_2 %	0.9	0.08	0.62	6.2
HfO_2 %	0.009	nd	0.007	0.112

CHAPTER SEVEN:
Discussion

7.1 Heavy Mineral Assemblages

High concentrations of heavy minerals within bulk wadi sediments samples were not detected except at two locations. This is consistent with the gamma radiation readings taken in the field during sampling. The most probable reason for the anomalies is over time accumulation of sediments from different directions in relatively low elevated portion of the study area. On the other hand, the major transparent heavy minerals species encountered were zircon, rutile, tourmaline and anatase (both detrital and authigenic) in decreasing order of abundance with some less amounts of garnet, apatite, dolomite, mica, staurolite and brookite concentrated with less frequency. This assemblage is expected, since the alluvium is derived from pre-existing sedimentary rocks. That is many species that could've been present might have disappeared from the original assemblages due to advanced digenetic and weathering processes in the sedimentary sources or post derived sediments respectively (Morton, 1985; Morton and Hallsworth, 2007). Zircon, rutile, tourmaline and anatase are regarded as of the most stable heavy mineral species in sandstones (Hubert, 1962; Pettijohn, 1975) hence their dominance in the alluvium deposits. Table 7.1 shows the order of resistivity of transparent heavy minerals grains as collected by (Mange and Wright, 2007) after several authors. It is evident that in all the different conditions, zircon, tourmaline and rutile are amongst most stable species found. On the other hand, the euhedral and crystal aggregate nature of some anatase grains found in grain mounts from different samples indicates according to Mange and Wright (2007) an authigenic origin within the source sedimentary strata.

The findings of this study mostly coincide with the findings of Madanat et al (2006) except with regard to the existence of monazite within the mineral assemblage, which wasn't

found in any of the grain mounts in this study. Shohadah (1993) studied the heavy mineral content of Dubaydib sandstone and didn't find any traces of monazite or any other mineral that could bear radioactive elements except for the cracked zircons. This absence of mineral species other than zircon bearing radioactivity as evident from the grain mounts is the strongest base for the argument that it is zircon (cracked or partially metamictized) most likely to be the main source of radiation in the wadi alluvium of the study area. Also statistics show a significant positive relation between the zircon contents and gamma-rays according to the correlation coefficient value for the total 40 samples and in addition to these facts it was found by (Madant et al, 2006) that a positive relationship exists between thorium and the presence of zircon grains within the DB2 member, which is expected to be the source of any appreciable amounts of heavy minerals in the wadi alluvium.

7.2 Geostatistical analysis

The geostatistical treatment of the variables studied showed that the gamma radiation and total heavy minerals content at first sight show erratic non-structured distribution, however, eliminating anomalous samples reduces the randomness and the spatial differences, which makes it possible to build models for the semi-variograms drawn with high reliability. Meanwhile transparent heavy mineral content HM, zircon and rutile contents in THM show high spatial dependence and kriging could be very well employed in estimating values of those variables at unanalyzed locations within the study area after transformation to logarithms. Tourmaline volume percentage however showed a pure nugget effect, which could be due to the large sampling intervals, and could be solved by reducing this intervals to account for small spatial variability.

Table.7.1. Resistance to chemical weathering of common transparent heavy minerals, inferred using different methods (after Mange and Wright, 2007).

	Petijohn (1941)	Bateman and Catt(1985)	Nickel(1973)			Gruner (1950)
Most	Persistence through geological time	Persistence in weathered cover-sands	Experimental dissolution at pH 3.6	Experimental dissolution at pH 5.6	Experimental dissolution at pH 10.6	Theoretical energy indices
Order of resistance of chemical weathering **Least**	Zircon Tourmaline Hornblende Garnets Sphene Augite Hypersthene	Zircon+ rutile + tourmalines Staurolite Kynaite Garnets Epidotes Hornblende+ Hypersthene Augite Olivines Apatite	Zircon+rutile+ hornblende Sphene Staurolite Tourmalines Epidot Garnet Apatite	Zircon+ rutile+ sphene Tourmalines +staurolite Epidote Hornblende Garnet Apatite	Zircon+ rutile+ staurolite+ garnet* Hornblende Apatite Sphene Tourmalines Epidote	Zircon Tourmaline Hornblende Garnets Sphene Augite

CHAPTER EIGHT: Conclusions and Recommendations

8.1 Conclusions

The mineralogical and geostatistical analysis done to fulfill the aims of this study led to the following conclusions:

1. The wadi deposits collected from 40 sample locations in the study area show no economically significant amounts of heavy minerals, except for the sample DBS46 and DBS24 (Fig 3.2) THM% values for these two samples are 15.628 and 1.069 respectively. It is those two samples locations that gave highest gamma-ray readings during the field survey; such that CPS recorded for them were 10100 CPS and 3100 CPS respectively.
2. The most abundant heavy mineral species encountered are zircon, tourmaline, rutile and anatase.
3. Zircon content in samples DBS 46 is found to be anomalously high comprising 79.051 % by volume of the total heavy mineral fraction in that sample. This high percentage of zircon content in the sample DBS46 coupled with the presence of highly cracked zircon grains (possibly metamict zircons as discussed previously), could be an explanation for the high radiation detected at the sampling location.
4. The XRF analysis for the 0.038-0.25 mm size fraction from the bulk sediment of sample DBS46 which indicated high Th content of 1880 ppm, U content of 170 ppm and Hf of 0.112%, might also point towards zircon source of radioactivity. Similar observations can be seen for sample DBS 24 and sample DBS 7 which contains 0.967 % THM and gamma radiation of 1450 CPS.
5. Spatial variability and geostatistical results along with the high correlation between the CPS and THM% indicate that gamma ray surveying could be used in

exploration for high concentrates of heavy minerals in the study area, with their source being the sandstones of DB2 member.

6. Tourmaline shows pure nugget effect; accordingly its spatial variability was studied using the IDW method.
7. Spatial variability maps for all variables show more or less similar trends of distribution.
8. The results of this study prove the applicability of kriging technique for determining heavy minerals as total and individual species spatial variability in wadi deposits in similar arid geologic environments where precursor rocks are of siliciclastics sedimentary type.

8.2 Recommendations

1. Though the application of Gamma Spectrometry in exploration for zircon proved to be useful its effectiveness need to be checked for on areas of large extent.
2. Detailed exploration and feasibility studies should be accomplished to evaluate the economic importance of Dubbaydib Member 2 mainly in terms of its Zr and radioactive elements i.e.U, Th and Hf content.

References

Abed, A.M. (2000), **Geology of Jordan, its environment and waters**. Publication of the Jordanian geologists association, p: 571, Amman, Jordan.

Abu Lihie, O. (1988), **Dubaydib sheet, 3148 I, 1:50,000 geological map series,** NRA, Geol. Dir., Geol. Map. Div., Amman

Amireh, B. S. (1990), **Mineral composition of the Cambrian-Cretaceous Nubian series of Jordan: Provenance, tectonic setting and climatological implications**. Sedimentary Geology, 71, 99-119, Elsevier Amsterdam.

Amireh, B.S. (1987), **Sedimentological and petrological interplays of the nubian series in Jordan with regard to palaegeography and diagenesis,** Ph.D.dissertation, university of Braunscchweiger, West Germany, p: 232.

Amireh, B.S. (1994), **Heavy and clay minerals as tools in solving stratigraphic problems: A case study from the Disi sandstone (Early Ordovician) and the Kurnub sandstone (Early Cretaceous) of Jordan.** N. J. Geol.Palaont. Mh. 4, 205-222, Stuttgart.

Amireh, B.S., Schneider, W., Abed A.M. (2001), **Fluvial-shallow marine-glaciofluvial depositional environments of the Ordovician system in Jordan**. Journal of Asian Earth Sciences 19, 45-60. Elsevier B.V.

Bateman, R.M. and Catt, J.A. (1985), **Modification of heavy mineral assemblages in English coversandsby acid pedochemical weathering**. Catena 12, 1-21.

Bateman, R.M. and Catt, J.A. (2007), **Provenance and Palaeoenvironmental interpretation of superficial deposits, with particular reference to post-depositional modification of heavy mineral assemblages.** Developments in Sedimentology, 58, 151-188, Elsevier B.V.

Bea, F. (1999), **Uranium.** In Encyclopedia of Geochemistry, p: 712, Kluwer academic publishers, London.

Bender, F. (1963), **Lithographic and time-stratigraphic subdivision of the "Nubian Sandstones" in south Jordan.** Dubetret, L (Ed) Lexique stratigraphique international, 3, Paris.

Bender, F. (1974), **Geology of Jordan**. *Gebrueder Borntraeger*, *Berlin*, p: 196.

Bhattacharyya, G. K. and Johnson, R. A. (1977), **Statistical concepts and methods,** p: 639, Wiley & Sons, New York.

Cambardella, C.A., Moorman, T.B., Noval, J.M., Parkin, T.B., Karlen, D.L., Turco, R.F. and Konopka, A.E. (1994), **Field-scale variability of soil properties in central Iowa soils.** Soil Science Society Am. J., 58, 1501-1511.

Chen, Y. and Jiao, X. (2001), **Semivariogram fitting with linear programming**. Computers and Geosciences, 27, 71-76.

Clark, I. (1979), **Practical Geostatistics,**p: 151, Geostokos Ltd, Alloa Business Center, Scotland.

Dickson, B.L. and Scott, K.M. (1997), **Interpretation of aerial gamma ray surveys-adding the geochemical factors.** AGSO Journal of Australian Geology and Geophysics, 17, 187-200.

Dill, H.G. (1998), **A review of heavy minerals in clastic sediments with case studies from the alluvial fan through the near shore marine environments.** Earth-Science Review 45, 103-132.

Elsner, H., (2010), **Heavy minerals of economic importance**. Federal institute for geosciences and natural resources (BGR) report, p.218, Hannover, Germany.

Ewing, R.C. (1994), **The metamict state,** 1993-The Centennial. The Nuclear instruments and Methods in Physics research, B91, 22-29.

Faure, G. (1998), **Principles and Applications of Geoshemistry (2nd ed), p: 600,** Prentince Hall, New Jersey.

Garnar, T.E. (1985), **Mineral sand products and their uses**. Presented at the Society of Mining, Metallurgy and Exploration, Inc., Fall Meeting and Exhibit, October 16, Albuqerque Convention Center, Albuquerque, New Mexico.

Garver, J. I. and Kamp, P. J.J. (2002), **Integration of Zircon color and zircon fission track zonation patterns in orogenic belts: applicationto the southern Alps, New Zeland.** Tectonophysics 349, 203-219. Elsevier B.V.

Gamma Design Software (2001), **GS+ Geostatisics for Environmental Sciences** (Version 5.1.1), professional edition.

Gruner, J.W. (1950), **An attempt to arrange silicates in the order of reaction energies at relatively low temperatures.** American Mineralogist 35, 137-148.

Haredy, R.A. (2008), **Heavy minerals in marine and fluvial sediments: provenance indicators and distributions in the tropical southeastern shelf of the gulf of Carpentaria and its hinterland North Australia**, PhD thesis , School of Earth and Environmental sciences, University of Wollongong.

Hedrick, J.B. (2005), **Rare earths, the lanthanides, yttrium and scandium**. Mining Engineering, 57(6), 50-52.

Heriawan, N. (2006), **http://dir.gmane.org/gmane.science.statistics.geostatistics**.

Hubert, J.F. (1962), **A zircon-tourmaline-rutile maturity index and the interdependance of the composition of heavy mineral assemblages with the gross composition and texture of sandstones.** Journal of Sedimentary Petrology 32, 440–450.

Huisman, D.J. and Klaver, G. Th. (2007), **Heavy minerals in the subsurface: tracking sediments sources in three dimensions.** Developments in Sedimentology, 58, 869-885, Elsevier, B.V.

International Atomic Energy Agency (IAEA), (2003), **Guidelines for radioelement mapping using Gamma-ray spectrometry data,** p: 173, IAEA, Austria.

Jalali, M. (2007), **Spatial variability in potassium release among calcareous soils of western Iran. Geoderma,** 140, 42-51. Elsevier B.V.

Jenkins, O.P. (1964), **Geology of placer deposits.** Mineral information services, 17, 1-9, California division of mines and geology, California.

Jewett, S. (2004), **Physics for scientists and engineers with Modern physics (6th ed),** p: 1552, Thomson learning, Brooks /Cole, USA.

Journel, A. G and Huijbregts, CH. J. (1978), **Mining Geostatistics**, p: 600, Academic press, London.

Kennedy, W.Q. (1964), **The structural differentiation of Africa in the Pan African (± 500 m.y.) tectonic episode.** Univ Leeds Res. Inst. Afr. Geol. Dept. Earth Sci. Annu. Rep. Sci. Results, 8, 48-49.

Klein, C. and Dutrow, B. (2008), **Mineral Science (23rd ed),** p: 675, Wiley & Sons, New York.

Komar, P.D. (2007), **The entrainment, transport and sorting of heavy minerals by waves and currents.** Developments in Sedimentology, 58, 3-48, Elsevier B.V. Amsterdam.

Kretz, R. (1983), **Symbols for rock-forming minerals.** American Mineralogist, 68, 277-279. Canada.

Krishnaswami, S. (1999), **Thorium**. In Encyclopedia of Geochemistry, p: 712, Kluwer academic publishers, London.

Limpert, E., Stahel, W.A. and Abbt, M. (2001), **Log-normal Distributions across the Sciences: Keys and Clues.** Bioscience, 51, 341-352.

MacRae, C.M., Wilson, N.C., Aral, H., Ryan, C.G. and Pownceby, M.I. (2003), **Zircon characterization- a new approach to an age old problem**. Heavy minerals 2003, Johannesburg, South African Institute of Mining and Metallurgy.

Makhlouf I. M. (1994), **Tempestite facies displaying hummocky cross-stratification and subaqueous channels in Ordovician shelf deposits South Jordan**. African Geoscience Review, 2, 91-99.

Makhlouf, I. (1998), **Storm generated channels in the middle Dubaydib sandstone formation, south Jordan.** Journal of King Saud University, Science, 10, 1-77, Riyadh.

Makhlouf, I. M. (1997), **Storm-Genereated Channels in the Middle Dubaydib Sandstone Formation, South Jordan**. J.King Saud Univ., 10, 61-77.

Mange, M.A. and Maurer, H.F.W. (1992), **Heavy minerals in colour**. London: Chapman & Hall. P: 147.

Mange, M.A. and Wright, D.T. (2007), **Heavy minerals in use**. Elsevier B.V. p: 1329.
Masri,A. (2007), **The Geology of Dubaydib and Jabal Ladghayn Area , map sheets No. 3148-I & 3148-II.** National Resources Authority Bulletin 65.

McCourt, W. (1987), **Geochronology of the Arabian-Nubian Shield of southwest Jordan.** NRA, Geol. Dir., Geol. Map. Div., internal report, p: 14, Amman.

McCourt, W. and Ibrahim, K. (1990), **The geology, geochemistry and tectonic setting of the granitic and associated rocks in the Aqaba and Araba complexes of southwest Jordan.** NRA, Geol. Dir., Geol. Map. Div., Bulletin 10, Amman.

Meinhold, G. (2010), **Rutile and its applications in earth sciences,** Earth-science Reviews,102, 1-28. Elsevier B.V.

Milliken, K. L. (2007), **Provenance and digenesis of heavy minerals, Cenozoic units of Northwestern gulf of Mexican sedimentary basin**. Developments in Sedimentology, 58, 247-261, Elsevier B.V.

Mittlefehldt, D.W. (1999), **Potassium.** In Encyclopedia of Geochemistry, p: 712, Kluwer academic publishers, London.

Morton, A.C. (1985), **Heavy minerals in provenance studies.** In Provenance of Arenites, Reidel, Dordrecht, 249-277.

Morton, A.C. and Hallsworth, C. (2007), **Stability of detrital heavy minerals during burial digenesis.** Developments in Sedimentology, 58,215-245, Elsevier B.V.

Musoli, C.P., Pinard, F., Charrier, A., Kangire, A., tenHoopen, G.M., Kabole, C, Ogwang, J., Bieyesse, D. and Cilas, C. (2008), **Spatial and Temporal analysis of coffee wilt disease caused by Fusarium hylarioides in Coffea canephora.** Eur. J. Plant Pathol, 122, 451-460.

Nickel, E., (1973). **Experimental dissolution of light and heavy minerals in comparison with weathering and intrastratal solution.** Contributions to Sedimentology 1, 1-68.
Okay, N. and Ergun, B. (2005), **Source of the basinal sediments in the Marmara Sea investigated using heavy minerals in the modern beach sands**. Marine Geology 216, 1-15.

Padmalal, D., Ramachandran, K.K. and Seralanth, P. (1998), **Significance of heavy mineral suite in riverine and esuarine sediments in the wouthwest coast of India-case study.** Indian journal of Marine Sciences 27, 185-189.

Patyk-Kara, N. G., Andrianova, E. A. and Dubinchuk, V. T. (2008), **Secondary alterations of zircons in placers.** Doklady Earth Sciences, 419: 253-256.

Perkins, D. (2002), **Mineralogy (2nd ed),** p: 483, Prentince Hall, New Jersey.

Pettijohn, F.J. (1941), **Persistence of heavy minerals and geologic age.** Journal of Geology 49, 610-645.

Pettijohn, F.J. (1975), **Sedimentary Rocks, (3rd ed.),** Harper and Row, New York.

Powell, J. (1989), **Stratigraphy and Sedimentation of the phanerozoic rocks in central and south Jordan, Part a: Ram and Khrayim groups.** NRA, Geol. Dir., Geol. Map. Div., Bulletin 11a, Amman.

Saffarini, G.A. and Lahawani, Y. (1991), **Multivariate statistical techniques in geochemical exploration applied to wadi sediments' data from an arid region: Wadi Dana, SW Jordan.** Journal of African Earth Sciences, 14, 417-427. Pergamon press Ltd, Great Britain.

Schuttenhelm, R.T.E. and Laban C. (2005), **Heavy minerals, provenance and large scale dynamics of seabed sands in the Southern North Sea: Baak's (1936) heavy mineral study revisited.** Quaternary International 133-134: 179-193.

Shatalov, V.V., Nikonov, V.I. and Kostar, M.L. (2008), **Prospects for zirconium and hafnium supplies for nuclear power in Russia up to 2030.** Journal of Atomic Energy, 105, 242-247, Springer, NewYork.

Shohadad, T.F. (1993), **Geochemical exploration for uranium and thorium in the Ordovician sandstone (Sabellarifex unit)/ south Jordan.** M.Sc thesis, p: 159, University of Jordan, Amman.

Suror, A.A., El-Kammar, A.A., Arafa, E.H. and Korany, H.M.(2003), **Dahab stream sediments, southeastern Sinai, Egypt: a potential source of gold, magnetite and zircon.** Journal of geochemical exploration, 77, 25-43. Elsevier B.V.

Van Loon, A.J. and Mange, M.A. (2007), **"In situ" dissolution of heavy minerals through extreme weathering, and the application of the surviving assemblages and their dissolution characteristics to correlation of Dutch and German silver sand.** Developments in Sedimentology, 58, 189-218. Elsevier B.V.

Warland, I. (2006), **The Eucla basin-new zircon province**. Presented at the south Australian resources and energy conference. Source: http://www.iluka.com/news.

Williams, G.E. and Steenkamp, J.D. (2006), **Heavy mineral processing at Richards bay minerals**. Southern African Pyrometallurgy 2006, Johannesburg.

Zumdahl, S. and Zumdahl, S. (2003), **Chemistry (6th ed),** p: 1102, Houghton Mifflin com., New York.

Appendices

Appendix A: Sample locations given in both International Geographic and UTM systems.

Samples	Geo Easting	Geo Northing	UTM Easting	UTM Northing
DBS1	35°46'25.00"	29°25'32.00"	769090	3258336
DBS2	35°46'11.00"	29°25'35.00"	768710	3258419
DBS3	35°45'58.00"	29°25'38.00"	768358	3258503
DBS4	35°45'43.00"	29°25'41.00"	767951	3258586
DBS5	35°45'36.00"	29°25'31.00"	767770	3258274
DBS6	35°45'55.00"	29°25'32.00"	768281	3258317
DBS7	35°45'53.00"	29°25'23.00"	768234	3258038
DBS8	35°45'53.00"	29°25'17.00"	768238	3257854
DBS9	35°46'14.00"	29°25'47.00"	768782	3258791
DBS10	35°46'7.00"	29°25'23.00"	768611	3258047
DBS12	35°45'59.00"	29°24'58.00"	768414	3257272
DBS13	35°46'15.00"	29°24'50.00"	768851	3257036
DBS14	35°46'11.00"	29°24'46.00"	768746	3256910
DBS15	35°46'10.00"	29°24'34.00"	768728	3256540
DBS16	35°46'24.00"	29°24'31.00"	769108	3256457
DBS17	35°46'31.00"	29°24'30.00"	769297	3256430
DBS18	35°46'32.00"	29°24'43.00"	769315	3256831
DBS19	35°46'31.00"	29°24'55.00"	769279	3257200
DBS20	35°46'38.00"	29°24'30.00"	769486	3256435
DBS21	35°46'52.00"	29°24'29.00"	769864	3256413
DBS22	35°46'56.00"	29°24'41.00"	769963	3256785
DBS23	35°46'60.00"	29°24'46.00"	770067	3256942
DBS24	35°46'47.00"	29°24'18.00"	769737	3256071
DBS25	35°46'33.00"	29°24'20.00"	769358	3256124
DBS26	35°46'20.00"	29°24'24.00"	769005	3256239
DBS28	35°46'27.00"	29°24'11.00"	769203	3255843
DBS29	35°46'41.00"	29°24'7.00"	769584	3255729
DBS31	35°46'13.00"	29°25'16.00"	768778	3257836
DBS32	35°46'11.00"	29°25'11.00"	768728	3257680
DBS37	35°46'24.00"	29°25'4.00"	769083	3257473
DBS39	35°46'28.00"	29°24'50.00"	769202	3257044
DBS40	35°46'38.00"	29°24'59.00"	769465	3257328
DBS41	35°46'47.00"	29°25'8.00"	769701	3257611
DBS43	35°46'51.00"	29°25'13.00"	769805	3257768
DBS45	35°46'33.00"	29°24'54.00"	769333	3257171
DBS46	35°46'24.00"	29°24'46.00"	769097	3256919
DBS48	35°46'59.00"	29°24'13.00"	770065	3255925
DBS49	35°46'59.00"	29°24'24.00"	770056	3256264
DBS50	35°47'14.00"	29°24'35.00"	770453	3256612
DBS52	35°47'28.00"	29°24'56.00"	770815	3257268

Appendix B: Gamma radiation readings as CPS and THM % values with corresponding Log transformed values.

Samples	CPS	Log10 CPS	% THM	log THM
DBS1	200	2.301029996	0.208	-0.681936665
DBS2	200	2.301029996	0.358	-0.446116973
DBS3	210	2.322219295	0.267	-0.573488739
DBS4	250	2.397940009	0.896	-0.04769199
DBS5	390	2.591064607	0.159	-0.798602876
DBS6	250	2.397940009	0.572	-0.242603971
DBS7	1450	3.161368002	0.967	-0.014573526
DBS8	300	2.477121255	0.283	-0.548213564
DBS9	180	2.255272505	0.4	-0.397940009
DBS10	200	2.301029996	0.57	-0.244125144
DBS12	220	2.342422681	0.198	-0.70333481
DBS13	200	2.301029996	0.281	-0.55129368
DBS14	260	2.414973348	0.074	-1.13076828
DBS15	200	2.301029996	0.062	-1.207608311
DBS16	200	2.301029996	0.098	-1.008773924
DBS17	250	2.397940009	0.49	-0.30980392
DBS18	290	2.462397998	0.216	-0.665546249
DBS19	200	2.301029996	0.094	-1.026872146
DBS20	250	2.397940009	0.063	-1.200659451
DBS21	250	2.397940009	0.563	-0.249491605
DBS22	290	2.462397998	0.1	-1
DBS23	400	2.602059991	0.055	-1.259637311
DBS24	3100	3.491361694	1.069	0.028977705
DBS25	170	2.230448921	0.317	-0.498940738
DBS26	150	2.176091259	0.296	-0.528708289
DBS28	200	2.301029996	0.316	-0.500312917
DBS29	170	2.230448921	0.302	-0.519993057
DBS31	400	2.602059991	0.37	-0.431798276
DBS32	250	2.397940009	0.124	-0.906578315
DBS37	340	2.531478917	0.0087	-2.060480747
DBS39	1267	3.102776615	0.165	-0.782516056
DBS40	220	2.342422681	0.137	-0.863279433
DBS41	200	2.301029996	0.177	-0.752026734
DBS43	150	2.176091259	0.194	-0.71219827
DBS45	250	2.397940009	0.343	-0.46470588
DBS46	10100	4.004321374	15.628	1.193903403
DBS48	180	2.255272505	0.285	-0.54515514
DBS49	150	2.176091259	0.154	-0.812479279
DBS50	150	2.176091259	0.326	-0.4867824
DBS52	150	2.176091259	0.117	-0.931814138

Appendix C: HM% values and corresponding Log transformed values.

Samples	HM/THM %	Log HM/THM %
DBS1	6.59	0.818885415
DBS2	5.854	0.767452718
DBS3	32.538	1.512390855
DBS4	7.773	0.890588668
DBS5	30.678	1.486827043
DBS6	16.688	1.222404291
DBS7	10.946	1.039255444
DBS8	12.352	1.091737283
DBS9	8.831	0.946009885
DBS10	16.912	1.22819497
DBS12	25.926	1.413735517
DBS13	39.881	1.60076604
DBS14	40.734	1.609957059
DBS15	35.77	1.55351894
DBS16	35.484	1.550032571
DBS17	55.224	1.74212786
DBS18	10.738	1.0309234
DBS19	38.814	1.588988402
DBS20	39.95	1.601516784
DBS21	23.219	1.365843512
DBS22	10.256	1.010978012
DBS23	71.362	1.853467013
DBS24	40.278	1.605067898
DBS25	45.581	1.658783849
DBS26	28.024	1.447530124
DBS28	35.946	1.55565057
DBS29	7.863	0.895588276
DBS31	52.703	1.721835337
DBS32	50.236	1.701015052
DBS37	28.39	1.453165393
DBS39	36.327	1.560229534
DBS40	15.714	1.196286749
DBS41	20.648	1.314877992
DBS43	9.732	0.9882021
DBS45	23.63	1.373463722
DBS46	87.154	1.940287324
DBS48	26.972	1.430913151
DBS49	33.641	1.526868897
DBS50	15.054	1.177651912
DBS52	17.38	1.240049772

Appendix D: Zircon % values and corresponding Log transformed values.

Samples	Zrn/THM%	Log Zrn/THM
DBS1	4.613	0.663983455
DBS2	2.439	0.3872118
DBS3	21.465	1.331730893
DBS4	2.691	0.429913698
DBS5	20.678	1.315508531
DBS6	8.85	0.946943271
DBS7	7.792	0.891648944
DBS8	5.584	0.74694541
DBS9	3.636	0.560623875
DBS10	10.662	1.027838678
DBS12	5.185	0.714748761
DBS13	18.45	1.26599637
DBS14	22.201	1.346372537
DBS15	22.193	1.346216013
DBS16	20.43	1.310268367
DBS17	17.413	1.2408736
DBS18	3.356	0.525821952
DBS19	24.259	1.384872894
DBS20	26.463	1.422639077
DBS21	11.082	1.044618146
DBS22	6.838	0.834929096
DBS23	56.808	1.7544095
DBS24	19.444	1.288785612
DBS25	24.957	1.397192379
DBS26	6.49	0.812244697
DBS28	20.27	1.306853749
DBS29	2.218	0.345961542
DBS31	29.73	1.473194909
DBS32	30.189	1.479848727
DBS37	17.797	1.2503468
DBS39	26.735	1.427080188
DBS40	7.143	0.85388065
DBS41	6.883	0.83777777
DBS43	5.353	0.728597243
DBS45	13.356	1.12567641
DBS46	79.051	1.897907368
DBS48	16.33	1.212986185
DBS49	23.66	1.37401474
DBS50	7.527	0.876621916
DBS52	11.23	1.050379756

Appendix E: Tourmaline% values and corresponding Log transformed values.

Samples	Tur/THM%	Log Tur/THM
DBS1	1.318	0.11991541
DBS2	5.122	0.709439574
DBS3	3.237	0.510142699
DBS4	3.139	0.496791316
DBS5	4.237	0.627058464
DBS6	3.413	0.533136288
DBS7	0.928	-0.032452024
DBS8	4.907	0.690816058
DBS9	3.377	0.528531061
DBS10	3.922	0.593507589
DBS12	10.37	1.015778756
DBS13	11.905	1.0757294
DBS14	5.019	0.700617196
DBS15	0.783	-0.106238238
DBS16	4.301	0.633569443
DBS17	15.92	1.201943063
DBS18	4.027	0.60498163
DBS19	6.199	0.792321636
DBS20	2.545	0.405687787
DBS21	7.916	0.898505786
DBS22	2.35	0.371067862
DBS23	2.582	0.411956238
DBS24	8.333	0.920801382
DBS25	11.438	1.058350092
DBS26	2.36	0.372912003
DBS28	2.162	0.334855690
DBS29	4.234	0.626750854
DBS31	8.559	0.932423026
DBS32	6.368	0.804003055
DBS37	15.254	1.183383742
DBS39	1.22	0.086359831
DBS40	5.714	0.756940236
DBS41	7.692	0.886039275
DBS43	3.163	0.500099192
DBS45	5.479	0.738701300
DBS46	0	0
DBS48	2.752	0.43964843
DBS49	3.697	0.567849451
DBS50	4.839	0.684755622
DBS52	4.012	0.603360924

Appendix F: Rutile % values and corresponding Log transformed values**.**

Samples	Rt/THM %	Log Rt/THM
DBS1	0.659	-0.181114585
DBS2	1.463	0.165244326
DBS3	5.792	0.762828553
DBS4	1.345	0.128722284
DBS5	5.424	0.734319681
DBS6	3.287	0.516799704
DBS7	1.855	0.268343914
DBS8	1.692	0.228400359
DBS9	1.039	0.016615548
DBS10	2.083	0.31868927
DBS12	3.704	0.568670978
DBS13	8.929	0.950802823
DBS14	8.301	0.919130414
DBS15	9.138	0.960851154
DBS16	9.677	0.985740741
DBS17	16.915	1.228272002
DBS18	2.461	0.391111614
DBS19	7.547	0.87777435
DBS20	9.16	0.961895474
DBS21	3.43	0.53529412
DBS22	1.068	0.028571253
DBS23	10.563	1.02378728
DBS24	5.556	0.744762237
DBS25	6.932	0.840858554
DBS26	6.195	0.792041311
DBS28	9.459	0.975845225
DBS29	1.21	0.08278537
DBS31	13.514	1.130783915
DBS32	11.792	1.071587471
DBS37	8.475	0.928139707
DBS39	7.755	0.889581802
DBS40	0.0001429	-3.844967771
DBS41	3.644	0.561578368
DBS43	1.217	0.085290578
DBS45	4.452	0.648555156
DBS46	7.708	0.886941706
DBS48	6.422	0.807670301
DBS49	5.73	0.758154622
DBS50	1.613	0.207634367
DBS52	1.872	0.272305844

Appendix G: Minor and trace heavy minerals as % from HM found in the wadi alluvium.

Samples	Anatase	Brookite	Apatite	Dolomite	Garnet	Biotite	Muscovite	Staurolite
DBS1	0	0	0	0	0	0	0	0
DBS2	0	0	0	0	0	0	0	0
DBS3	4.712	1.571	0	0	0	0	0	0
DBS4	7.692	0	0	0	0	0	0	0
DBS5	1.105	0	0	0	0	0	0	0
DBS6	6.818	0	0	0	0	0	0	0
DBS7	3.39	0	0	0	0	0	0	0
DBS8	1.37	0	0	0	0	0	0	0
DBS9	8.824	0	0	0	0	0	0	0
DBS10	1.45	0	0	0	0	0	0	0
DBS12	11.429	0	0	0	2.857	8.571	2.857	0
DBS13	1.493	0	0	0	0	0	0	0
DBS14	12.322	0	0	0.474	0	0	0	0
DBS15	0.73	0	0	0	0	0	0	0
DBS16	3.03	0	0	0	0	0	0	0
DBS17	9.01	0	0	0	0	0	0	0
DBS18	6.25	0	0	0	0	2.083	0	0
DBS19	2.083	0	0	0	0	0	0	0
DBS20	2.55	0	0.637	1.274	0	0	0	0
DBS21	2.273	0	1.136	0	0	0	0	0
DBS22	0	0	0	0	0	0	0	0
DBS23	0.658	0	1.316	0	0	0	0	0
DBS24	3.448	0	13.793	0	0	0	0	0
DBS25	4.943	0	0	0	0	0	0	0
DBS26	15.789	0	1.053	0	0	0	0	0
DBS28	5.263	0	0.752	0	0	0	0	5.263
DBS29	2.564	0	0	0	0	0	0	0
DBS31	1.709	0	0	0	0	0	0	0
DBS32	2.817	0	0	0.939	0	0	0	0
DBS37	2.985	0	0	0	0	0	0	0
DBS39	1.685	0	0	0	0	0	0	0
DBS40	7.576	0	0	1.515	0	0	0	0
DBS41	5.882	0	1.961	0	0	0.983	0	2.941
DBS43	0	0	0	0	0	0	0	0
DBS45	0	0	0	1.449	0	0	0	0
DBS46	0.454	0	0	0	0	0	0	0
DBS48	5.442	0	0	0	0	0	0	0
DBS49	0.549	0	0	0	1.099	0	0	0
DBS50	7.143	0	0	0	0	0	0	0
DBS52	0	0	1.538	0	0	0	0	0

التغييرات المكانية للمعادن الثقيلة والنشاط الاشعاعي بالقرب من وادي المزراب، جنوب شرق الأردن، ومضامينها الاستكشافية

إعداد
ابتسام البيك

المشرف
الاستاذ الدكتور غازي سفاريني

المشرف المشارك
الاستاذ الدكتور هارالد دل

ملخص

للمعادن الثقيلة من مثل الزركون والروتايل والاباتيت والمونازيت أهمية اقتصادية بارزة وتطبيقات صناعية وتكنولوجية متعددة الأطياف في حياتنا المعاصرة. وتعرف التوضعات الاقتصادية للمعادن الثقيلة أنها تلك الحاوية على تراكيز تزيد عن 1% من وزنها من هذه المعادن, ومعظمها من أنواع رسوبية سيليسية.

تمثل هذه الدراسة فحوصات على رسوبيات أودية تقطع الصخور الرسوبية لتكوين دبيدب الغني بالمعادن الثقيلة بهدف التعرف على أنواعها المعدنية وتحري احتمالية وجود علاقة بين المعادن الشائعة منها في المنطقة والإشعاعية السائدة وبالتالي تحري مدى ملائمة استخدام تقنية قياس إشعاعات جاما لأغراض التنقيب عن هذه المعادن.

لتحقيق أهداف هذه الدراسة جرى أخذ 40 عينة على شبكة شبه متسامة تغطي ما مساحته 3 كم^2، كما جرى قياس الإشعاعية عند مواقع أخذ العينات، ثم جرى فصل المعادن الثقيلة باستخدام السوائل الخاصة بذلك. وتم بعد التعرف على المعادن شبه الشفافة فتبين أن الرئيسية منها أنواع ثلاثة هي الزركون والروتايل والتورمالين أما المعادن الفرعية فهي معادن الأناتيس والغارنت والدولوميت والأباتيت. وباستخدام المايكروسكوب الالكتروني الماسح تم التعرف على المظهر الخارجي للمعادن المفصولة ودراسة تركيبها الكيميائي. ثم جرى حساب الشيوع النسبي لكل نوع وعملت خرائط تبين التغيرات المكانية للنشاط الإشعاعي السائد باستخدام تقنية الكريجينج.

واستخدمت بعد ذلك الخرائط التي تم الحصول عليها في تحري وجود ارتباط بين التغير المكاني لشيوع المعادن الثقيلة و النشاط الإشعاعي . وعلى الرغم من تدني تراكيز المعادن الثقيلة إلا أن خرائط التوزع المكاني تشير إلى زيادة في تراكيز هذه المعادن في اتجاه شمالي غربي وعلاقات ارتباط وثيقة بين تغيرات النشاط الإشعاعي وشيوع العناصر الثقيلة.

ولمعرفة مصادر النشاط الإشعاعي جرى تحليل عينات من الرسوبيات باستخدام تقنيات التضوء بالأشعة السينية فتبين أن الإشعاعية أكثر ارتباطا بعنصر الثوريوم ونتائج تحلله الإشعاعي منها بعنصر اليورانيوم كما تبين خرائط التوزع المكاني لمعدن الزركون.

اختتمت الدراسة بتوصيات بإجراء دراسات مفصلة على مساحات أكثر اتساعا في نفس المنطقة لتأكيد ما توصلت إليه هذه الدراسة وإمكانية استخدام التقنيات المتبعة في التنقيب عن المعادن الثقيلة في بيئات جيولوجية مشابهة.